UNIVERSIDADE FEDERAL DE SANTA CATARINA

CENTRO TECNOLÓGICO

PROGRAMA DE PÓS-GRADUAÇÃO EM ENGENHARIA CIVIL

Aline Kirsten Vidal de Oliveira

Automatic Fault Detection of Photovoltaic Solar Generators Applying Aerial Infrared Thermography

Florianópolis

2022

Aline Kirsten Vidal de Oliveira

Automatic Fault Detection of Photovoltaic Solar Generators Applying Aerial Infrared Thermography

Florianópolis

2022

Aline Kirsten Vidal de Oliveira

Automatic Fault Detection of Photovoltaic Solar Generators Applying Aerial Infrared Thermography

O presente trabalho em nível de doutorado foi avaliado e aprovado por banca examinadora composta pelos seguintes membros:

Prof. Roberto Zilles, Dr.
Universidade de São Paulo - USP

Prof. Arno Krenzinger, Dr.
Universidade Federal do Rio Grande do Sul - UFRGS

Prof. Roberto Lamberts, PhD
Universidade Federal de Santa Catarina – UFSC

Certificamos que esta é a **versão original e final** do trabalho de conclusão que foi julgado adequado para obtenção do título de doutora em Engenharia Civil no Programa de Pós-Graduação em Engenharia Civil da Universidade Federal de Santa Catarina.

Prof. Philippe Jean Paul Gleize, Dr Coordenador do Programa de Pós-Graduação	Prof. Ricardo Rüther, PhD Orientador

Florianópolis, 2022.

ACKNOWLEDGEMENTS

friends I gained by marriage, especially the colleagues of Faselit that made a very busy and tough year way funnier.

Finally, I want to thank my partner in research, in surfing and in life, Matheus Körbes Bracht. This work would never be possible without your encouragement and support. I feel very lucky to have found you.

"Há uma piada entre até quem não é do mercado que diz que, em algum momento, as máquinas vão tomar o controle da sociedade. Pode até ser — ainda que o nível do aprendizado de máquina hoje esteja longe disso. Mas, agora, a gente precisa prestar atenção e notar os passos não das máquinas, mas de quem as controla."

(Felitti, 2022)

RESUMO

A termografia aérea (aIRT) é uma técnica de inspeção de sistemas fotovoltaicos (FV) que vem ganhando atenção nos últimos anos por ser um método de inspeção rápido, não-destrutivo e sem contato necessário com o módulo solar FV, além de poder ser aplicado em condições operacionais em tempo real. No entanto, a avaliação visual das imagens capturadas pela aIRT e a análise de um grande número de imagens é um processo demorado e trabalhoso. Este trabalho propõe um método para automatizar o procedimento de detecção de falhas combinando a aIRT com orto-georreferenciamento e um algoritmo de aprendizado profundo (Deep Learning – DL). O trabalho inicia com uma revisão da literatura sobre métodos para a automatização das diversas etapas do processo de aIRT. Com isso, são escolhidos os métodos de DL para a detecção de falhas em imagens (Mask-RCNN) e o método de produção de ortomosaico para a visualização de falhas nas usinas FV. Para o treinamento do método de detecção de falhas, foi necessária a criação de um banco de dados de imagens de aIRT. Para isso, uma campanha de voos sobre usinas FV brasileiras foi realizada. Com os dados obtidos, foi formado o banco de dados de imagens aIRT que foi utilizado para treinar um algoritmo de DL para detecção de falhas. As imagens com suas falhas detectadas foram então utilizadas para formar um orthomosaico com as falhas da usina FV. O método foi testado com dois casos testes de duas pequenas usinas FV e os resultados obtidos demonstraram a viabilidade de utilizar o método para facilitar a localização de falhas de sistemas FV. Especialmente no caso de detecção de pontos quentes e subséries FV (*substrings)* desconectadas, a técnica provou ter alta acurácia (em torno de 10% de falsos positivos), em um curto espaço de tempo, com poucos recursos computacionais necessários. Mesmo com conjuntos de dados pequenos, foi possível detectar visualmente as diferentes falhas nos ortomosaicos térmicos produzidos. O desenvolvimento do método tem uma importância grande para o desenvolvimento da energia solar, especialmente no Brasil, onde as usinas de grande porte (que ocupam centenas de hectares) começam a dominar o espaço, e pode ser desenvolvido com um maior conjunto de dados para melhorar a inspeção utilizando aIRT em qualquer lugar deste grande país e do mundo.

Palavras-chave: Detecção de falhas; Energia Solar Fotovoltaica; Termografia Infravermelha Aérea; Inteligência Artificial.

RESUMO EXPANDIDO

Introdução

Atualmente, a energia fotovoltaica (FV) é o segmento de energia renovável que mais cresce no mundo. No Brasil, o final do ano de 2022 marca o momento em que a geração solar FV passa à frente da geração eólica em capacidade instalada, ficando atrás apenas da geração hidrelétrica de grande porte. À medida que a competitividade da tecnologia aumenta, a sua confiabilidade é uma grande preocupação no setor e métodos confiáveis e econômicos de operação e manutenção (O&M) para usinas FV são de extrema importância para garantir a segurança, disponibilidade e produtividade dos sistemas. A termografia infravermelha (IRT) é um dos métodos mais populares e confiáveis de diagnóstico de falhas de sistemas FV, pois é um método não destrutivo, requer instrumentação mínima e pode ser realizada sem interromper a operação de usinas FV. O método se baseia nas mudanças de temperatura nos módulos FV quando eles estão operando sob condições anormais, sendo os defeitos nos mesmos passíveis de detecção através de seus padrões térmicos. Para acelerar o procedimento de detecção de falhas para usinas FVs em escala de megawatts ou sistemas FV com acesso físico limitado, como em telhados ou fachadas, a IRT pode ser combinada com veículos aéreos não tripulados (VAnTs, ou drones). A termografia aérea (aIRT) tem a vantagem de ser um método de inspeção rápido e eficiente para a detecção de séries de módulos FV abertos/desconectados, módulos quebrados, subséries desconectadas, curto-circuitos, entre outros. No entanto, a avaliação visual das imagens capturadas pela aIRT e a análise de muitos quadros de imagem é um processo lento e repetitivo, sujeito a erro. Este trabalho propõe um método original e inovador para automatizar o procedimento de detecção de falhas combinando a aIRT com o uso de ortomosaicos e um algoritmo de aprendizado profundo (Deep Learning – DL). O trabalho vem de encontro à necessidade do desenvolvimento de ferramentas rápidas e de baixo-custo e que estejam disponíveis no mercado para a inspeção de grandes usinas FV, aumentando a confiabilidade da energia solar e contribuindo para a disseminação de uma fonte limpa de energia elétrica.

Objetivos

O objetivo desta tese é propor um método original e inovador para a detecção e classificação de falhas em módulos solares FV através de imagens aéreas IRT, combinando algoritmos de ortomosaicos e de DL. Especificamente, objetiva-se:

- Revisar a literatura acadêmica/científica para entender os métodos atuais utilizados para a automatização de inspeções de aIRT em usinas solares FV;

- Efetuar inspeções de aIRT de diferentes usinas FV para detectar falhas e adquirir imagens aIRT de módulos com diferentes tipos de falhas;

- Analisar e processar as imagens aIRT capturadas para criar um conjunto de dados de amostras classificadas em categorias de possíveis falhas em módulos FV;
- Treinar e refinar um algoritmo de DL para detectar falhas em módulos FV em imagens aIRT;
- Desenvolver um método para obter automaticamente um mapa de uma usina FV com suas falhas destacadas.

Método

Esta tese é composta de três artigos científicos (dois já publicados em revistas científicas internacionais Qualis A1 e um recentemente submetido também a revista científica internacional Qualis A1) que investigam os procedimentos da técnica de aIRT e a possibilidade de automatização do método de análise das falhas detectadas. O trabalho inicia com uma revisão da literatura sobre métodos para a automatização das diversas etapas do processo de aIRT (Artigo 1). Com a revisão, foram escolhidos os métodos de DL para a detecção de falhas em imagens (Mask-RCNN) e o de produção de ortomosaico para a visualização de falhas nas usinas FV.

Para o treinamento do método de detecção de falhas, foi necessária a criação de um banco de dados de imagens de aIRT. Para isso, uma campanha de voos sobre quatro usinas FV brasileiras em escala comercial foi realizada (Artigo 2), analisando falhas de módulos FV de duas tecnologias diferentes: c-Si e CdTe. Diferentes métodos de voos e diferentes equipamentos foram testados para ajudar a aprimorar os procedimentos de aIRT.

Com os dados obtidos, foram escolhidas 83 imagens para compor o banco de dados para o algoritmo de detecção automática de falhas. Estas imagens foram marcadas para destacar as falhas existentes nas mesmas e assim treinar o algoritmo para detectá-las (Artigo 3). As imagens resultantes com as falhas destacadas foram então utilizadas para formar um ortomosaico da planta FV. O método foi testado com dois casos testes de duas pequenas usinas FV (1 MW e 400 kW). O ortomosaico das usinas com as falhas anotadas foi gerado utilizando o software ContextCapture®.

Resultados e Discussão

Os resultados da revisão da literatura mostraram que a maioria dos estudos focados na automatização do processo de aIRT estudam a detecção e classificação de falhas em usinas FV. Dentre esses estudos, o uso de algoritmos DL tem proporcionado bons resultados com precisão de até 90% na detecção e classificação de falhas em 10 tipos diferentes de anomalias detectadas em segmentos de módulos extraídos de imagens aIRT. Por outro lado, poucos estudos exploraram a automação de outras partes do procedimento de aIRT, como a otimização do planejamento de trajetória (nove trabalhos) para o voo de inspeção, a criação de ortomosaicos da planta FV (14 estudos) que é realizado para facilitar a localização das falhas no campo e a detecção de sujeira, e sua diferenciação das falhas reais nos módulos FV (oito estudos). Para a automação desses procedimentos, diferentes algoritmos foram investigados,

incluindo filtros de processamento digital de imagens (DIP) e métodos como detecção de bordas e limiarização; algoritmos DL como Fast RCNN, ImageNET e VGG16; e outros algoritmos baseados em aprendizado de máquina usados para tarefas de classificação, como SVMs, KNNs e RFs. No entanto, a precisão, robustez e generalização dos algoritmos desenvolvidos ainda são os principais desafios desses estudos, principalmente quando se trata de um número grande de classes de falhas e da inspeção de plantas FV de grande porte. Portanto, o procedimento autônomo e a tarefa de classificação ainda devem ser explorados para aumentar a precisão e aplicabilidade do método aIRT.

Durante a campanha de voos em usinas FV no Brasil, os resultados mostraram que os problemas mais comuns detectados com a aIRT foram os pontos quentes devido à sujidade e à vegetação, que causavam o sombreamento das células FV. Entre as falhas reais, as mais comuns, em número de ocorrências, foram subséries de células desconectadas, seguidas de séries desconectadas, defeitos de pontos quentes e módulos com vidros quebrados. No entanto, ao comparar a quantidade de energia perdida causada por cada falha, os maiores prejuízos são causados por séries desconectadas, seguidas por subséries desconectadas e pontos quentes, com vidro frontal quebrado por último.

Após a etapa de aquisição de dados e formação do banco de dados para treinamento do algoritmo de detecção de falhas, foram realizados vários testes ajustando os hiperparâmetros da rede Mask-RCNN e ajustando o formato da anotação do conjunto de dados. Os melhores resultados obtidos utilizando o algoritmo com o conjunto de dados de validação (10% do número total de amostras) atingiram uma precisão média de 90,5% e um F1-score de 69,0%. Considerando o pequeno conjunto de dados utilizado para treinamento, esses valores são razoáveis e podem ser melhorados adicionando mais amostras. Após a aplicação do algoritmo de DL nas imagens dos dois casos testes, as imagens resultantes, com suas falhas detectadas, foram processadas para a produção de um ortomosaico de cada usina. Os resultados obtidos demonstraram a viabilidade de utilizar o método para facilitar a localização de falhas dentro das usinas FV. Especialmente no caso de detecção de pontos quentes e subséries desconectadas, a técnica provou ter alta precisão (em torno de 10% de falsos positivos), em um curto espaço de tempo, com poucos recursos computacionais necessários. Mesmo com conjuntos de dados pequenos, foi possível detectar visualmente as diferentes falhas nos ortomosaicos térmicos produzidos. A proposta do método tem uma importância grande para o desenvolvimento da energia solar e o método pode ser aprimorado com um maior conjunto de dados para melhorar a inspeção utilizando aIRT.

Considerações Finais

Os resultados deste trabalho contribuem com o desenvolvimento da técnica de inspeção aIRT, principalmente no contexto das usinas FV brasileiras, que estão caminhando para portes da ordem de 1GWp, ocupando áreas de várias centenas de hectares. Primeiramente, a revisão da literatura proporciona uma visão geral dos diferentes algoritmos usados para automatizar as muitas partes do processo de inspeção e fornece uma compreensão clara dos métodos mais comuns e eficazes a serem usados e desenvolvidos.

Os resultados das inspeções realizadas no país também são extremamente importantes porque mostram as falhas mais comuns que podem acontecer no início

da operação de usinas FV e, a partir disso, os operadores podem decidir como resolvê-los e evitá-los, reduzindo o downtime e maximizando o tempo de operação e geração de energia das usinas FV. Além disso, são apresentados os impactos técnicos e econômicos destes problemas para o operador dos sistemas FV.

Por fim, esta tese fornece uma abordagem inovadora que combina um algoritmo de DL com técnicas de produção de mosaicos para oferecer uma maneira simples e eficaz de detectar e localizar falhas em usinas FV usando IRT de forma automática. Este método é inovador tanto pela nova combinação de técnicas de DL e fotogrametria, como também pelo treinamento de uma rede de segmentação de instâncias usando dados coletados no Brasil. Isso é relevante porque o país está sujeito a condições ambientais específicas, como alta irradiância e temperatura, e condições de layout particulares que não são difundidas nos países que desenvolveram conjuntos de dados de aIRT anteriormente, ou seja, Europa e Ásia. Portanto, o desenvolvimento de algoritmos de automatização com conjuntos de dados locais é extremamente valioso e pode ser aperfeiçoado com um maior conjunto de dados para melhorar a inspeção de aIRT em todo o país.

Palavras-Chave: Detecção de falhas; Energia Solar Fotovoltaica; Termografia Infravermelha Aérea; Inteligência Artificial.

ABSTRACT

Aerial thermography (aIRT) is an inspection technique for photovoltaic (PV) systems that has been gaining attention in recent years as it is a fast, non-destructive inspection method with no contact required with the module. In addition, it can be applied in real-time operational conditions. However, visually evaluating the images captured by aIRT and analyzing many image frames is a time-consuming and labor-intensive process. This work proposes a method to automate the fault detection procedure combining aIRT with orthomosaicking and a deep learning (DL) algorithm. The work begins with a review of the literature on methods for automating the various stages of the aIRT process. Thus, the DL methods are chosen for the detection of faults in images (Mask-RCNN) and the orthomosaic production for the visualization of faults in PV plants. To train the failure detection method, it was necessary to create an aIRT image database. For this, a campaign of flights over Brazilian PV plants was carried out. With the obtained data, the aIRT image database was produced, which was used to train a DL algorithm for fault detection. The images with their detected faults are then used to form an orthomosaic with the faults of the PV plant. The method was tested with two test cases of two small PV plants and the results obtained demonstrated the feasibility of using the method to facilitate the location of faults in PV systems. Especially in the case of detection of hot spots and disconnected substrings, the technique proved to have high accuracy (around 10% false positives), in a short time, with few computational resources needed. Even with small datasets, it was possible to visually detect the different faults in the thermal orthomosaics produced. The development of the method is of great importance for the development of solar energy and can be developed with a larger dataset to improve inspection using aIRT in Brazil.

Keywords: Fault detection; Photovoltaic Solar Energy; Aerial Infrared Thermography; Artificial Intelligence.

LIST OF FIGURES

Figure 3-6 - Examples of vegetation and soiling over PV modules: (a) Soiling pattern image over many c-Si modules, taken with System 2. (b) Bird droppings image over one c-Si module, taken with System 1. (c) Vegetation image over many c-Si modules

LIST OF TABLES

ACRONYMS

Ac	Accuracy
AI	Artificial Intelligence
aIRT	Aerial Infrared Thermography
ANN	Artificial Neural Network
AP	Average Precision
AUROC	Area under the Receiver Operating Characteristic
CdTe	Cadmium Telluride
CNN	Convolutional Neural Network
c-Si	Crystalline Silicon
DIP	Digital Image Processing
DL	Deep Learning
EL	Electroluminescence
FN	False Positive
FoV	Field of View
FP	False Positive
GB	Gigabyte
GPS	Global Positioning System
GW	Gigawatt
IEC	International Electrotechnical Commission
IOU	Intersection over Union
IRT	Infrared Thermography
kW	Kilowatt
KNN	K-Nearest Neighbors
MB	Megabyte
mc-Si	Multicrystalline Silicon
MCC	Matthews correlation coefficient
ML	Machine Learning
MW	Megawatt
O&M	Operation and Maintenance
PB	Paraíba

PID	Potential Induced Degradation
Pr	Precision
PTP	Partial True Positive
PV	Photovoltaic
RCNN	Regional Convolutional Neural Network
Re	Recall
RF	Random Forest
RGB	Red Green Blue
RN	Rio Grande do Norte
RTK	Real Time Kinematic
SIFT	Scale Invariant Feature Transform
SVM	Support Vector Machine
TN	True Negative
TP	True Positive
UAV	Unmanned Aerial Vehicle

1. INTRODUCTION

Solar photovoltaic (PV) energy is currently the fastest-growing renewable energy technology worldwide, with more than 150 GWp installed in 2021 alone (Renewable Capacity Statistics 2022IRENA, 2022), and over 1 TWp of cummulative capacity worldwide. Such technology adoption is mainly due to significant cost reductions, primarily driven by technological advancements, high learning rates, policy support and innovative financing models. For these reasons, solar PV will play a crucial role in the fight against climate change and is expected to exceed an installed capacity of 5,200 GWp before the end of the current decade (World Energy Transitions Outlook 2022: 1.5°C PathwayIRENA, 2022).

Solar PV is especially important in Brazil, where the high irradiances and policy incentives contributed to the close to 25 GWp of installed capacity by the end of 2022, which translates into more than 10% of the electricity generation installed capacity of the country (ABSOLAR, 2022). This growth has been driven by a combination of small-scale distributed generation as well as utility-scale systems that can occupy an area as large as 1200 hectares (AGÊNCIA NACIONAL DE ENERGIA ELÉTRICA (ANEEL), 2021; BADRA, 2021).

The wide-scale adoption of this technology is highly dependent on its economic viability, which relies on its reliability, predictability and life span (IRENA, 2017). In addition, failures in installations can impose hazard risks, produce extra costs and increase scepticism about the technology. Quantifying electrical or mechanical stresses from installation and operation is both a matter of safety and financial return. Therefore, quality assurance is of utmost relevance in PV power plants, and developing fast and efficient methods for inspecting PV modules is critical in order for this technology to scale. With the advances in data analytics, sensors and artificial intelligence, a system supervisory platform is one applied solution for monitoring a power plant. These platforms acquire and control data from remote measurement devices (such as inverter current sensors) and enable the visualization of the performance status of the plant (Advanced asset management tools in photovoltaic plant monitoring: UAV-based digital mappingNICCOLAI *et al.*, 2019). However, these systems typically measure each string's power, current and voltage, making it hard to

detect and locate faults that affect a particular module or component (ABUBAKAR *et al.*, 2021). They also cannot detect non-energy, latent risk factors, such as hot spots or sub-string failures, that do not reduce power production in the short term but can cause damage to the system in the long run (HØIAAS *et al.*, 2022). Therefore, onsite inspections are still a necessary component of proper operation and maintenance.

Manual inspection of PV plants is becoming practically impossible as their sizes expand due to long assessment time, low efficiency, demand for skilled workers and a relatively high error rate. For this reason, alternative methods are employed nowadays for inspection and monitoring. I-V curve measurements have been broadly used to assess the performance and efficiency of PV modules. However, this method requires the disconnection of the PV system, interrupting its operation (KÖNTGES *et al.*, 2014). Photoluminescence and Electroluminescence, imagining techniques that capture photons emitted by the radiative recombination of excited charge carriers, are other methods commonly used to evaluate PV modules (OLIVEIRA, A. K. V. De *et al.*, 2019). However, they require expensive cameras and can only be done at night, imposing challenges to a rapid and low-cost inspection (DOLL *et al.*, 2018; ULRIKE JAHN *et al.*, 2018).

On the other hand, infrared thermography (IRT) is a reliable and precise fault diagnosis method that requires minimal instrumentation and can be carried out during regular operation. The technique measures the radiation emitted by the modules in a range between 7 μm and 13 μm using commercially-available cameras (BUERHOP *et al.*, 2022; TSANAKAS *et al.*, 2016). Because all modules, in principle, receive the same amount of irradiance, faults that somehow prevent the conversion of photons into electricity will irradiate heat, which IRT can then detect. It, therefore, has the potential to identify the exact physical location of PV module defects such as disconnected strings, broken modules and substring interruptions (BUERHOP, CI *et al.*, 2012).

IRT has proved to be an effective and reliable method for PV plant inspection. However, as PV power plants become more extensive, performing it with a handheld camera is neither time-efficient nor scalable. For this reason, combining IRT cameras with Unmanned Aerial Vehicles (UAVs), known more colloquially as drones, can improve cost-effectiveness in large systems, reduce the inspection time, and facilitate inspections for systems that are difficult to access, such as roof-mounted systems

(QUATER *et al.*, 2014). This technique has been called Aerial Infrared Thermography (aIRT) and has the potential to revolution PV plant operation and maintenance (O&M). This thesis addresses aIRT, the advantages and challenges associated with the technology, and proposes a novel method to increase its time efficiency and accuracy.

1.1. PROBLEM AND RELEVANCE OF THIS WORK

As previously stated, with the development of PV, PV plants are becoming larger and are being installed in remote territories. Subsequently, research regarding aIRT has significantly increased in previous years. The process for an aIRT inspection consists of three primary stages: acquisition, analysis of the data, and remediation actions. For the acquisition step, the UAV flies a designated rote over the site, taking successive pictures or recording videos to create an imagery database that covers all modules in the PV plant.

The acquired data is then analyzed, and an actionable report is produced. However, the visual assessment of the images captured by aIRT and the analysis of several image frames is time- and computer-intensive. Not only is it a long and tedious process, but it is also prone to human error. One potential solution to address this issue is to use artificial intelligence to perform fault detection in aIRT images. That is possible by combining aIRT with classic computer vision algorithms, as proposed by many authors using different strategies, like Hough Line Transform (SHA *et al.*, 2019), k-means (SALAZAR; MACABEBE, 2016), and HOG Features (MONTOYA *et al.*, 2019). Another approach to the problem is to use deep learning (DL) algorithms to train a dataset and correctly detect PV module faults, mimicking the human brain. Some studies assess this strategy using classic DL algorithms such as ImageNet (Computer vision tool for detection, mapping, and fault classification of photovoltaics modules in aerial IR videosBOMMES *et al.*, 2021), Yolo (GERD IMENES *et al.*, 2021) and Faster RCNN (WEI *et al.*, 2019).

However, these algorithms' computational time and intensity are still relatively high, thus limiting potential adoption (DUNDERDALE *et al.*, 2020). Furthermore, developing accurate classification algorithms that are robust enough to detect and classify faults in the most varied types of images (e.g., a domain shift between training

and test data) remains an unsolved problem (BUERHOP *et al.*, 2022). Most of the developed algorithms in the literature used data collected in Asia and Europe, presenting installation and environmental conditions that are much different than in the Sun Belt countries, meaning that these solutions are often inadequate for such areas. This is the case in Brazil, where the absence of aIRT datasets collected has prevented the development of algorithms to detect such faults in Brazilian solar PV systems properly. This thesis aims to address this challenge by performing a flight campaign in typical PV plants in Brazil and developing a fault detection algorithm specifically adapted to the country's power plant layout and environmental conditions.

An additional challenge related to the analysis of faults in PV power plants is the correct localization of the defects in conformity with the operator's nomenclature of strings and modules. This list is crucial so that repairs can be planned with complete knowledge of the site's condition. Since most of the technicians replacing broken modules and repairing connections on-site will not have an IRT camera on hand, an error in the fault list can cause a healthy module to be replaced while failing to address the root issue. Registering the physical location of the faults identified via aIRT is highly challenging, namely because aIRT videos are repetitive and display only a small section of the plant with only a few PV modules at any given time (BUERHOP *et al.*, 2022).

To perform this process automatically, a highly accurate Global Positioning System (GPS) position data is necessary (ADDABBO *et al.*, 2018; ISMAIL *et al.*, 2020), as well as it is high computational time. Applying aerial photogrammetry using aIRT images is one potential solution to this problem. Photogrammetry is a scalable process that corrects the perspective distortions of the images. This makes it possible to create an orthorectified mosaic, the so-called orthomosaic, that completely covers the inspection site (ZEFRI *et al.*, 2021). It improves sight perspective by giving a more comprehensive view of the modules, boosting resolution, and making defect localization easier (Survey on PV Modules' Common Faults After an O&M Flight Extensive Campaign Over Different Plants in ItalyGRIMACCIA *et al.*, 2017). This allows users to accurately locate the system faults with detailed site mapping.

Recent research has demonstrated that orthomapping combined with automatic fault detection algorithms enables efficient inspections of PV power plants. These

studies mostly use simple DIP techniques to detect faults and combine them with orthomosaicking techniques (LÓPEZ-FERNÁNDEZ *et al.*, 2017; PARK; LEE, 2019; TSANAKAS *et al.*, 2017). Considering this, this thesis proposes a method combining a DL algorithm for fault detection with orthomosaicking techniques to reconstruct a PV power plant orthophoto that highlights the detected faults by the automatic algorithm.

1.2. OBJECTIVES

1.2.1. General objective

This doctoral thesis proposes a method for detecting and classifying faults on PV modules through aerial IRT images, combining orthomosaicking and deep learning algorithms.

1.2.2. Specific objectives

The general objective was divided into four specific goals:
a) Review academic literature to understand the current methods used for the automatization of aIRT inspections of PV plants;
b) Perform aIRT inspections of different PV power plants in order to detect faults and acquire aIRT images of modules and modules with different types of faults;
c) Analyze and process the captured aIRT images in order to create a dataset of samples classified in categories of possible PV module faults;
d) Train and refine a deep learning algorithm to detect PV modules faults in aIRT images;
e) Develop a method to automatically obtain a map of a PV power plant with its detected faults.

1.3. STRUCTURE OF THE THESIS

This thesis consists of three contextual chapters regarding the Introduction, Discussions and Conclusions, and three journal papers that together describe the activities performed during this doctorate work. Each article is presented in a chapter, and Table 1-1 gives an overview of them. The co-author of one of the papers (the only co-author besides the supervisor and co-supervisor of the thesis) provided a shared authorship agreement, as shown in Appendix A. The journal papers were transcribed to this document, but adjustments in their format were made to comply with the ABNT (Brazilian Association of Technical Standards) requirements. Also, all the references were presented at the end of this document for conciseness. An overview of all the chapters is presented in this section.

Table 1-1 – Papers written in the context of this thesis.

Title	Journal	Year	Status
Automatic Inspection of Photovoltaic Power Plants Using Aerial Infrared Thermography: A Review	Energies	2022	Published
Aerial infrared thermography for low-cost and fast fault detection in utility-scale PV power plants	Solar Energy	2020	Published
Automatic Fault Detection of Utility-Scale Photovoltaic Solar Generators Applying Aerial Infrared Thermography and Orthomosaicking	Solar Energy	2022	Under review

The first chapter provides an introduction to the importance of the research topic. It explains the value of monitoring PV systems and the problems associated with inspecting large PV plants. It shows the relevance of aIRT for fast and efficient PV plant inspections and presents the challenges of analyzing a large amount of the produced data. It highlights the significance of this thesis, which focuses on the automation of detecting faults on aIRT images. The chapter also synthesis the general and specific goals of this work, announcing the following chapters.

Given the importance of aIRT and the need for automating the process of processing aIRT images, this thesis reviews the state-of-art techniques and automation methods. The second chapter then presents a literature review on strategies for automating various tasks of the aIRT framework for PV system inspections. The study was published as a paper in the journal *Energies* in 2022. In addition to presenting different methods reported in the literature, the chapter assesses the subject's main challenges and research opportunities. Algorithms for digital image

processing (DIP), classification, and deep learning techniques are among the related studies, with the majority based on a large dataset of acquired aIRT images.

For this reason, acquiring images to create an image dataset is crucial in developing an automatic fault detection algorithm. Therefore, the third chapter of this thesis presents the results of an aIRT flight campaign in the northeast of Brazil over four utility-scale PV plants. This analysis was published in 2020 in the Solar Energy Journal and also presents the differences in the acquired images when using different flight strategies and equipment. The findings also show the most common faults that can occur right after the beginning of the operation of PV power plants and how operators can prevent such defects from occurring and remediate problems when necessary.

Finally, the fourth chapter of this thesis describes a novel method to automatically detect faults in PV systems using aIRT and to obtain a map of the faults of the power plant. The procedure consists of training a deep learning algorithm for instance segmentation, a technique chosen based on the literature review presented in Chapter 2. The algorithm was trained using images obtained during the flight campaign described in Chapter 3. The review paper also supported the construction of a map with the faults of the PV plant, using the technique of orthomosaicking, listed in the review as a knowledge gap that needed further investigation. The method was tested on a 3 MW power plant case study, demonstrating promising results. It was described in the format of a paper submitted to the Solar Energy journal and is now under review.

The last chapter presents the final discussions and conclusions obtained with this doctorate thesis. It discusses the primary outcomes reached throughout the development of this work and offers potential research opportunities about the automation of aIRT inspection that can be explored in future work. Figure 1-1 presents a flowchart that summarizes this thesis's previously described structure, focusing on each paper's role in developing the method proposed in this work.
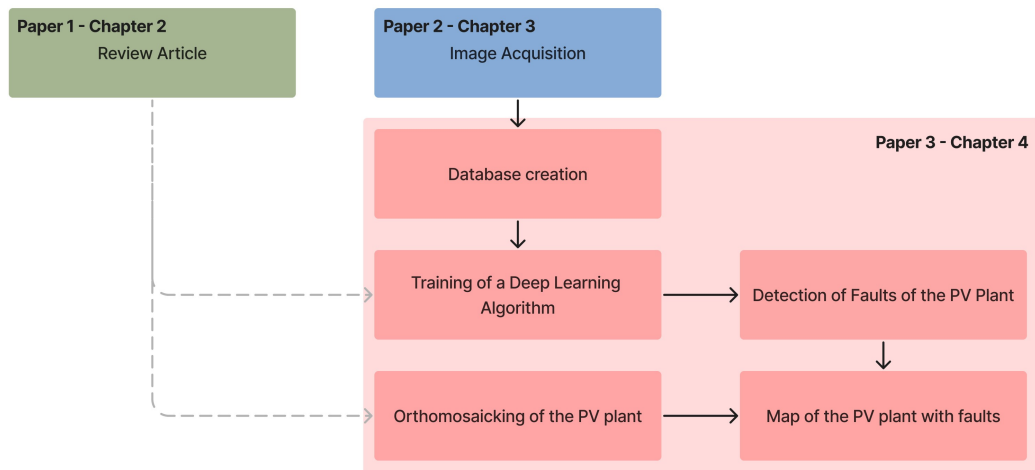
Figure 1-1 – Flowchart of the structure of the thesis.

1.4. CONTRIBUTION AND INNOVATION

Research regarding aIRT in PV power plants has increased in the last few years. Such a trend is directly linked to the expansion of this clean energy source, which is occupying increasingly larger territories. This thesis aims to contribute to developing the inspection technique by improving and automating the processes to increase time and cost-efficiency, specifically in the context of the Brazilian power plants.

The first contribution of this work is a comprehensive examination of the literature for different strategies for automating the inspection framework. It was published as a literature review, which outlines the area´s main developments, as well as its main challenges. This overview of the different algorithms used to automatize the many parts of the inspection process provides a clear understanding of the most common and effective methods to be used and further developed. It also presents research prospects for further scientific progress and can even help the industry understand the gaps and opportunities for investments in the area.

Other contributions of this research are aligned with the importance of gathering aIRT data in power plants in Brazil. This data collection is essential to increase knowledge about the inspection procedures and better understand the main faults found in power plants in the country. These contributions are based on the results of the flight campaign carried out over four PV power plants in northeast Brazil, where

most of the large power plants in the country are installed. The flight campaign was published as a research paper that presented the outcomes of different flight strategies and equipment for the aIRT inspection, providing important conclusions for improving the technique. An unprecedented survey of Brazil's most common faults in power plants was presented, showing significant results for PV plant operators that can better understand Brazil's failure rates and mechanisms and plan repairs and preventive measures. Module manufacturers also can benefit from these results and fabricate more resilient equipment for Brazilian's climate and conditions.

The publication also demonstrated aIRT effectiveness, estimating the power loss of the detected faults and their economic and technical impact. This is a significant contribution not only on the scientific side but also to draw the attention of power plant operators to the importance of regular inspections. It contributes to increasing the adoption of the aIRT technique and the better performance of PV modules. Therefore, it impacts the reliability and safety of this clean energy source, with an expected consequence of higher acceptance and adoption of the technology.

Finally, this research provides an innovative approach that combines DL algorithms with mosaicking techniques to offer a simple and effective way to detect and locate faults in PV plants using aIRT automatically. This method is innovative via the new combination of DL and orthomosaicking techniques and the training of an instance segmentation network. It was described and submitted in a journal paper that evaluates the proposed framework highlighting its main challenges, shortcomings, and workarounds. The study also presents the impact of different flight configurations and datasets on the processing time and results of the proposed workflow. The results were obtained by testing the proposal with test commercial PV plants, evaluating the challenges imposed by real datasets. Therefore, it contributes to scientific and industrial advancement by describing a method that can effectively detect and visually present faults and showing the gaps and advantages of the process for further development.

The work is also innovative because it trains a machine learning (ML) algorithm using data collected in Brazil. This is relevant because Sunbelt countries are subject to specific environmental conditions, such as high irradiances and temperatures, including extreme over-irradiance events (NASCIMENTO *et al.*, 2019) and specific

spectral distribution of irradiance (BRAGA *et al.*, 2019). Also, Brazilian power plants have particular layout conditions that are not widespread in the countries that have previously developed aIRT datasets, namely Europe and Asia. Particularities of Brazilian large-scale PV power plants include the type of soil of the terrain and the low latitudes of most of the power plants and, therefore, the low tilt angles of the solar panels. The application of automation algorithms developed with these datasets in power plants in Brazil is challenging because of the differences in contrast and layout between the data used for training and application, which is called domain shift in the literature. These algorithms are not usually generalized and robust enough to overcome the different faults and layouts that are common in Brazil. Therefore, developing a local framework is extremely valuable and can be further developed with a larger dataset to improve aIRT inspection throughout the country.

2. LITERATURE REVIEW ON AUTOMATIC INSPECTIONS USING AIRT

This chapter is the transcription of the following paper:

Automatic Inspection of Photovoltaic Power Plants Using Aerial Infrared Thermography: A Review

Authored by: Aline Kirsten Vidal de Oliveira, Mohammadreza Aghaei and Ricardo Rüther.

Abstract

In recent years, aerial infrared thermography (aIRT), as a cost-efficient inspection method, has been demonstrated to be a reliable technique for failure detection in photovoltaic (PV) systems. This method aims to quickly perform a comprehensive monitoring of PV power plants, from the commissioning phase through its entire operational lifetime. This paper provides a review of reported methods in the literature for automating different tasks of the aIRT framework for PV system inspection. The related studies were reviewed for digital image processing (DIP), classification and deep learning techniques. Most of these studies were focused on autonomous fault detection and classification of PV plants using visual, IRT and aIRT images with accuracies up to 90%. On the other hand, only a few studies explored the automation of other parts of the procedure of aIRT, such as the optimal path planning, the orthomosaicking of the acquired images and the detection of soiling over the modules. Algorithms for the detection and segmentation of PV modules achieved a maximum F1 score (harmonic mean of precision and recall) of 98.4%. The accuracy, robustness and generalization of the developed algorithms are still the main issues of these studies, especially when dealing with more classes of faults and the inspection of large-scale PV plants. Therefore, the autonomous procedure and classification task must still be explored to enhance the performance and applicability of the aIRT method.

2.1. INTRODUCTION

As the world experiences a continuously growing share of photovoltaics (PVs) in the energy mix, increasing the performance and reliability of PV installations is of utmost importance. In this context, infrared thermography (IRT) has become a well-established and competitive fault detection method for the condition monitoring and maintenance of PV systems (TSANAKAS *et al.*, 2016). It provides reliability and accuracy in the detection of typical PV module faults such as bypassed or disconnected substrings, microcracks, soldering problems, shunted cells and disconnected modules. Another feature of this technique is the possible large-scale applicability, through the combination of IRT cameras with an unmanned aerial vehicle (UAV), configured for aerial infrared thermography (aIRT) (BUERHOP, CI *et al.*, 2012; TSANAKAS *et al.*, 2016).

The first description of the potential of using aIRT in the literature was given in 2012 by Denio (2012). This was followed by the publication of the results of an experimental setup that inspected 60 different PV plants of up to 1 MWp, based on a remote-controlled drone (BUERHOP, Claudia *et al.*, 2012). Since then, several publications have demonstrated the technique's capability to detect failures in photovoltaic systems quickly and efficiently from the commissioning phase of the power plant through its expected 25 years of operation (BUERHOP-LUTZ *et al.*, 2016; CIOACA *et al.*, 2015; Overview on Photovoltaic Inspections Procedure by means of Unmanned Aerial VehiclesNICCOLAI *et al.*, 2019; OLIVEIRA *et al.*, 2020; ULRIKE JAHN *et al.*, 2018).

To further improve the time and cost efficiency of the method, the automation of the entire procedure of the aIRT technique has been assessed in recent years by several research groups worldwide. However, this is a complex task, since it includes not only the automation of the inspection itself (flight path planning and autonomous flight), but also the analysis of a large amount of data for the detection of PV modules, detection of faults, classification and localization of these faults in the field. A significant amount of progress has been made recently in this area, using either simple digital image processing (DIP) techniques or more complex algorithms such as deep learning (DL).

This paper aims at reviewing the reported studies in the literature on the automation of the inspection procedure of PV plants using aIRT.

2.2. METHOD OF REVIEW

The literature search for conference and journal papers was carried out in the scientific databases IEEE Xplore and ScienceDirect, and on the web scientific indexing services Web of Science and Google Scholar. The keywords used included PV systems, inspections and thermography synonyms. Keywords related to aerial and UAVs were not included to not limit results and exclude the automatic assessment of ground-based thermographic images, besides reducing false positives related to the development of UAVs powered by PV modules. The string used for the search was "(photovoltaic OR PV OR (PV AND modules)) AND (faults OR detection OR classification) AND (automatic OR (artificial AND intelligence) OR processing) AND (thermography OR thermal OR infrared)" and initially returned 183 papers. The papers were filtered to fit the theme and classified according to application and automation algorithm. Papers that focused on the automatic assessment of visual images were not excluded since, normally, aIRT-aimed UAVs also have a visual camera coupled to them, which is also used in the inspection to better classify faults.

The list of papers was expanded using references of the original papers and the references already known by the authors. When overlapping work was found in multiple publications (e.g., preprint in a conference and full paper in a journal), only the publication deemed most important was included.
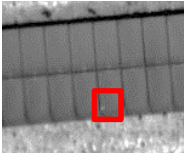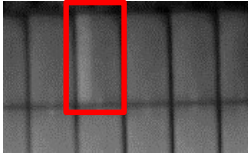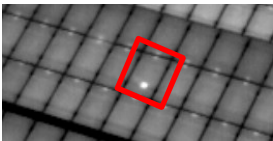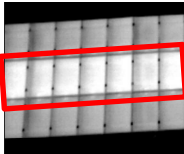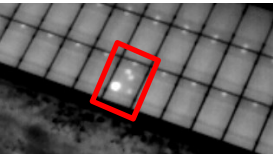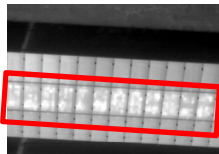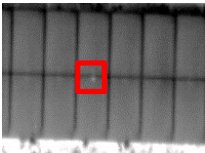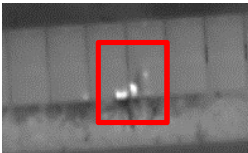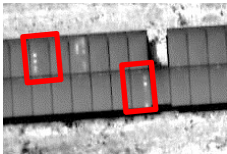
2.3. INFRARED THERMOGRAPHY (IRT)

Infrared thermography (IRT) is a technique that assesses the radiation emitted by the surface of any body in the infrared wavelength spectrum between 1.4 and 15 µm. IRT cameras used in PV inspections normally have the capability of measuring wavelengths in the mid-infrared wavelength range of 7–14 µm. This is a good compromise between costs and product availability, according to measuring conditions in the field (TSANAKAS *et al.*, 2013).

In a PV plant, PV modules that are close to each other receive almost the same amount of irradiance. Some 20% of this irradiance will be converted to electricity; however, most of the photons which are not converted into electricity will produce heat in the cell. This will increase the temperature of these damaged cells and modules, and the faults will appear in the acquired IRT images as temperature differences (KUMAR *et al.*, 2020), like a "temperature signature".

IRT has been shown to be a reliable and non-destructive tool for detection of different types of faults in PV cells, modules and strings, as they have an effect on the PV module thermal behavior. Table 2-1 presents some thermal signatures which have been identified and classified in previous studies (BUERHOP, CI *et al.*, 2012; KÖNTGES *et al.*, 2014) and are standardized according to the international standard IEC TS 62446-3 Edition 1.0 2017-06 (INTERNATIONAL ELECTROTECHNICAL COMMISSION (IEC), 2017).

Table 2-1 - Examples of IRT images of typical faults in PV systems.

IRT image	Description	IRT image	Description
	Suspicious conductor strip (INTERNATIONAL ELECTROTECHNICAL COMMISSION (IEC), 2017; VATH, 2016)		Disconnected substring (INTERNATIONAL ELECTROTECHNICAL COMMISSION (IEC), 2017; WEINREICH *et al.*, 2011)
	Overheated cell (VATH, 2016)		Disconnected string (INTERNATIONAL ELECTROTECHNICAL COMMISSION (IEC), 2017)
	Module with broken front glass (INTERNATIONAL ELECTROTECHNICAL COMMISSION (IEC), 2017)		String in short circuit (patchwork) (INTERNATIONAL ELECTROTECHNICAL COMMISSION (IEC), 2017; VATH, 2016)
	Heated module junction box (INTERNATIONAL ELECTROTECHNICAL COMMISSION (IEC), 2017; WEINREICH et al., 2011; VATH, 2016))		Partly shaded cells (not a defect) (INTERNATIONAL ELECTROTECHNICAL COMMISSION (IEC), 2017; VATH, 2016)
	Substring in short circuit (INTERNATIONAL ELECTROTECHNICAL COMMISSION (IEC), 2017; WEINREICH *et al.*, 2011)		

2.4. UNMANNED AERIAL VEHICLES (UAVS)

Unmanned aerial vehicles (UAVs) are aircrafts that are capable of remote or autonomous operation. They were initially developed for military applications, but due to recent developments, they are now available for civil activities and commonly used in applications such as rescuing and disaster relief, energy power line monitoring and environmental and forest control (AGHAEI *et al.*, 2015). UAVs are becoming more popular especially in the energy and agriculture sectors, due to their fast large-area coverage, precise imagery, high flexibility, light weight, low cost and ability to operate in hostile environments (GRIMACCIA *et al.*, 2015; TSANAKAS; BOTSARIS, 2012). Several countries have established legal guidelines for the use of UAVs. The rules can include limitations of flight areas, license requirements and insurance (GALLARDO-SAAVEDRA *et al.*, 2018).

UAVs can carry various cameras and sensors to collect data and can be classified by size, range or endurance (AGHAEI *et al.*, 2014). The most appropriate UAV equipment type for thermographic inspections is multicopters, which use rotary blades to generate lift, because of their stability and easy usability. They can be classified by the number of motors (tricopters, quadcopters, hexacopters and octocopters), with quadcopters being the most popular on the market (GALLARDO-SAAVEDRA *et al.*, 2018). They can also be classified by autonomy levels, being manually operated, semi-autonomous (i.e., need of a human operator for mission planning and for taking some of the movement decisions) or fully autonomous (i.e., all decisions for a delegated mission are made by the UAV based on sensor observations) (ELMOKADEM; SAVKIN, 2021).

2.5. AERIAL INFRARED THERMOGRAPHY

In the past, IRT inspections of PV systems were performed on the ground or on lifting platforms with handheld IRT cameras. This procedure cannot provide fast and accurate coverage of the power plant and is dependent on human labor and competence, besides being very time-consuming and labor-intensive. As a result, the inspection accuracy is susceptible to human error. A possible solution to the problem

is to combine the IRT sensor with aerial technologies such as UAVs. This procedure is known as aIRT and increases the cost effectiveness of IRT inspection, allowing the technique to be employed for large-scale PV plants or roof-mounted PV systems with limited access (AGHAEI, 2016; AGHAEI *et al.*, 2019; BIZZARRI *et al.*, 2019; CIOACA *et al.*, 2015).

This method has shown its potential in recent years, but its use can still be expanded to increase and simplify routine inspections of PV power plants and revolutionize the future of PV plant monitoring procedures (AGHAEI *et al.*, 2015). For this method to achieve its full potential, however, it should be combined with automation algorithms and technologies, such as automated route planning and defect identification.

Aerial IRT uses visual and IRT cameras that are mounted on the UAV. The equipment provides real-time and precise imagery, allowing a time-efficient inspection. The procedure can detect faults of different types, such as cell cracks, corrosion spots, broken cells, hot spots, snail trails, discoloration, soiling, disconnected modules or strings and potential-induced degradation (PID) (QUATER *et al.*, 2014; TSANAKAS; BOTSARIS, 2012). According to the inspection goal and the PV plant layout, aIRT can be performed from different altitudes and directions to identify specific defects or faults, also depending on the time available for the inspection (LEVA *et al.*, 2015).

The aIRT process is carried out in three stages: acquisition of imagery, assessment of data and remediation actions. For the acquisition step, the UAV must fly a designated route acquiring successive photos or videos over the site to build an imagery database covering all modules in the system. As the equipment has a limited battery capacity, each flight has a duration of around 20 min (OLIVEIRA *et al.*, 2020)

During the flight, the weather conditions, wind speed and sunlight reflection must be monitored, as they can affect the measurements and consequently the quality of the aIRT images. Additionally, the velocity of the UAV and the orientation and angle of the IRT sensor must be controlled to avoid self-shading, blurred images and other reflections. aIRT should be performed on cloudless, sunny and clear days, with minimum irradiance of 600 W/m^2 on the plane of the PV array under inspection. The flight path and velocity should be planned beforehand in order to optimize the coverage

and to avoid any drift during the flight (AGHAEI *et al.*, 2017; LEVA *et al.*, 2015; QUATER *et al.*, 2014; VERGURA, 2021).

The acquired data are then analyzed, and an action report is produced. With a detailed site mapping, it is possible to obtain an accurate location of the system faults, and the remediation can be planned based on full knowledge of the site state. The report is passed to the stakeholders for remediation actions such as assessment of connections or replacement of modules or fuses.

2.6. AERIAL INSPECTION ALGORITHMS

2.6.1. Digital Image Processing

The field of digital image processing (DIP) has been an object of increasing interest because it allows many applications such as: remote sensing, component defect detection, biomedical engineering, geoprocessing, metallography and industrial automation applications. DIP aims to transform and analyze images by extracting relevant information, highlighting and identifying patterns and objects (GONZALEZ; WOODS, 2002; PLATINI REGES *et al.*, 2015).

A digital image consists of a set of a finite number of elements (i.e., pixel), each one with a specific location and intensity. DIP techniques apply several operations to these pixels to transform the images, allowing the automatic interpretation of them by systems or machines. These operations include image rotation, thresholding, binary image analysis, brightness and contrast adjustment, filtering, resizing and interpolation (AGHAEI *et al.*, 2017; GONZALEZ; WOODS, 2002).

The methods of DIP are normally simple but can often solve problems in a more time- and computing-efficient way than DL techniques. Pixel thresholding or algorithms such as the scale-invariant feature transform (SIFT) are normally very general, do not require a large dataset to be trained and can be replicated in other images. DIP can even be combined with DL to take the best from both methods to automate image processing and recognition (O'MAHONY *et al.*, 2020; OLIVEIRA, A. K. V. *et al.*, 2019).

2.6.2. Deep Learning (DL)

Artificial neural networks (ANNs) are the most popular technique in machine learning (ML) and were first developed based on the structure and operation of the human brain. They are commonly used because they can deal with highly nonlinear systems and allow constant updates in the model (MAYO; LEUNG, 2018). They are composed of a set of simple, connected processors called neurons that produce a sequence of activation calculations. The fundamental property of an ANN is its ability to learn from the environment (read a set of examples), through an iterative process of adjustments applied to synaptic weights and bias levels. Learning a task consists in finding weights that make the ANN exhibit a desired output when processing an input. Depending on the problem and how the neurons are connected, this process may require chains of consecutive computational stages, where each one modifies the aggregate activation of the network. DL is about accurately assigning credit across many of these stages, using convolutional neural networks (CNNs) (JUNIOR, 2011; SCHMIDHUBER, 2014).

CNNs were inspired by the human visual system's structure and are the state-of-the-art method for image classification (KAMILARIS; PRENAFETA-BOLDÚ, 2018; MALOF *et al.*, 2016; MEHTA *et al.*, 2017; VOULODIMOS *et al.*, 2018). They are easy to train if there is a substantial number of labeled images that represent distinct categories.

They are layered sequences, and each has a specific function in the propagation of the input signal. There are three main types of neural layers: (i) convolutional layers, (ii) pooling layers and (iii) fully connected layers. Figure 2-1 illustrates the CNN architecture and its three main layers for a task of object detection in an image:

- Convolutional layers: responsible for extracting attributes from the input volumes.
- Pooling layers: responsible for reducing the spatial dimensions of the input volume after the convolutional layers, reducing the computational work of the network.

- Fully connected layers: perform the final classification of the images, in the same way as a conventional neural network.

In the end, the CNN output is the probability that the input image belongs to one of the classes for which the network was trained (CARNEIRO; SILVA, 2017).
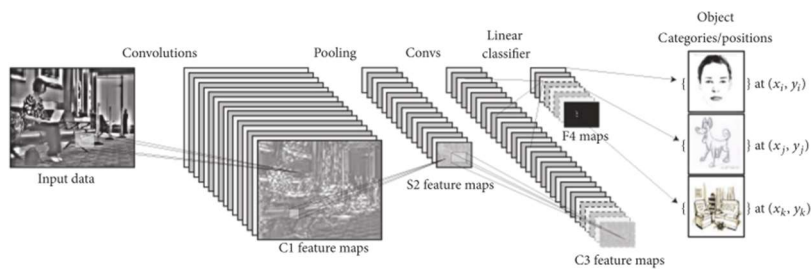
Figure 2-1-Example architecture of a CNN for an object detection task
(VOULODIMOS *et al.*, 2018).

2.6.3. Other Machine Learning Techniques

Other ML techniques are also used in the automation of aIRT inspection, especially for classification in combination with other techniques. Among them, support vector machines (SVMs) are supervised ML algorithms that are usually used for classification and regression analysis of data, as they are based on a decision function that divides the classes by decision planes. SVMs work relatively well when there is a clear separation between classes, and they are more effective in high-dimensional spaces (KARIMI *et al.*, 2018; SERFA JUAN; KIM, 2020).

Another commonly used classifier is the random forest (RF), which is an algorithm that builds several decision trees on multiple random portions of the data for training. In these trees, different binary classifications concatenated in a tree structure are performed, for different input features, and a combination of the nodes is used to calculate the result. The most common result among the trees is "elected" as the output of the classifier (DA COSTA *et al.*, 2019; HANAFY *et al.*, 2019).

On the other hand, k-nearest neighbors (KNN) is a classification supervised algorithm that does not require training, as the samples are classified by a metric of distance, where the k-nearest points to the test sample are defined as a class (HANAFY *et al.*, 2019).

For clustering, the most popular method is k-means clustering, which is an unsupervised ML algorithm. This method consists of dividing data in k clusters that will be grouped by the mean distance between points (ET-TALEBY *et al.*, 2020; WAQAR AKRAM *et al.*, 2019).

2.6.4. Algorithm Evaluation Metrics

Performance indices quantify the capacity of an algorithm to identify the events of interest. The accuracy (Ac) of an algorithm is the percentage of correct predictions over the test dataset. The precision index (Pr) provides the proportion of all segments that were identified in one class that in fact belong to this class (results of true positives over all the positives). The recall (Re) measures how well the algorithm can identify each class among the dataset (results of true positives over all images in a dataset that were originally labeled as positives). The F1 score is calculated by the harmonic mean of Pr and Re. A good algorithm should have all of these metrics close to 100% for all the classes (ZECH; RANALLI, 2020).

Other less common metrics are also used in the papers covered by this work. The Matthews correlation coefficient (MCC) is a coefficient related to accuracy, which does not penalize classes of different sizes (DOTENCO *et al.*, 2016). The Dice coefficient and the Jaccard index are often used for evaluating segmentation tasks. The first represents the overlapping between the predicted result with the ground truth, and the second measures the similarity of the predicted result to the ground truth (MEHTA *et al.*, 2017; ZHANG *et al.*, 2019). The Jaccard index is also known as Intersection over Union (IOU). The area under the receiver operating characteristic (AUROC) is an index obtained by integrating the curve of the true positives of a task over the false positives at various decision thresholds (Anomaly Detection in IR Images of PV Modules using Supervised Contrastive LearningBOMMES *et al.*, 2021).

In this paper, when available, the preferred metrics are F1 score and precision indices, in order to provide a comparison between different works, whenever possible.

2.7. APPLICATIONS OF AUTOMATIZATION ALGORITHMS

2.7.1. Automatic Path Planning

In an automatic aIRT mission, the UAV flies over a set of waypoints that cover all modules of the PV plant. Therefore, an optimized path-planning algorithm aiming at an optimal path for time and battery efficiency is essential (SIZKOUHI *et al.*, 2022). Figure 2-2 depicts the coverage area by a UAV based on the field of view (FoV) and resolution of the camera on board as well as the essential parameters used for path planning (SIZKOUHI *et al.*, 2022).

Available market software packages already provide an automatic flight based on a so-called "lawn mower" flight pattern. However, they do not always provide the most efficient flight and do not guarantee a centralized view to the PV arrays, especially in power plants installed over complex topography.

Studies aiming at optimizing path planning include different approaches to the problem. In the study developed by Salahat et al. (2019), the traveling salesman shortest path algorithm was used to generate a path that includes a randomly selected set of modules that represent the entire PV plant, allowing an optimization of the battery use. Ding et al. (2020) based their method on density clustering, Boustrophedon path planning and Bezier Curves. Luo et al. (2017) also based their algorithm for path planning optimization on Bezier curves in a joint approach with particle swarm optimization (PSO), taking into consideration the flight attitude, gimbal limitation and path length.

Image stitching and DIP techniques were used by Henry et al. (2020) to find contours of the power plant and generate a "lawn mower" path over it. A similar approach, using DL, was adopted by Moradi Sizkouhi et al. (2019; 2022), which is also complemented with a dynamic path planning, that deviates the previous flight plan to take closer photos when faults are detected. Pérez-González et al. (2021) also used DL to detect the area of the PV plant and then used different algorithms to determine the best flight path, wherein exact cellular decomposition boustrophedon and grid-based wavefront coverage algorithms produced the best results.

Other real-time algorithms have been proposed that calculate the optimized path of the UAV during the flight. In Roggi et al. (2020), the UAV corrected the pre-planned "lawn mower" path according to the images that it acquired and the image processing techniques that are applied. A vision-based flight control was also proposed by Xi et al. (2018), which performs a real-time direction and velocity correction.
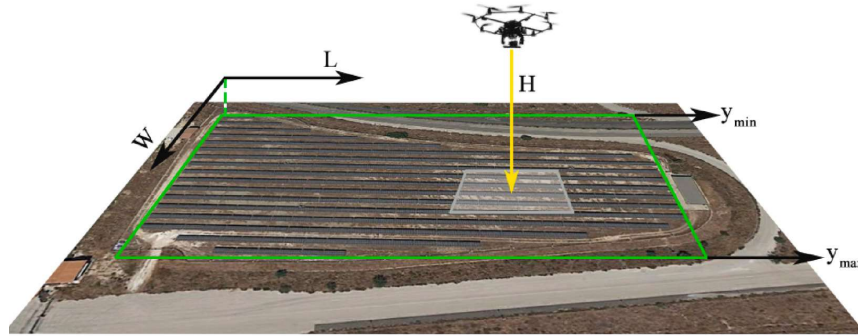
Figure 2-2 - Path planning procedure of a PV power plant (SIZKOUHI *et al.*, 2022).

2.7.2. Detection of PV Systems

Although not always related to aerial inspections, the detection of PV systems in aerial imagery (UAV or satellite imagery) has been proposed by many authors and even used for path planning before the aIRT flight (MORADI SIZKOUHI *et al.*, 2019; PÉREZ-GONZÁLEZ *et al.*, 2021). Table 2-2 presents a summary of methods used in the literature for detecting PV systems in aerial imagery. The table presents the best metrics obtained in each study, the type of image data used as input and the type of detection output obtained with each method. The detection output was classified into three categories:

a) Boxes: the output is given by the coordinates of a box or polygon placed around the PV system;

b) Mask: the output is a binary image where the pixels corresponding to the segment of the PV system are represented by the value 1 and the rest of the image is represented by 0;

c) Binary: for each image, the presence or absence of a PV system is the result of the algorithm (1 or 0).

Figure 2-3 shows two examples of two types of detections, by the coordinates of boxes around the detected PV panels (left) and masks of the segment of the PV

system (right). Besides developing an algorithm for the detection of PV arrays, Wu et al. (2017), also matched them to their string identifiers.

Table 2-2 - Summary of methods for detecting PV systems using aerial imagery.

(Ref)	Algorithm	Best results	Output Type	Images
(MALOF *et al.*, 2016)	RF and DL	Pr: 90%	Mask	Aerial imagery
(ZHANG, D. *et al.*, 2017)	Adaptive clustering method based on k-means	Loss rate is lower than 5%	Mask	Aerial imagery
(SHEN *et al.*, 2017)	GLCM algorithm	Pr: 93.16% F1: 77.8%	Mask	aIRT
(WU *et al.*, 2017)	Feature description vector according to PV modules' different colors	-	Boxes	UAV
(WANG *et al.*, 2018)	DIP and k-means classifier	Pr>99%	Boxes	Aerial imagery
(CAMILO *et al.*, 2018)	DL (Segnet)	Pr: 90%	Mask	Aerial imagery
(GIRARD; TARABALKA, 2018)	DL (PolyCNN)	IoU: 79.5%	Mask	Google earth
(GOLOVKO *et al.*, 2019)	DL (Faster-RCNN, based on the classifier ResNet-50)	Pr: 92.9%	Boxes	Google earth
(ZHANG *et al.*, 2019)	DL (Res-UNet)	Ac: 97.11%	Mask	System IRT images
(SIZKOUHI *et al.*, 2020)	DL (Mark-RCNN and VGG16)	Ac: 96.99%	Mask	UAV
(ZECH; RANALLI, 2020)	DL(U-net)	F1: 82%	Mask	Google earth
(MORAGUEZ *et al.*, 2020)	DL	F1: 92.2%	Binary	Satellite imagery
(MAYER *et al.*, 2020)	DL	Pr: 92.66% Re: 97.43%	Mask	Google earth
(RICO ESPINOSA *et al.*, 2020)	DL (CNN for semantic segmentation)	Average error of 5.75%	Mask	UAV
(LI, Q. *et al.*, 2020)	K-means, SVM and CNN	MCC: 0.17	Mask	Identify solar in rooftops
(HUERTA HERRAIZ *et al.*, 2020)	DIP (edge detection) and DL (RCNN)	Pr: 92.25%	Mask	Panels in aIRT images
(COSTA *et al.*, 2021)	DL algorithms	F1: 95.38%	Mask	Aerial imagery
(WANG, Q. *et al.*, 2021)	DIP (Transform Invariant Low-rank Textures (TILT) algorithm for orthographic view and Otsu's method for segmentation)	-	Mask	Panels in aIRT images
(SOUFFER *et al.*, 2021)	Unsupervised Segmentation Parameters Optimization (USPO) and RF classifier	F1: 98.7%	Mask	UAV
(PÉREZ-GONZÁLEZ *et al.*, 2021)	DL server	-	Mask	UAV
(SIZKOUHI *et al.*, 2022)	Mask-RCNN structure	Ac: 96.99%	Mask	UAV
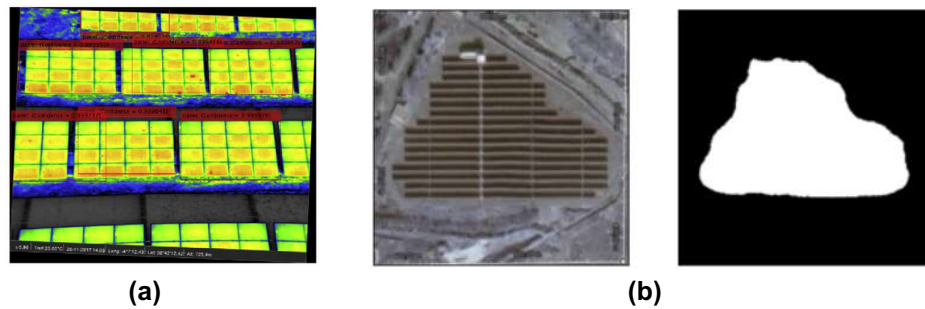
Figure 2-3 - Examples of detection types for the detection of PV systems using aerial imagery: (**a**) boxes (HUERTA HERRAIZ *et al.*, 2020); (**b**) mask (PÉREZ-GONZÁLEZ *et al.*, 2021).

2.7.3. Detection of PV Modules

The detection of the area of the modules is an important step in the image processing task, which is required for both detecting modules with defects and locating them in the power plant.

The first attempts to automatize the segmentation of the PV modules in IRT images appear to have been made in 2015, with images obtained with a moving cart, using simple DIP methods (GAO *et al.*, 2015). Other attempts were described in Menéndez et al. (2018), Montanez et al. (2020), and Wu et al. (2018). Uma et al. (2019) did the same using a k-means clustering algorithm. In 2021, Xie et al. (2021) used a Segnet, a CNN used for segmentation.

For aerial images, Tribak and Zaz (Remote solar panels identification based on patterns localization2018), Salamanca et al. (2017) and Perez et al. (2019) published results on detecting PV modules in aerial visual images, and many studies used different techniques to detect and segment PV module boundaries in aIRT data. Table 2-3 shows the studies related to DIP and DL algorithms. In this case, the detection result of the algorithm can be given by a box or polygon around the PV module, a mask of the segment of the module or lines that mark the borders of the modules in a PV panel.

The best metric among the studies was obtained with a combination of many algorithms (DIP, SVM and DL) (DÍAZ *et al.*, 2020). On the other hand, the worst metrics were obtained with simple DIP filters (ALFARO-MEJÍA *et al.*, 2020).

It is important to note that not all studies are comparable, because not all have presented metrics for their performance, and they have different dataset sizes, which

make the comparison difficult. The studies described by Carletti et al. (2020) and Bommes et al. (Computer vision tool for detection, mapping, and fault classification of photovoltaics modules in aerial IR videos2021), besides detecting the PV module, also developed ways to track the modules in subsequent frames of a video. A tracking system was also developed by Xie et al. (Abnormal target tracking and localization algorithm for UAV PV inspection scenarios2020) using a AlexNet CNN.

Table 2-3 - Summary of methods for detecting PV modules in aIRT using DIP and DL algorithms.

(Ref)	Algorithm	Best results	Output type
(DOTENCO et al., 2016)	DIP (Normalization and Thresholding)	F1: 92.76%	Boxes
(ARENELLA et al., 2017)	DIP (Edge extraction by Hough transform)	-	Boxes
(KIM et al., 2017)	DIP (Thresholding)	Pr: 96.9%	Mask
(LÓPEZ-FERNÁNDEZ et al., 2017)	RANSAC (Random Sample Consensus) algorithm	-	Boxes
(MUHAMMAD et al., 2017)	DIP (not detailed)	Pr: 82%	Boxes
(PV plant digital mapping for modules' defects detection by unmanned aerial vehiclesGRIMACCIA et al., 2017)	DIP (Thresholding in HSV color space)	-	Mask
(ADDABBO et al., 2018)	DIP (Template matching algorithm)	F1: 83.0%	Boxes
(CARLETTI et al., 2020)	DIP (Canny Edge and morphological filters)	F1: 87%	Boxes
(ALFARO-MEJÍA et al., 2020)	DIP (ACM LS and filtering by area, Hough Transform)	Re: 70%	Boxes
(JEONG et al., 2020)	DIP (Thresholding in HSV color space and MSER algorithm)	Ac: 98%	Boxes
(GRECO et al., 2020)	DL (YOLOv3)	F1: 95%	Boxes
(DÍAZ et al., 2020)	DIP + Support Vector Machine (SVM) and DL (Mask RCNN)	F1: 98.9%	Boxes
(NIE et al., 2020)	DIP (Hough line detection, Sobel operator)	-	Lines
(Photovoltaic panel anomaly detection system based on Unmanned Aerial Vehicle platformXIE et al., 2020)	DIP (Sobel and canny operator, HoughPLine,)	Pr: 90.91%	Lines
(WANG, N. et al., 2021)	DIP (LSD algorithm and k-means clustering)	Pr: 77.3% F1: 86.3%	Mask
(FERNÁNDEZ et al., 2020)	DIP (k-means clustering and thresholding)	Ac: 98.46%	Mask
(Computer vision tool for detection, mapping, and fault classification of photovoltaics	DL (Mask RCNN)	Pr: 90.01% F1: 90.51%	Mask

modules in aerial IR videosBOMMES *et al.,* 2021)			
(ZEFRI *et al.,* 2022)	DIP (Geometry coercion, clustering and angularity-based segment filtering)	-	Mask

2.7.4. Orthomosaicking

The localization of faults within a power plant is a challenging issue that can be addressed by creating an orthomosaic of the PV power plant (OLIVEIRA *et al.,* 2021). Image mosaicking, also known as image stitching, is a computational technique that detects overlapping key points in spatially subsequent photos and uses them to create a so-called panorama picture (PV plant digital mapping for modules' defects detection by unmanned aerial vehiclesGRIMACCIA *et al.,* 2017).

To improve the sight perspective and enable an expanded view of the localization of faults in both visual and thermal images of PV power plants, some researchers used commercially available software packages to create orthomaps with aerial imagery. Lee and Park (2019) and Zefri et al. (Thermal Infrared and Visual Inspection of Photovoltaic Installations by UAV Photogrammetry—Application Case: Morocco2018) used the software Pix4D capture to process thermal and visual images and create orthographic images with temperature information. Oliveira et al. (2021) compared the use of two software (DroneDeploy and ContextCapture) to create an orthomosaic of a 1 MW PV power plant. Higuchi and Babasaki (2018) used the software OpenDroneMap to generate the orthographic image of a 2 MW PV power plant.

Grimaccia et al. (PV plant digital mapping for modules' defects detection by unmanned aerial vehicles2017), Aghaei et al. (2017) and Ismail et al. (2020) have proposed methods for the orthomosaicking of visual images of PV power plants using DIP techniques. Tsanakas et al. (2017) used the method of aerial triangulation, and Lafkih and Zaz (2017) and Zefri (2021, 2022) used the SIFT technique to perform the task. To optimize the mosaicking of visual PV images, Qi et al. (2020) used a Faster RCNN to detect key points in aerial sequence images in the world coordinate system, so it avoids redundant information generated by traditional methods. López-Fernández et al. (2017) developed a tool that creates a 5D point cloud of the power plant, where

each coordinate point has a temperature and an intensity value associated with it. After segmenting the modules in a dataset, Costa et al. (2021) used a sliding window algorithm with over-lapping pixels, combining frames side by side to reconstruct orthomosaics of power plants.

2.7.5. Soiling

A common cause of hot spots in PV power plants is soiling and shadow over the modules, which hinders the evaluation of results since they are not considered real defects of the PV modules (OLIVEIRA *et al.*, 2020). Cipriani et al. (2020) approached this issue by using a CNN to differentiate hot spots caused by faults from soiling, obtaining an accuracy of up to 98%.

Another solution to the problem is the analysis of the visual images that are normally taken together with the IRT images in the UAV, which enables the operator to discard hot spots caused by soiling. Automation of the task of detecting soiling in individual modules was proposed by Yang et al. (2020), Pivem et al. (2019) and Qasem et al. (2016) using DIP techniques. Similar techniques were employed by Wen et al. (2021), and by Karaköse and Firildak (2015) to detect shadows over PV systems. Hanafy et al. (2019) compared different ML algorithms (KNN, NN, RF and SVM) to classify modules in different categories of cleanliness and obtained an accuracy of over 90% using an SVM algorithm. Mehta et al. (2017) proposed a method that uses a weakly supervised CNN-based classification network to predict power loss, detect soiling and categorize it given a PV module image. This method obtained an accuracy of about 87% on a test dataset of about 50 images.

2.7.6. Detection and Classification of Faults

The manual assessment of aIRT imagery is a time- and computing-consuming task; therefore, its automation is the most explored part of the aIRT framework in the literature. This detection can either be processed on board, during the UAV flight, as shown in the example in Figure 2-4, or in a computer software, after the acquisition of images has been carried out by the UAV (Figure 2-5). Both Figure 2-4 and Figure 2-5

show the procedure of the inspections for the two different approaches, including all tasks being automatized in each case.

In 2002, Pilla et al. (2002) used the Sobel and canny edge operators to detect cracks in IRT PV cell images. In 2003, Wang et al. (2003) used thresholding and a fuzzy classifier to detect faults in IRT images. After that, in 2011, Vergura and Falcone (2011) used DIP techniques to analyze IRT images for faults. Since then, many other studies have used mostly DIP techniques to segment faults in IRT images. Table 2-4 presents a summary of the main algorithms for the detection and classification of faults in IRT images. In this case, the results can be in the form of a segmentation of the faults (mask), the detection of modules with faults and the classification of these faults in categories. Some methods presented high metrics when used in association with a classification algorithm, such as an SVM (NATARAJAN *et al.*, 2020). Many papers do not present a metric for the performance evaluation of the algorithms proposed, especially for the case of fault segmentation (masks). It is important to note that a comparison between metrics is not always possible, because the dataset size and number of classes differ among studies.
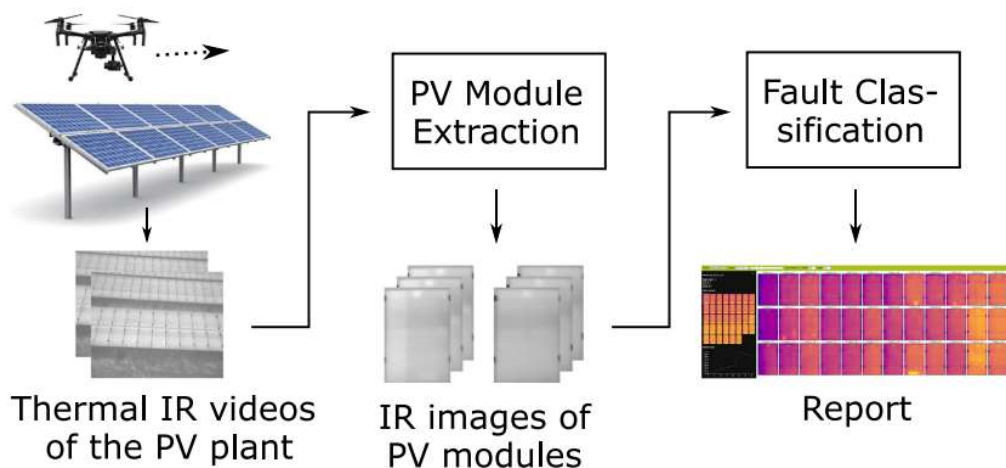
Figure 2-4 - Overview of a tool for semi-automatic inspection of large-scale PV plants using IRT videos acquired by a UAV (Computer vision tool for detection, mapping, and fault classification of photovoltaics modules in aerial IR videosBOMMES *et al.*, 2021).
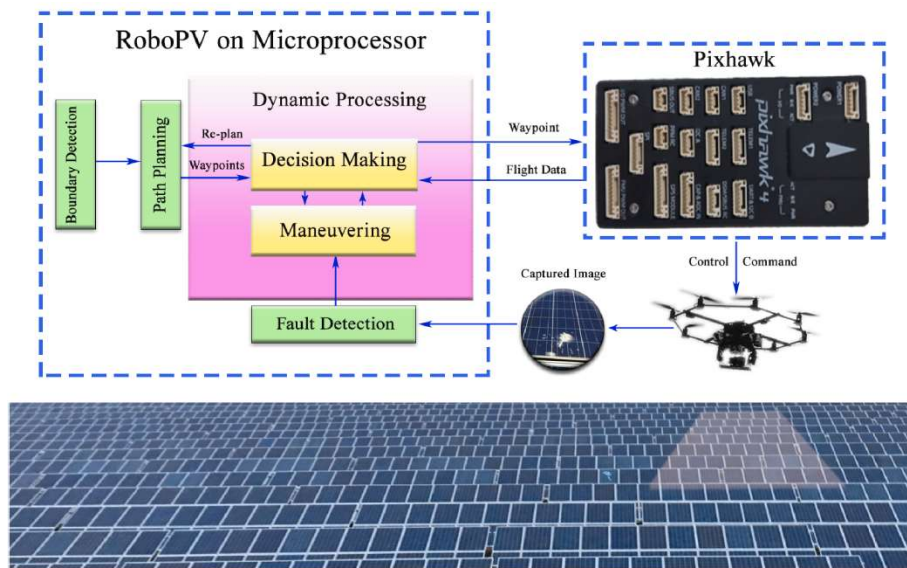
Figure 2-5 - Overview of the on-board software package RoboPV, developed to perform the autonomous aerial monitoring of large-scale PV plants using UAVs (SIZKOUHI *et al.*, 2022).

Table 2-4 - Summary of methods for detecting and classifying faults in IRT images of PV modules.

(Ref)	Algorithm	Best results	Output type
(GAO *et al.*, 2015)	DIP filters	Pr: 97.40%	Detection of modules with faults
(TSANAKAS *et al.*, 2015)	Histogram analysis, Thresholding and Canny edge	-	Faults mask
(J. VANEK *et al.*, 2016)	DIP and ANN	Ac: 80%	Faults mask
(GUERRIERO *et al.*, 2016)	Filter by temperature values	-	Detection of hot spot, cracks and soldering issue
(NGO; MACABEBE, 2016)	K-Means color quantization and Density-Based Spatial Clustering of Application with Noise (DBSCAN)	-	Faults mask
(VERGURA; MARINO, 2017)	DIP (thresholding and clustering)	-	Detection of modules with faults
(JAFFERY *et al.*, 2017)	DIP and Fuzzy Rule on temperature data	-	Classification in 6 anomaly types
(MENÉNDEZ *et al.*, 2018)	Filtering by temperature values	Pr: 96.52%	Detection of modules with hot spots
(ALAJMI *et al.*, 2019)	Thresholding in HSV color space	Ac: 100% (only 3 images)	Detection of modules with faults
(NIAZI *et al.*, 2018, 2019)	nBayes classifier	Ac: 94.1%	Classification in healthy, shaded, and defective modules
(UMA *et al.*, 2019)	DIP filters	-	Detection of delamination, snail trails and bubbled faults
(HAQUE *et al.*, 2019)	ANN and Discrete wavelet transform	Ac: 100%	Combination of IRT with electrical data - Classification in 5 anomaly types

(DHIMISH; BADRAN, 2019)	Fuzzy inference system (FIS) using Mamdani-type fuzzy controller	Ac: 96.7%	Combination of IRT with electrical data – detection and classification of hot spots
(DU *et al.*, 2020)	GoogleNet VS LeNet-5 and VGG-16	Ac: 97.9%	Classification in 6 cell anomaly types
(AKRAM *et al.*, 2020)	DL and Transfer Learning	Ac: 99.23%	Detection of modules with faults
(NATARAJAN *et al.*, 2020)	DIP and SVM	Ac: 97%	Detection of modules with faults
(MONTANEZ *et al.*, 2020)	Histogram analysis of segmented module	-	Detection of modules with faults
(BALASUBRAMANI *et al.*, 2020)	Fuzzy classifier based on temperatures of the module	Ac: 94%	Detection of EVA discoloration and delamination faults
(NAJIAH NURUL AFIFAH *et al.*, 2021)	Multilevel Otsu thresholding	Ac: 91.81%	Faults mask
(LE *et al.*, 2021)	DL and SVM	Ac: 86%	Classification in 12 anomaly types
(KIM *et al.*, 2021)	DIP (adaptative histogram equalization), DL and SVM	Ac: 92.96%	Detection of modules with faults
(KURUKURU *et al.*, 2021)	DIP filters and SVM classifier	Ac: 94.4%	Classification in 10 anomaly types

Table 2-5 shows the summary of studies of the detection and classification of faults in visual images. The faults detected in this case are mostly related to visible problems, such as delamination, burn marks and glass breakages. An important issue that makes the comparison between studies difficult is the difference between the data resolution used as input for each one of them, as images vary from PV cells (BAIG *et al.*, 2018) to aerial images (VENKATESH; SUGUMARAN, 2022).

Table 2-5 - Summary of methods for detecting and classifying faults in visual images of PV modules.

(Ref)	Algorithm	Best results	Detection type
(REGALADO *et al.*, 2014)	Color base segmentation based on k-means clustering	-	Detection of cracks, interconnects problems and discolored areas.
(BAIG *et al.*, 2018)	Luminance filters	-	Cell faults detection
(SHIHAO DING ; QIANG YANG ; XIAOXIA LI ; WENJUN YAN ; WEI RUAN, 2018)	DL	Ac: 98.9625%	Classification in 8 anomaly types of faults in aerial images
(ZYOUT; OATAWNEH, 2020)	Different CNNs	Ac: 93.3%	Detection of faults
(RICO ESPINOSA *et al.*, 2020)	CNN for semantic segmentation	Ac: 75%	Detection of glass breakage, shadows, and dust.
(LI *et al.*, 2019; Edge Computing Enabled Unmanned Module Defect Detection and Diagnosis System	DL and SVM	Ac: 99.8%	Classification in 6 anomaly types of faults.

for Large-scale Photovoltaic PlantsLI, X. *et al.*, 2020; An Unmanned Inspection System for Multiple Defects Detection in Photovoltaic Plants2020)			
(PATEL *et al.*, 2020)	Kirsch edge detection	-	Detection of glass breakage
(REN *et al.*, 2020)	Yolo, MobileNet-SSD network	Pr: 89.2%	Classification in 3 anomaly types of size of hot spot (not made in real PV system)
(SRIDHARAN; SUGUMARAN, 2021)	DL	Ac: 95.07%	Detection of burn marks, delamination, discoloration, glass breakage and snail trail
(LI *et al.*, 2021)	K-means, SVM and CNN	MCC: 1.0	Detection of damaged modules in rooftops
(VENKATESH; SUGUMARAN, 2022)	Naïve Bayes, SVM, k-nearest neighbor, decision tree, RF and pre trained DL models	Ac: 100%	Detection of burn marks, delamination, discoloration, glass breakage and snail trails
(MORADI SIZKOUHI *et al.*, 2021)	DL	Ac: 93%	Masks of bird droppings

Table 2-6 and Table 2-7 present a summary of the methods for detecting and classifying faults in aIRT images of PV systems, using DIP and DL algorithms, respectively. In general, the algorithms with the highest results are the ones dedicated to the detection of faults or the classification of a few types of faults, with the classification of many classes of faults being a much more complex task. It is noticeable that the DIP algorithms have comparable results to DL techniques, even though most of them use smaller datasets, and therefore their generalization capabilities can be jeopardized.

Some of the challenges for the development of a robust automatic classification of faults include the reflections and shadows from surroundings and the lack of a standardized image database (with standard flight directions and weather conditions). When using DL, the computation requirements, the need for a large dataset with annotated data and the processing time must also be overcome.

Table 2-6 - Summary of methods for detecting PV modules in aIRT using DIP and classification algorithms (continues).

(Ref)	Algorithm	Best results	Detection type
(AGHAEI et al., 2015)	Thresholding, temperature filtering	-	Detection of faults
(ARAICA; RUÍZ, 2015)	DIP filters	F1: 99.4%	Detection of faults
(R. RASCH, G. BEHRENS, F.U. HAMELMANN, S. HANTELMANN, R. DREIMANN, 2015)	Canny edge, thresholding		Faults mask
(DOTENCO et al., 2016)	Statistical classification of faults	F1: 93.88%	Classification in 3 classes of faults
(SALAZAR; MACABEBE, 2016)	DIP and k-means clustering	-	Detection of faults
(LIN et al., 2016)	Histogram filtering	-	Detection of hot spots
(ZHANG, P. et al., 2017)	Thresholding module segment	-	Detection of faults
(PV plant digital mapping for modules' defects detection by unmanned aerial vehiclesGRIMACCIA et al., 2017)	Thresholding by module luminance distribution	-	Classification in 3 classes of faults
(KIM et al., 2016, 2017)	Mean and std of luminance of area of module	Ac: 97%	Detection of faults
(ARENELLA et al., 2017)	DIP filters	-	Faults mask
(LÓPEZ-FERNÁNDEZ et al., 2017)	Temperature segmentation	Ac: 100%	Faults mask
(AROSH et al., 2017)	Non-uniform illumination (NUI) boundary detection	-	Hot spots detection and analysis of visual images for soiling or shadowing in laboratory setup
(ALSAFASFEH et al., 2018)	Thresholding, pixel seed and canny edge	-	Faults mask
(ADDABBO et al., 2018)	Normalized Cross Correlation as a similarity measure for template matching	F1: 75%	Detection of faults
(WU et al., 2018)	DIP filters	-	Faults mask

Table 2–6 - Summary of methods for detecting PV modules in aIRT using DIP and classification algorithms (conclusion).

(Ref)	Algorithm	Best results	Detection type
(ERGÜZEN; SAIT, 2019)	Thresholding	-	Faults mask
(SHA et al., 2019)	Gaussian filter, Hough Line	-	Detection of hot spots
(MONTOYA et al., 2019)	Hog Features and Cascade Object Detector	-	Detection of hot spots
(LIAO; LU, 2020)	Thresholding	-	Faults Masks
(Photovoltaic panel anomaly detection system based on Unmanned Aerial Vehicle platformXIE et al., 2020)	Statistics of the luminance	Pr: 92.71%	Classification in 3 classes of faults

(Ref)	Algorithm	Best results	Detection type
(UMAIR *et al.*, 2020)	DIP for feature extraction +different algorithms for classification (SVM, n-Bayes, KNN…)	Ac: 92%	Detection of faults
(ET-TALEBY *et al.*, 2020)	K-means clustering	-	Faults mask
(JEONG *et al.*, 2020)	Temperature based thresholding	Ac: 97%	Detection of faults
(FERNÁNDEZ *et al.*, 2020)	Temperature based thresholding	Pr: 97.6%	Classification of size and severity of faults
(CARLETTI *et al.*, 2020)	Water filling and temporal tracking algorithms	F1: 72%	Detection of hot spots
(SEGOVIA RAMÍREZ *et al.*, 2021)	Statistical analysis of temperature of modules	Ac: 96%	Classification in 6 classes of faults
(WANG, Q. *et al.*, 2021)	Robust PCA decomposition and thresholding	F1: 78.23%	Faults mask
(LIAO; LU, 2021)	Filtering and probability density functions	-	Fault detection using both visual and aIRT images

Table 2-7 - Summary of methods for detecting PV modules in aIRT using DL and classification algorithms (continues).

(Ref)	Algorithm	Best results	Detection type
(PIERDICCA *et al.*, 2018)	U-Net, LinkNet, FPN, Mask RCNN	Dice: 0.841 IOU: 0.741	Faults mask
(WEI *et al.*, 2019)	Hough line transformation and canny operator and Faster-RCNN	F1: 95.15%	Detection of reflections and hot spots
(HIGUCHI; BABASAKI, 2018)	VGG	Pr: 49.11%	Detection of substring, module, and string failures
(OLIVEIRA, A. K. V. *et al.*, 2019)	DIP and DL	-	Faults mask
(NIE *et al.*, 2020)	DL	Pr: 95%	Detection of hot spots
(DUNDERDALE *et al.*, 2020)	RF, SVM, VGG-16, MobileNet	Ac: 91.2%	Classification in disconnected substring, patchwork, hot spots, soiling, and string problem
(HUERTA HERRAIZ *et al.*, 2020)	RCNN	Pr : 91%	Detection of hot spots

Table 2–7 - Summary of methods for detecting PV modules in aIRT using DL and classification algorithms (conclusion).

(Ref)	Algorithm	Best results	Detection type
(MANNO *et al.*, 2021)	Thresholding, CNN, and Multi-Layer Perceptron	Ac: 100%	Detection of hot spots
(Anomaly Detection in IR Images of PV Modules using Supervised Contrastive LearningBOMMES *et al.*, 2021)	DL (ResNet-34) and k-nearest neighbour classifier	AUROC from 73.3% to 96.6%	Faults Masks
(FONSECA ALVES *et al.*, 2021)	DL using a Nadam optimizer	Ac: 66.43%	Classification in 11 anomaly types

| (Computer vision tool for detection, mapping, and fault classification of photovoltaics modules in aerial IR videosBOMMES *et al.*, 2021)	ResNet-50 with ImageNet	Ac: 90%.	Classification in 10 anomaly types
(AHMED *et al.*, 2021)	ICNM and transfer learning	Ac: 97.62%	Detection of bird drops, hot spots, patchwork, disconnected string, disconnected substring.
(HWANG *et al.*, 2021)	DIP and XGBoosz (algorithm for statistical characteristics of the temperatures) as input preparation for a CNN	Ac: 93.8%	Classification in hot spots, PID and disconnected modules
(GERD IMENES *et al.*, 2021)	YOLOv3	Ac: 75%	Classification in 5 faults classes using composites (aIRT and visual images)
(ZEFRI *et al.*, 2022)	DL	F1: 94.52%	Classification in 5 faults classes using composites

2.7.7. Other Applications

Imaging techniques have been employed in some other applications to facilitate the analysis of PV modules. An example is the detection of blurred images that was addressed by Tribak and Zaz (Solar Panels Frames Quality Assessment2018) with image processing techniques in order to filter frames of videos before employing mosaicking techniques. Similar techniques were used by Shen et al. (2020) to correct the angle distortion of IRT images.

2.8. DISCUSSION

This review has shown that different automatization algorithms, including DIP, DL and classification techniques, have been employed for automating different tasks of the aIRT procedure for inspecting PV power plants. Among the conclusions, this review showed that only a few among the selected studies have assessed two important aspects of the autonomous inspection procedure, namely, the optimization of the flight path (nine papers), and the detection of soiling (eight papers). These two topics are of great importance to increase time efficiency in aIRT and therefore should be further investigated. The latter goal of detecting soiling over PV modules and differentiating it from actual faults of the modules was investigated by some authors, e.g., Dunderdale

et al. (2020) and Arosh et al. (2017), together with the detection and classification of other faults.

For the task of performing the orthomosaicking of aIRT images to facilitate the localization of the faults in the field, four papers employed existing software to per-form the task, while ten studies approached the development of algorithms to create the orthomosaic of the PV plant. However, most of the proposed methods are based on DIP techniques; therefore, the resulting mosaic consists of a simple image, without additional GPS information. The correlation of orthomosaic images with GPS coordinates and the identification of modules and strings according to the site nomenclature are areas that require further investigation.

Another approach to the challenge was developed by Wu et al. (2017) with the development of an algorithm that detects PV arrays in power plants and performs the automatic correlation with their string identifiers. This is a promising strategy that could also be used to facilitate the localization of detected faults in the field through aIRT. Besides the study carried out by Wu et al. (2017), another 20 studies among the selected literature focused on the development of algorithms to detect PV systems and panels in aerial imagery. However, only three of these studies focused on aerial IRT images of the PV plants, obtaining up to 93.16% precision in the results (SHEN *et al.*, 2017). On the one hand, 18 papers presented the results of developed algorithms for the detection of individual PV modules in aIRT images, of which three of them applied DL techniques. Although the methods are hardly comparable given their different structures for results (i.e., mask, box or line), their different dataset sizes and the different evaluation metrics used, a method that combined many algorithms (DIP, SVM and DL) for detecting PV modules in aIRT images and obtained an F1 score of 98.4% can be highlighted (DÍAZ *et al.*, 2020). On the other hand, the worst metrics were obtained with simple DIP filters (ALFARO-MEJÍA *et al.*, 2020), which although providing fast results with small datasets required for training, are characterized by a lack in generalization. This is important for the replication of the algorithm in images acquired in different conditions and with a different quality. The algorithms proposed by Carletti et al. (2020), Xie et al. (Abnormal target tracking and localization algorithm for UAV PV inspection scenarios2020) and Bommes et al. (Computer vision tool for detection, mapping, and fault classification of photovoltaics modules in aerial IR

videos2021) also performed the tracking of the modules in subsequent frames of an aIRT video. This task is of utter importance for the cross-correlation of detected modules and faults, as well as their location in PV plants.

Most of the selected studies have assessed autonomous fault detection and classification in PV plants through visual (12 papers), IRT (22 papers) and aIRT images (43 papers). Among these studies, 35% used DL techniques for the detection or classification of PV faults, with an increase in developed algorithms using CNNs in recent years. Still, DIP-based algorithms also presented high accuracy results, even though most of them use smaller datasets, and therefore their replication in other sets of data is possibly not feasible. The combination of DL or DIP techniques with classifier algorithms was a promising approach in recent studies. In the field, fault detection can either be processed on board, during the UAV flight, or subsequently through a post-processing procedure after the flight. For the first case, the high computational requirements and the processing time of DL are still a challenge, as even in high-performing computers, the processing of a set of images of a large-scale PV power plant (that consists of some gigabytes of data) can take hours when using a DL algorithm. In the same way as in the detection of PV systems and modules, many types of outputs for the algorithms are possible, namely the segmentation of the faults, the detection of damaged modules or even the classification of faults in separate classes. The classes also differ among authors, and these differences represent a great challenge not only for the comparison between studies, but also for the exchange of data, experiences and algorithms among researchers in PV community, which hinders the advancements in this area. The exchange of data to enable the development of larger and more generalized datasets that consider different environmental conditions is also deaccelerated by data protection clauses.

Besides the different result types, the different evaluation metrics (or the lack of them), dataset sizes and image resolutions of the inputs also make the comparison between studies difficult. However, in general, the algorithms with the highest metrics are the ones dedicated to detecting and classifying a few types of faults compared to those that carry out the classification of many classes of faults. This proves that detection and classification of multiple faults is a complex task and further investigation is required. On this subject, the algorithm developed by Bommes et al. (Computer

vision tool for detection, mapping, and fault classification of photovoltaics modules in aerial IR videosBOMMES *et al.*, 2021) can be highlighted for its encouraging results, with an accuracy of 90% in the detection and classification of faults in ten different anomaly types. In summary, to achieve the goal of an entirely autonomous aIRT procedure, advances in some of the tasks related to the technique must be achieved. Even tasks that were already the focus of many research studies, such as the detection and classification of faults, should be further explored to contemplate different types of datasets and conditions. The exchange of data and academic collaborations are fundamental to allow for a fully automatic procedure that not only detects modules and faults on PV modules but also provides information about the type and location of the faults, in a simple and accessible manner, to enable quick remediation measures.

2.9. CONCLUSIONS

This paper has conducted a comprehensive review of the literature for methods of automating different tasks of the aIRT framework of PV power plants, since it is a subject that has been intensely investigated by researchers in recent years. Most of these studies (77 studies) focused on the autonomous fault detection and classification of PV plants in visual, IRT and aIRT images. Among these studies, the use of DL algorithms has provided good results with an accuracy of up to 90% in the detection and classification of faults in 10 different anomaly types detected in module segments extracted from aIRT images. On the other hand, only a few studies have explored the automation of other parts of the procedure of aIRT, such as the optimization of the path planning (nine papers) for the inspection flight, the orthomosaicking of the PV plant (14 studies) that is performed to facilitate the localization of the faults in the field and the detection of soiling, and its differentiation from actual faults on PV modules (eight studies). Algorithms for the detection and segmentation of PV modules were presented in 38 papers and achieved a maximum F1 score of 98.4%.

For the automation of these procedures, different algorithms have been investigated, including DIP filters and methods such as canny edge detection and thresholding; DL algorithms such as Fast RCNN, ImageNET and VGG16; and other ML-based algorithms used for classification tasks such as SVMs, KNNs and RFs.

However, the accuracy, robustness and generalization of the developed algorithms are still the main challenges of these studies, especially when dealing with more classes of faults and the inspection of large-scale PV plants. With the ever-increasing capacity and size of utility-scale PV power plants, reaching the scales of gigawatts and hundreds of hectares, automation is increasingly becoming a matter not only of scientific interest, but also of economic importance. Therefore, the autonomous procedure and classification task must still be explored to enhance the accuracy and applicability of the aIRT method.

3. AIRT FLIGHT CAMPAIGN ON PV POWER PLANTS IN BRAZIL

This chapter is the transcription of the following paper:

Abstract
The uptime of utility-scale solar photovoltaic (PV) power plants is of utmost importance for meeting contractual energy yields and expected capacity factors. Aerial Infrared Thermography (aIRT) is a non-destructive, no-downtime, fast and cost-effective method for monitoring large-scale PV power plants and assisting in fault detection. The use of aIRT techniques aims at increasing the quality and service life of PV plants especially in sunny and developing countries such as Brazil, where there is a shortfall of specialised workforce and the costs for a detailed supervisory system of utility-scale PV power plants are high. This paper presents an analysis of an aIRT flight campaign over four utility-scale PV plants in the northeast of Brazil. Two types of measurement equipment have been tested and compared, resulting in more stability and efficiency using a commercially available solution. This solution was also equipped with a RGB camera that accelerated the inspections, since it helped to differentiate defects from hot spots caused by soiling and vegetation over the modules, which were common. Different methods for fault detection were also tested and it was concluded that post-flight image analysis provides faster results. The most common faults that can happen in the early operation of PV power plants and how operators should address and prevent them were also discussed. The most common defect detected during the campaign were disconnected cell substrings. However, disconnected strings had the most impact on the power plants energy performance.

3.1. INTRODUCTION

Globally, renewable energy has contributed to a paradigm change in the electricity market. Mainly European and some North American countries and, in more recent years, China has sped up this growth through energy policy. Utility-scale photovoltaics (PV) is now one of the key players in this development, and Brazil has also seen a major expansion in installed PV capacity over the last couple of years, with the first gigawatts of power plants coming online (AGÊNCIA NACIONAL DE ENERGIA ELÉTRICA (ANEEL), 2021). As installations increase in number and scale, the need for novel methods to ensure the reliability and performance of PV systems grows. Approximately 8 GWp of PV plants will become operational in the forthcoming years in Brazil (AGÊNCIA NACIONAL DE ENERGIA ELÉTRICA (ANEEL), 2021). Most of them use single-axis tracking technology with bifacial PV modules, and are located in the northeastern region of the country (see Figure 3-1). This region is characterised by high levels of solar radiation (i.e. above 2000 kWh/m^2 annual irradiation) and semi-arid climate in remote sites with difficult access, including hundreds of kilometres of unpaved roads (BRAZILIAN MINISTRY OF MINES AND ENERGY, 2018). In addition, the impact of high-operating temperatures, extreme over-irradiance events caused by cloud-edge and cloud-enhancement effects (NASCIMENTO *et al.*, 2019), and soiling on the output of PV power plants is far more extreme in warm and sunny countries than in more temperate climates where most of the 600 GW PV plants operate worldwide (JÄGER-WALDAU, 2020; RÜTHER *et al.*, 2017).

Figure 3-1 - Brazilian map presenting in red the location of PV power plants that were contracted through regulated and PV-dedicated energy auctions. Based on ANEEL (2020). Darker shades of red indicate a multiple PV power plants in the same place.

In addition, the lifespan and the durability of PV modules depend on the degradation and failure modes, which may be created during PV module production, transportation and installation. Usually, PV modules are transported by trucks in ship containers, forcing harsh conditions on a glass product such as a PV module. Not only will the transport of the modules but also their storage and poor handling during installation implicate in potential faults and reduction of performance sooner or later after the beginning of operation. Another critical concern is the quality of these PV modules. Studies have shown that the quality control methods and qualification tests adopted in current standards are not sufficiently strict to cover the lifetime stress and the evolution of micro-cracks that PV modules experience in working conditions (FERRARA; PHILIPP, 2012).

For all these reasons, after PV modules have been installed on their mounting structure and during plant commissioning, an effective inspection method covering a

larger area in a short time is crucial. Early fault identification ensures high uptimes and might prevent outages or expensive repair steps. In recent years, advanced inspection methods and techniques have been developed for performance assessment, such as real-time tracking, I-V curve tracing, infrared thermography (IRT), and electroluminescence (EL). In particular, IRT, as a non-destructive method, is one of the key techniques for fault inspections and has proven to be effective on detecting faults in PV modules. It requires only a minimum of instrumentation and is carried out under operating conditions, without interrupting the energy production of the PV plant (BUERHOP, CI et al., 2012). Nevertheless, this method is time consuming, not cost-effective and not practical for large-scale PV power plants because it requires expert manpower, and takes a long time to be performed. For this purpose, Unmanned Aerial Vehicles (UAVs) have been fitted with IRT cameras to inspect wide areas quickly, and this technique is known as aerial infrared thermography (aIRT) (BUERHOP et al., 2016; CIOACA et al., 2015).

The aIRT technique has already been proven to be a simple and efficient tool for detecting and classifying faults. It has been effectively applied for the control and commissioning processes of utility-scale PV power plants (AMSTAD et al., 2019; MORADI SIZKOUHI et al., 2019). It also offers an easy recognition of problems caused by environmental events such as hailstorms, windstorms, and lightning, as exemplified in Oliveira et al, (OLIVEIRA et al., 2018). The aIRT technique can assess a greater number of modules in a short time with no system shutdown (trackers only have to be in stow mode). The method is even more efficient when it combines RGB and IRT cameras in the same UAV, allowing a simultaneous analysis.

aIRT is an opportunity for increasing the quality of PV plants and it is especially advantageous in countries such as Brazil, where the lack of specialised workforce and the high costs for a detailed supervisory system of the power plants make a fast and cost-effective method for monitoring a power plant are even more welcome.

Many studies showed the potential for the automation of the inspection process, since the speed in which the inspections are held generate a great amount of images to be treated and analysed (An Unmanned Inspection System for Multiple Defects Detection in Photovoltaic PlantsLI, X. et al., 2020; NIAZI et al., 2019; OLIVEIRA, A. K. V. et al., 2019; ROGGI et al., 2020; SIZKOUHI et al., 2020). With the data produced

from all the performed inspections, it becomes now possible to analyse specific failures occurring at various stages of installed PV systems and on the economic effect of these defects on commercial installations, where uptime is paramount. Additional analysis of these inspections could lead to findings about the quality of the equipment employed and of the installation process, and the financial return of routine inspections. A similar measurement campaign was previously carried out in Italy (Survey on PV Modules' Common Faults After an O&M Flight Extensive Campaign Over Different Plants in ItalyGRIMACCIA *et al.*, 2017), and carried out aIRT inspections for smaller PV power plants that have been operating for at least four years in more temperate climate conditions.

In this context, the purpose of this paper is to summarise the main conclusions of a very comprehensive flight campaign carried out in Brazil over a variety of utility-scale, single-axis tracking PV power plants of both c-Si and thin film CdTe technologies during their commissioning phase. It describes common defects found in the different plants displaying UAV-captured image data and the association between visible and IRT sensors. It also offers some evidence of typical faults identified and relative failure rates, and correlates results with related research observations in recent literature. The flight campaign applied different techniques and tested different sensor technologies in each one of the inspected PV power plants, in order to compare different methods for aIRT inspections with the aim of increasing the uptime of these plants.

The paper is structured as follows. Section 2 summarises the method of aIRT as well as the faults it can detect and the procedures adopted for this study Then, Section 3 describes the test sites where the inspections were carried out. In Section 4, the results are presented and discussed and in Section 5 the main findings of the study are summarised.

3.2. AERIAL INFRARED THERMOGRAPHY (AIRT)

As in theory, all PV modules receive the same amount of irradiance in a PV plant, the modules or cells that do not turn photons into electricity convert them into heat. IRT measures the radiation emitted from the surface of any object within the spectrum of infrared wavelengths between 1.4 and 15 μm (TSANAKAS *et al.*, 2013). Energy losses

will therefore be revealed as temperature variations in the IRT images. These thermal differences have been defined and listed in previous research (BUERHOP *et al.*, 2007; BUERHOP, CI *et al.*, 2012; KÖNTGES *et al.*, 2014) and are now standardised in the international standard IEC TS 62446-3 Version 1.0 (INTERNATIONAL ELECTROTECHNICAL COMMISSION (IEC), 2017).

Traditionally, IRT assessments are carried out with handheld IRT cameras in the field or on lift platforms to maximise coverage. This method relies on human effort and expertise and is very time-consuming and labour-intensive. As a result, the precision of the testing is vulnerable to human error, and it increases the complexity of the inspection method. IRT cameras can be combined with aerial equipment such as UAVs (drones) to increase cost-effectiveness and allow inspections on roof-mounted PV systems with limited access or large-scale PV power plants, in the so-called aIRT. This method increases the speed of the inspections, but they provide lower images resolutions than the traditional IRT method. (QUATER *et al.*, 2014; TSANAKAS; BOTSARIS, 2012; TSANAKAS *et al.*, 2016). The next subsections describe the aIRT techniques, and the equipment and procedures adopted in this paper.

3.2.1. aIRT Measurement Equipment

For the right choice of measurement equipment for aIRT inspections, many aspects must be considered. For the camera, the resolution is a key factor because it determines the maximum flight height, which strongly influences the time requirements for inspection. This is critical, especially for large-scale PV power plants, because normally the minimum irradiance conditions are met only for around six hours per day in the locations of this study. Other important characteristics are thermal sensitivity, accuracy, temperature range, camera weight and lens type. In addition, the camera type and the camera software that are offered are relevant. For the UAV system, the battery flight time, stability of the system, maximum altitude, flight duration, maximum payload and full compatibility between instruments are issues that have to be considered, and which impact on the quality of the flight as well as the costs of the equipment (GALLARDO-SAAVEDRA *et al.*, 2018).

In this experiment, two different measurement systems were used for the aerial inspections, each of them were employed in different test sites, in order to compare two different types of equipment. Both are described in Table 3-1 and were previously tested in order to demonstrate the efficiency in detecting all desired faults. System 1 was developed by coupling an IRT surveillance camera to a light consumer UAV. The camera is non-radiometric, which means that it differentiates temperatures with different shades of grey, but it does not provide information about the temperature at each point. For this retrofit, it was necessary to remove the RGB camera of the UAV and to develop a new data transmission system, as described in Oliveira *et al.* (2018). For this reason, there is no integration between UAV and IRT camera, which creates challenges for inspection, such as not being able to see the camera image in the same device that controls the UAV.

System 2 is a high-end, commercially-available professional UAV solution that integrates a high quality radiometric IRT camera with an RGB camera in a robust UAV, which offers better image quality, flight autonomy, stability, and insulation against electromagnetic interferences. The equipment also includes image-processing software that facilitates the detection of faults. However, this equipment is much more expensive (almost three times the price) than System 1, what raises the question of the necessity of such sophisticated equipment. While the equipment cost for these valuable analyses is a negligible fraction of the typical costs associated with large-scale PV power plants, these services are typically offered and carried out by third parties to whom they represent a considerable cost. Both systems are presented in Figure 3-2.

Table 3-1 - AIRT measurement systems features.

System Features	System 1	System 2
UAV equipment	DJI Phantom 3 Professional	DJI Matrice 200
IRT camera	MicroCAM 2	FLIR Zenmuse XT2
UAV Weight	1,280 g	3,800 g
System flight autonomy	13 min.	20 min.
IRT camera sensitivity	< 60 mK	< 50 mK
Spectral range	7 – 17 µm	7.5 – 13.5 µm
Pixel pitch	17 µm (640x480)	17 µm (640×512)
Frame rate	30 FPS	30 FPS
IRT camera weight	80 g	588 g

Transmitter	BosCam FPV Transmitter	Built-in
Antenna	Cloverleaf 5.8 GHz	Built-in
RGB camera	None (removed)	12 MP, 1/1.7" CMOS
Price	US$ 6,000.00	US$ 15,000.00

Figure 3-2 - aIRT measurement systems applied with extra lightweight IRT camera adapted to commercial drone (System 1 (left) in Table 3-1, and high-end, fully commercial IRT+RGB drone System 2 (right) in Table 3-1).

3.2.2. Inspection Procedure

In order to optimise flight time, video images are acquired instead of still images, also because it facilitates fault detection. It also helps on the differentiation between faults and measurement artefacts, as the reflection of the sun or other rows of modules move following the UAV movement.

During the flight, different environmental stress factors, such as weather, air turbulence, and sunlight reflection, can influence the inspection and, consequently, the quality of the aIRT images. The ideal conditions for aerial IRT monitoring can be summarised as follows (AGHAEI *et al.*, 2017; LEVA *et al.*, 2015; QUATER *et al.*, 2014).

a) The orientation of the UAV-mounted IRT sensor should be perpendicular to the PV modules and should be kept constant;

b) The flight altitude should be at least five meters to prevent any UAV self-shading during the inspection;

c) The IRT inspection should be carried out on cloudless, bright, and dry days. The wind speed should not exceed 4 m/s since higher wind speeds will create air turbulence and disturb the UAV during the inspection procedure;

d) The optimal period for UAV IRT inspection is about midday, when the direction of the sun is more perpendicular to the PV modules in stow mode in single-axis

tracking large-scale PV power plants. The irradiance should be over 600 W/m^2 on the plane of the PV array under inspection;

e) The flight path should be planned before each inspection task and the route should be well documented.

For all the inspections, the UAV route is a route orthogonal to the single-axis tracking PV system tracking tables planned in advance, in order to optimise and to obtain a shorter flight time and a better view of all PV modules.

In one of the power plants (Plant 1), the flights were carried out manually and the fault analysis was held in real-time. This means that every time a fault was detected, the UAV was manoeuvred closer to the damaged module, for a better visualisation, and a specialist was sent to the fault in order to check it, making notes and capturing images with handheld RGB and IRT cameras. This process is illustrated in Figure 3-3.
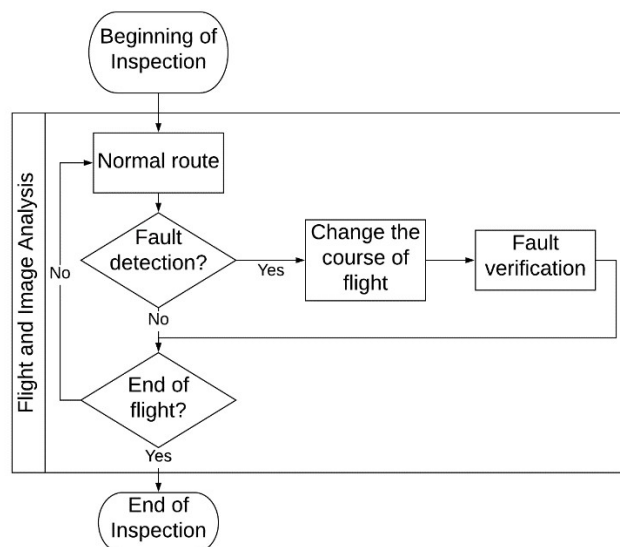
Figure 3-3 - Flowchart illustrating the process of real-time fault analysis of the power plant (i.e. the detection and analysis of the faults are carried out during the flight).

For the other three inspections, the route of the UAV was initially programmed and automatically carried out by the drone software. Furthermore, the fault analysis was evaluated after the flights, by analysing the images captured. Figure 3-4 presents the flowchart that illustrates this process. In the image, the grey boxes indicate steps that can be held outside of the power plant, reducing on-site time.
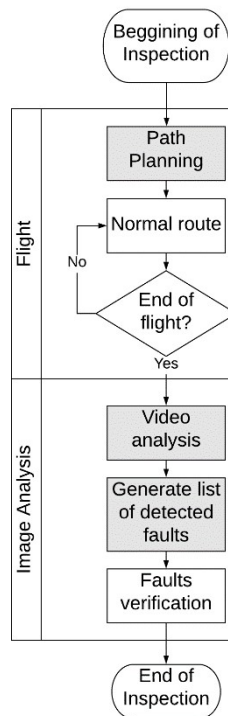
Figure 3-4 - Flowchart illustrating the process of post-flight fault analysis of a PV power plant (i.e. the detection and analysis of faults are carried out after the flight).

In order to compare both measurement systems employed and also the two different methods of inspection tested, the duration of the inspections were also registered. The duration of the inspection includes not only flight time but also image analyses and images captured with handheld cameras, for verifying faults. With these records, it is possible to calculate an estimation of the amount of MW inspected per person per day, in order to have a metric for comparison between methods according to the amount of manpower required. This does not mean, however, that a person alone can perform any inspection, since regulation on work in power plants requires that any inspection be done at least in pairs. For the comparison between inspection times, it is important to notice that the workforce that performed the inspections were highly skilled and had experience with aIRT in power plants. The real-time approach was only tested using the measurement system 1, limiting the comparison of productivity of this method with the post-flight analysis approach.

3.2.3. Image analysis and faults classification

The fault diagnosis occurs by evaluating the PV module's thermal pattern, which is uniform for healthy modules, and which is very clearly impacted by failures evidenced by the IRT image. Examples of detectable failures include: cracks, corrosion, disconnected strings, shading, dirt, broken glass, among others. The classification of detected faults is performed based on IEC TS 62446-3: 2017 (International Electrotechnical Commission and International Electrotechnical Commission (IEC), 2017).

The effect that such faults have on the power plant varies in amount of power loss that they cause and in the risks of greater damage, as fire hazard for example, which might lead to considerable downtimes. A hot spot; example, can cause indetectable power loss at first (less than 3 %), but this loss of power can increase over time, as the high temperatures damage the cell or other elements of the model, such as solder joints (Köntges et al., 2014; Ndiaye et al., 2013; Ogbomo et al., 2018)

The data collected are then processed and an actionable report is generated. Through precise site planning, it is possible to provide an exact position of the system faults and remediation may be scheduled based on a complete awareness of the site condition. The report is then sent to stakeholders for correction activities such as connection review or element replacement.

3.3. EXPERIMENTAL SITES

The inspections were carried out in four different PV power plants, totalling around 130 MW and over 600 thousand individual PV modules. All inspected PV plants follow the trend of most of Brazilian utility-scale PV systems, consisting of N-S single-axis trackers, each one moving some hundreds of PV modules simultaneously. The inspections were carried out as part of the commissioning phase of the corresponding PV plants. Table 3-2 presents some characteristics of the inspected sites. According to the PV module technology (i.e. crystalline Si or thin-film CdTe), measurement system, and approach, the height of the flight was defined for each site, after initial tests.

Table 3-2 - Details of the utility-scale PV power plants inspected in this paper, all located in the sunny and warm Brazilian northeast region. Annual irradiation data is based on Pereira et al. (2017).

PV Plant	Location	PV Installed Capacity	PV Technology	Drone used (from Table 3-1)	Height above sea level (m)	Annual irradiation (kWh/m^2)
Plant 1	Rio Grande do Norte (RN)	36.7 MW	CdTe	System 1	50	2,150.9
Plant 2	Paraíba (PB)	31.2 MW	c-Si	System 1	250	2,211.9
Plant 3	Paraíba (PB)	31.5 MW	c-Si	System 2	257	2,194.7
Plant 4	Paraíba (PB)	31.5 MW	c-Si	System 2	257	2,194.7

All sites are located in the countryside of the states of Paraíba (PB) and Rio Grande do Norte (RN), in the Northeast of Brazil, known for its hot climate and high irradiances. Figure 3-5 presents a map of Brazil with annual averages of the daily average of latitude-tilted irradiation, highlighting the two states in discussion. The annual irradiation averages in the region exceed 6 kWh/m^2 per day (> 2100 kWh/m^2.year) and the mean annual temperature is about 26°C.
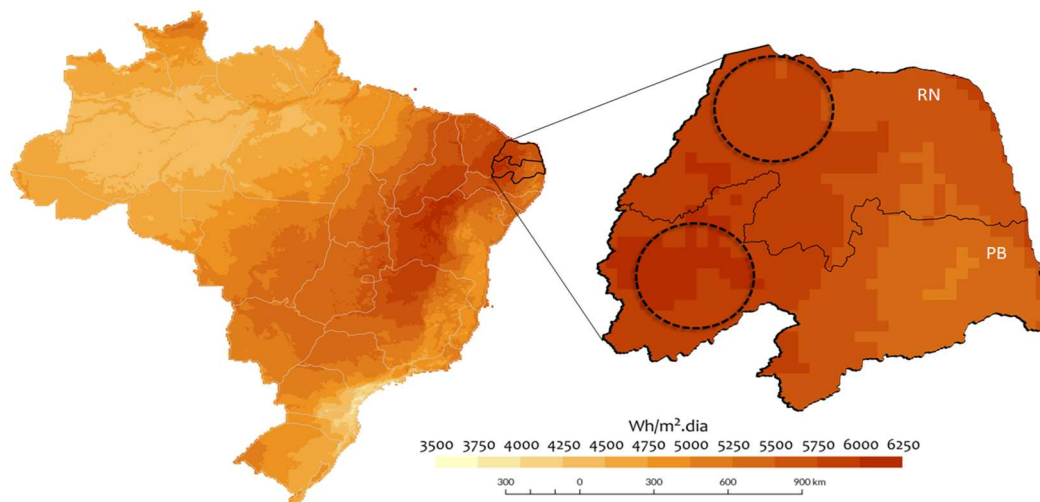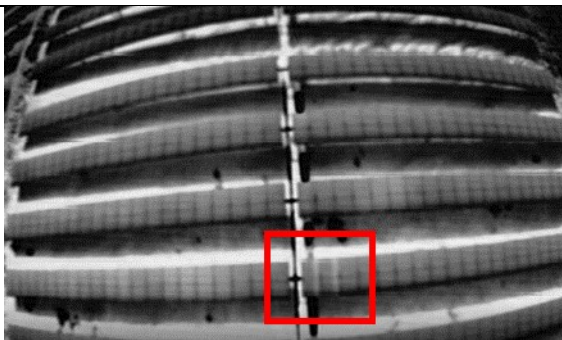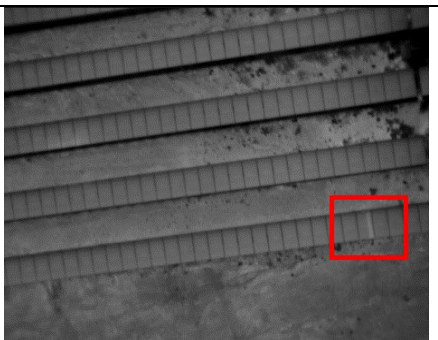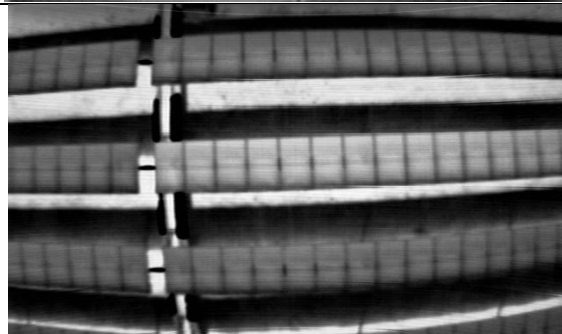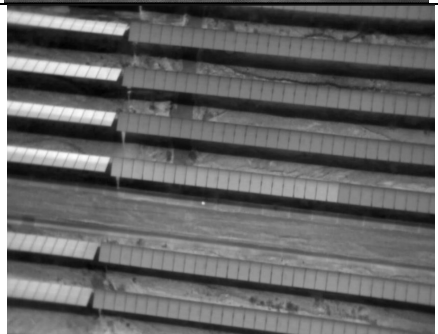
Figure 3-5 - Brazilian map with annual averages of the daily total irradiation at latitude tilt, highlighting the two states where the utility-scale PV power plants are located (RN and PB). The circled areas represent the location of the power plants, coinciding with the highest annual irradiation levels in the country. Based on Pereira et al. (2017).

3.4. RESULTS AND DISCUSSION

3.4.1. aIRT Measurement System

The inspections carried out with System 2 were faster and easier, because of the integrated solution provided by that equipment. The drone presents a better GPS system, which made the inspections quicker and safer. Besides, because System 1 consists of an adapted solution, its transmission and image quality were inferior. System 2 also offered the convenience of taking aIRT and RGB images simultaneously, unlike the first equipment that required additional flights with conventional UAVs. Table 3-3 compares the outcomes of the two systems for the detection of the most common faults. The poorer image quality and resolution of System 1 is clear on the images, on top of the "fisheye" effect of the camera, which also made the visualization of faults more difficult. The disconnected substrings faults are highlighted in red in order to facilitate visualization.

Table 3-3 - Comparison of both aIRT measurement systems results.

Fault	System 1	System 2
Disconnected Substring		
Disconnected String		

3.4.2. Real-time vs post-flight fault analysis

Table 3-4 presents the duration of each inspection. The table also presents an estimation of the amount of MW inspected per person per day, showing the high productivity obtained in the inspections of plants 3 and 4.

In terms of comparing the different approaches on the PV power plant fault analysis, the analyses carried out after the flight proved to be more efficient. The measurement time in the power plant was longer for the real-time approach and demanded double the workforce (four people instead of two) to enable checking and locating the faults during the flight. The real-time approach also complicated the detection of faults because of the difficulties of analysing videos in the field, as the screen is severely affected by glare, reflections of the sun and dirt from the soil. Another reason for the longer time needed for the real-time analysis was the manual flight. The programmed automatic route provides more stable and quicker flights, but unfortunately do not yet allow real-time analysis, since it is not viable to stop at each fault detected to take notes and take a closer look during automatic route flights. Given these outcomes, it is suggested that inspections are held with automatic path planning, prior to the measurements and that the analysis of the footage is carried out immediately afterwards. There is also the possibility to repeat the flight over some areas, in order to check ambiguous results after the first analysis. Plant 1 was also the only power plant to employ thin film CdTe modules, which have a slightly lower efficiency and therefore a larger area for the same amount of power.

The duration of the inspection also differs between power plants due to the different heights used for the UAV flights. As mentioned before, the altitudes were defined according to initial tests, aiming to provide the best results given the employed measurement system and PV module technology. The higher image quality of the measurement System 2, allowed an inspection from a higher altitude, which sped up the inspection process. One further factor that impacted the duration of the inspection is the presence of an RGB camera in measurement System 2, which minimises field time due to the effects of soiling and vegetation over the PV modules. For the case of Plant 2, an additional flight with an RGB UAV was performed, to check for such problems, which also takes extra time not only for the flight but also for the analysis of

the RGB images. This additional inspection step can be reduced by performing aIRT right after the cleaning and the vegetation pruning at the power plant. Considering that in a day is possible to work for 4 to 6 hours due to environmental conditions, the results of plants 3 and 4 are very similar to other studies as Ulrike Jahn et al (2018). The study affirms that a PV plant of 4 MWp requires 5 to 10 hours for an aIRT inspection, when all required conditions are met.

Table 3-4 - Results of the aIRT flight inspections in each utility-scale PV power plant in northeast Brazil.

PV Plant	Drone used	PV Technology	Fault Analysis	Inspection Duration	Flight Altitude	Team Size	MW inspected per person per day
Plant 1	System 1	CdTe	Real-time	9 days	15 m	4 people	1.02
Plant 2	System 1	c-Si	Post-flight	7 days	20 m	2 people	2.23
Plant 3	System 2	c-Si	Post-flight	4 days	30 m	2 people	3.94
Plant 4	System 2	c-Si	Post-flight	4 days	30 m	2 people	3.94

The results shows that the economy of acquisition costs of System 1 does not worth the extra inspection time required using this solution, as the difference is dissolved in the many inspections that the robustness of System 2 can perform. The cost disparities are much smaller than workmanship costs that are fixed for every inspection.

3.4.3. Hot-spots caused by soiling and vegetation

The most common problems found in the inspections were hot spots caused by soiling and vegetation resulting in shading of PV cells, affecting some hundreds of modules during the inspections. The faults are not always distinguishable from actual hot spots defects through the visual aerial images, so all hot spots that are not visible caused by soiling or vegetation have to be verified with a ground inspection to complete the diagnosis. When a hot spot is found in a soiled PV module, the procedure is to

clean the module in order to re-evaluate the thermal pattern to know whether the hot spot was caused by soiling or actual damage. These situations are not accounted for as faults in this analysis because they are not considered damages or defects of the power plant and can be easily fixed. However, they cause power losses and create fire hazard risks, which can severely affect uptime.

Figure 3-6 presents different examples of soiling and vegetation detected during a flight campaign. On the images, it is possible to compare the effect of such problems detected with the two different measurements systems and over different PV module technologies. Figure 3-6 (a) shows a soiling pattern caused by wind over many PV modules, but which only causes hot spots over some of them due to the amount of soiling. The soiling pattern consists of white lines on the lower corner of the modules, as can be better seen in the detail of the image. Figure 3-6 (b) presents a hot spot caused by a bird dropping over a module in an image taken with measurement System 1. Because this UAV had its RGB camera removed, the visual picture (on the right side) was taken with a second UAV. Therefore, the images are taken from slightly different positions. This problem slows the association of the two images to compare IRT and RGB images to correctly classify faults. Figure 3-6 (c) and Figure 3-6 (d) present images of modules covered with vegetation. However, due to the difference of measurement system used and PV module technologies employed, it is clear that the detection is quite different for the two cases.
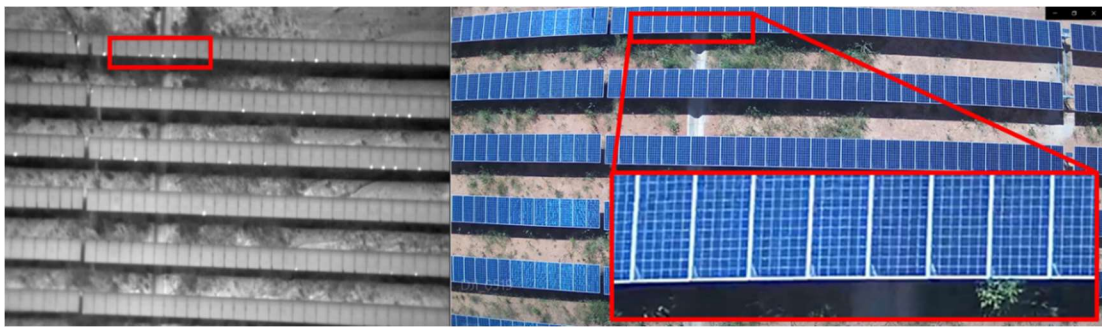
(a)
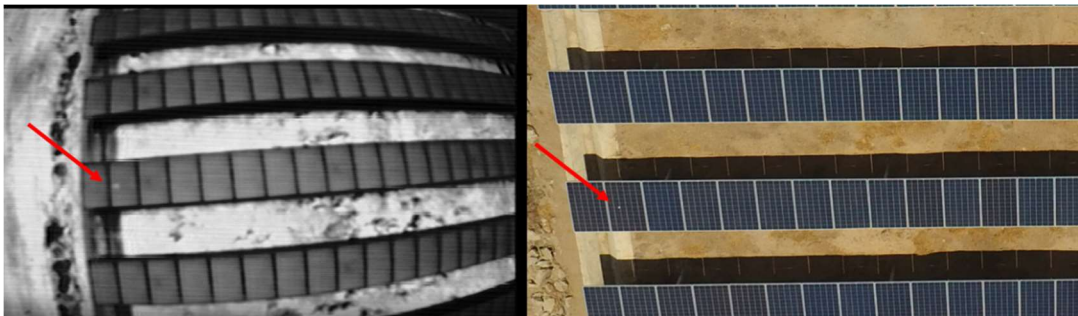
(b)
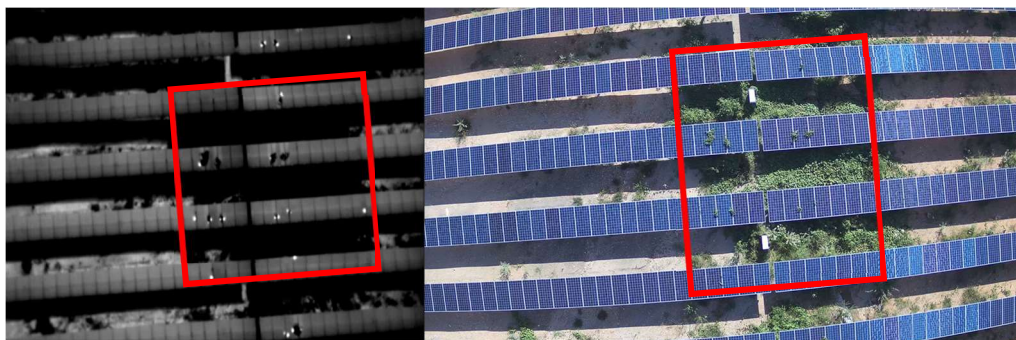
(c)
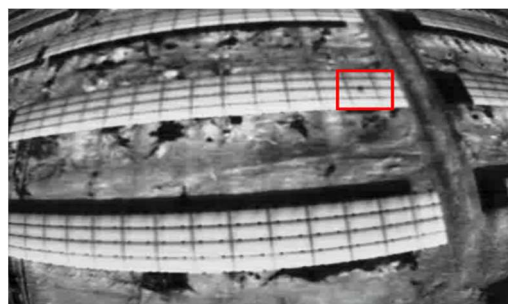
(d)

Figure 3-6 - Examples of vegetation and soiling over PV modules: (a) Soiling pattern image over many c-Si modules, taken with System 2. (b) Bird droppings image over one c-Si module, taken with System 1. (c) Vegetation image over many c-Si modules taken with System 2. (d) Vegetation image over one CdTe PV module, taken with System 1.

3.4.4. Most common defects detected on the sites

The most common defects found in the inspections were:

- disconnected substrings: disconnection of the cell strings of the module inside the junction box, causing one third of the module to be in open circuit;
- disconnected strings: interruption of the connection one full string with the system, due to failures of connection, fuses, or string boxes problems, causing many modules to be in open circuit;
- modules with broken glass: modules with the front glass broken due to shock with rocks or other objects during construction or thermal stress due to other failures that generate hot spots;
- modules with hot spots defects: points of higher temperature over the modules caused by failures such as delamination points, cracks due to mechanical stress, corrosion, soldier joint defects and others.

Table 3-5 presents the number of occurrences of each of these faults in each inspected site as well as the number of modules affected by each fault (a disconnected string affects 15 to 21 modules, for example). These four problems are considered defects in the PV power plant and are discussed in order of most common occurrence in the next subsections.

The table also estimates the power loss caused by each fault. For the calculation of power loss of each fault, the nominal datasheet peak power of each module was used, considering that disconnected substrings cause a loss of one third of the PV module, and disconnected strings cause the loss of power proportional to the number of modules in each string. For the case of hot spots and broken glass PV modules, a loss rate of 2% of the power of the PV module was applied, assuming that in the commissioning phase of the power plant the impact of the failure is minimal. This impact can grow linearly or exponentially over time. These power losses estimations do not account for the possible power mismatch that the faults brings to the whole system. Disconnected substrings, for example, reduce the string voltage and affect all string parallel to it, due to voltage mismatch.

From the table we see that despite not being the most common fault, disconnected strings cause the major loss of power in a power plant, since it affects many modules at once.

Table 3-5 - Most common PV module defects detected in the four utility-scale PV power plants in Brazil.

PV Plant	Number of detected faults				Number of affected modules				Estimated Power Loss (kW)			
	Disconnected substrings	Disconnected strings	Broken module	Other types of hot-spots	Disconnected substrings	Disconnected strings	Broken module	Other types of hot-spots	Disconnected substrings	Disconnected strings	Broken module	Other types of hot-spots
Plant 1	0	26	5	1	0	390	5	1	0	44.85	0.01	0.01
Plant 2	86	8	0	2	86	168	0	2	9.46	55.44	0	0.01
Plant 3	39	2	5	0	39	30	5	0	4.29	9.90	0.03	0
Plant 4	34	1	5	0	34	21	5	0	3.74	6.93	0.03	0
Total	159	37	15	3	159	609	15	3	17.49	117.12	0.08	0.02

3.4.4.1. Disconnected substrings

The most common defects detected are disconnected cell substrings, which are usually a manufacturing defect. PV modules are healthy and have an open-circuit voltage according to the product's datasheet as they leave for transport to the PV power plant site, what is confirmed by the measurements and the flash report that is carried out before the modules leave the manufacturer's plant. After transport and installation, through thermal or mechanical stress, these cells strings became disconnected in the junction box, causing the bypass diode to take on the full current of the string. Besides the loss of one-third of the PV module peak power, the fault causes unnecessary stress to the bypass-diode. These results can be compared to a flight campaign in Italy (Survey on PV Modules' Common Faults After an O&M Flight Extensive Campaign Over Different Plants in ItalyGRIMACCIA *et al.*, 2017), in which a similar approach to this work was adopted, only that the experiments were carried out in much smaller PV plants using PV modules that already had operated for

some years, and which were produced with manufacturing technologies no longer in use. In that study, disconnected substrings were not as common as in the study carried out in Brazil, which raises the question of the quality of PV modules produced under the very demanding price reduction pressure the PV industry has suffered in recent years.

Figure 3-7 presents two examples of detection of disconnected cell substrings, one detected with each measurement system. System 2 allows a clear detection of this defect, and the worse image quality of System 1 results in a more difficult detection. Commonly, as shown in the picture taken with System 1, many modules with this defect are found side-by-side. There are cases with more than four modules in a string with the same defect. This happens because this defect is a manufacturing problem: since the modules installed close to each other are usually taken from the same pallet, they are more likely to have come from the same PV module production batch, and to be installed and transported together. Figure 3-7 (c) shows a hand-held IRT image of a PV module with a disconnected substring. The image shows that the temperature difference between the affected and the non-affected substrings is around 3 K, value that fits with what is stated in the IEC 62446-3 (differences of 2 to 7 K for disconnected substrings) (INTERNATIONAL ELECTROTECHNICAL COMMISSION (IEC), 2017). This defect does not occur in CdTe modules, because thin film PV modules do not usually have bypass diodes separating the module in substrings.

(a)   (b)   (c)
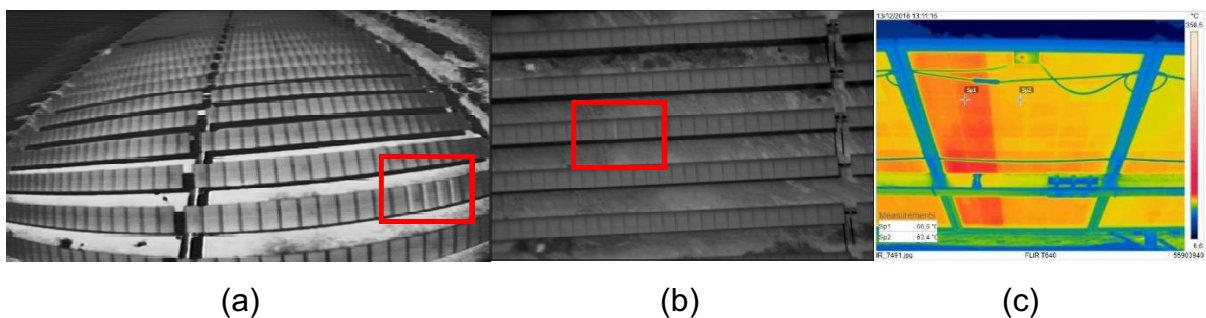
Figure 3-7 - Examples of disconnected cell substrings in individual PV modules detected during the flight campaign: (a) four defective modules, in the image taken with measurement System 1, and (b) one defective module, which was taken with measurement System 2. Image (c) shows a disconnected substring IRT image taken with a hand-held camera.

3.4.4.2. Disconnected strings

String disconnection is a failure that causes the highest fraction of energy losses in a PV power plant energy production, since it affects many modules at once and it is also quite common. Some examples of disconnected strings are shown in Figure 3-8. The three images were taken in different PV power plants, which have different string and table configurations. In Figure 3-8 (a) and Figure 3-8 (c) the detection is easier because strings are all wired in the same table, and this provides contrast to the disconnected ones. On the other hand, for the power plant shown in Figure 3-8 (b), the inspection should be carried out above a certain height that allows a good comparison with other tables, to enable the detection. For Figure 3-8 (a) and Figure 3-8 (b), the images were taken with measurement System 1, in two PV power plants using different PV module technologies. For Figure 3-8 (c), the image is taken with System 2. It is visible that this type of fault is easily recognised with both systems, even with the lower camera resolution of System 1. The disconnection can also easily be seen even under bad environmental conditions, such as clouds and low irradiance. Figure 3-8 (a) presents also the open string IRT image taken with a hand-held camera. The image shows that the difference of temperature between disconnected and connected strings is around 4 K, what matches the IEC 62446-3, which affirms normal temperature difference for disconnected strings is between 2 to 7 K (INTERNATIONAL ELECTROTECHNICAL COMMISSION (IEC), 2017)p.

Disconnected strings also slow down the inspection process, since this type of defect disguises other faults, as the only problems that can be detected in a disconnected string are short-circuited PV modules or substrings. Therefore, the string needs to be reconnected and the thermal pattern of the PV modules re-evaluated. The causes for string disconnections vary from different equipment defects: trackers, inverters, and fuses and diodes due to extreme-overirradiance events (NASCIMENTO *et al.*, 2019), besides scheduled disconnections for maintenances, or power restrictions. Disconnected strings can be detected more easily through the supervisory system when current monitoring is carried out at a string or stringbox level (depending on topology and PV module technology). However, with the ever-growing cost pressure on new PV power plants, and also because normally the supervisory system

is not fully functional by commissioning phase, the aIRT is still a fast method to perform this inspection. For medium-size PV power plants, one can raise the question of the viability of having a supervisory system on the string level. Depending on the maintenance and equipment costs, a continuous aerial inspection can provide a better economic balance.

(a)

(b)   (c)
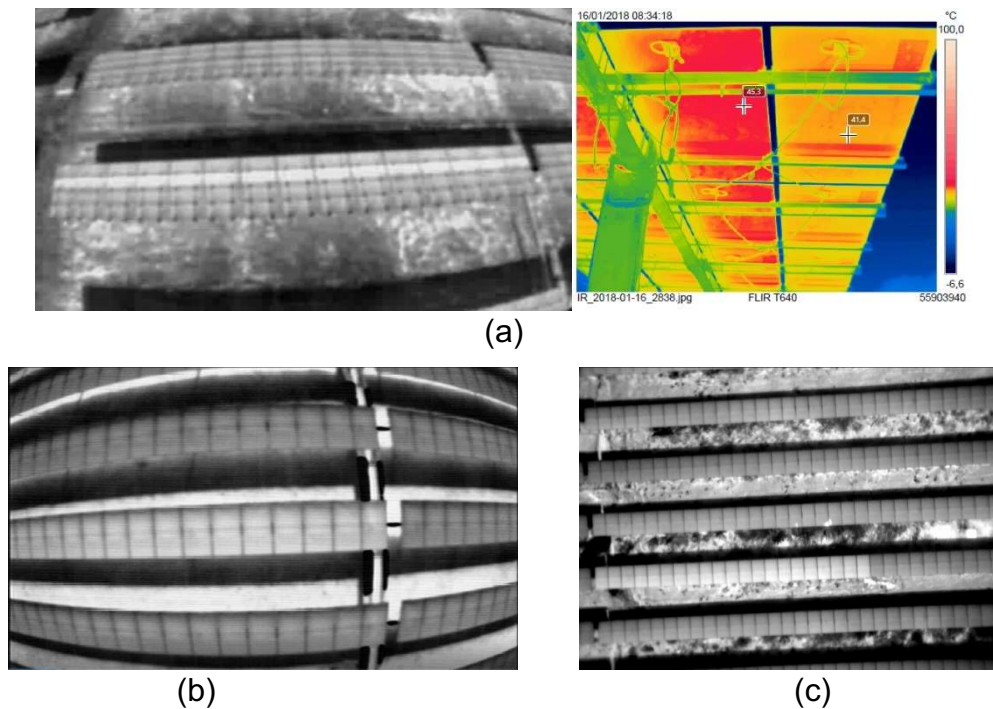
Figure 3-8 - Examples of disconnected PV strings: (a) thin film CdTe PV module disconnected string, taken with System 1 and accompanied by an IRT image taken with a hand-held camera. (b) c-Si disconnected string, taken with System 1. (c) c-Si disconnected string, taken with System 2.

3.4.4.3. Broken PV modules and other types of hot-spots in c-Si PV modules

Broken modules were not so commonly found and were mainly caused by installation events. Other types of hot spots defects were even rarer since the power plants were connected only for a short-time period. This is an interesting result in comparison with Grimaccia et al. (Survey on PV Modules' Common Faults After an O&M Flight Extensive Campaign Over Different Plants in Italy2017), where problems detected as hot spots defects were the main findings of the flight campaign in Italy. Faults that result in hot spots are most frequently found in PV power plants that

have been operating for at least a few years or have undergone severe weather events. They do not typically induce a substantial loss in PV output at an early level; therefore, they are not generally identified by the supervisory systems. They are, however, a possible cause of fire hazards in the power plant or electrical shocks. The breakages also usually increase moisture infiltration and are normally followed by corrosion, discolouration or delamination issues (NDIAYE *et al.*, 2013).

Figure 3-9 presents examples of modules with hot spots. Both cases shown in the images are c-Si modules with broken front glass. Figure 3-9 (a) shows an example of the aIRT image and its correspondent RGB image. The detail of the image shows that, in this case, the broken module is not visible through the visual inspection, even though the problem is clear through the IRT image. In these cases, the identification of the broken module is performed through ground inspection. There are cases when the fault can be identified in the RGB images my using different camera angles. Nevertheless, the RGB image enables the operator to discard the hypothesis of vegetation or soiling over the module, assuring that the hot spot represents a module fault. This combination of RGB and aIRT image reduces on-site time and extra work. Figure 3-9 (b) presents another example of broken front glass that creates a hot spot with high temperature differences, which must be replaced immediately.
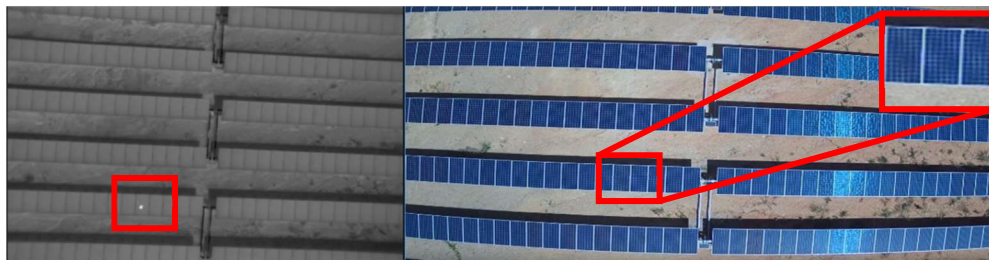
(a)
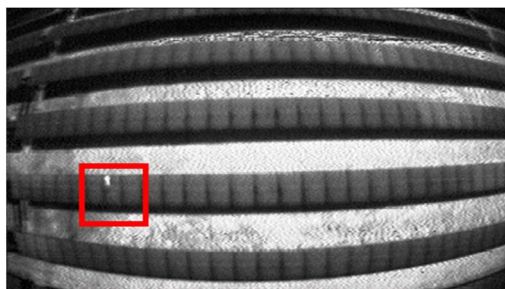
(b)

Figure 3-9 - Examples of hot pots detected in c-Si PV modules: (a) aIRT image of PV module with broken glass detected with System 2 and its RGB equivalent. (b) aIRT image of PV module with broken glass detected with System 1.

3.4.4.4. Broken PV modules and other types of hot-spots in CdTe PV modules

Figure 3-10 presents three images with different types of hot spots defects detected in Plant 1 (CdTe modules). Figure 3-10 (a) shows an example of a module with broken glass that resulted in temperature differences of more than 30 K above the module temperature, despite IEC 62446-3 affirming these defects normally causes differences of 0 to 7 K.

(a)

(b)

(c)
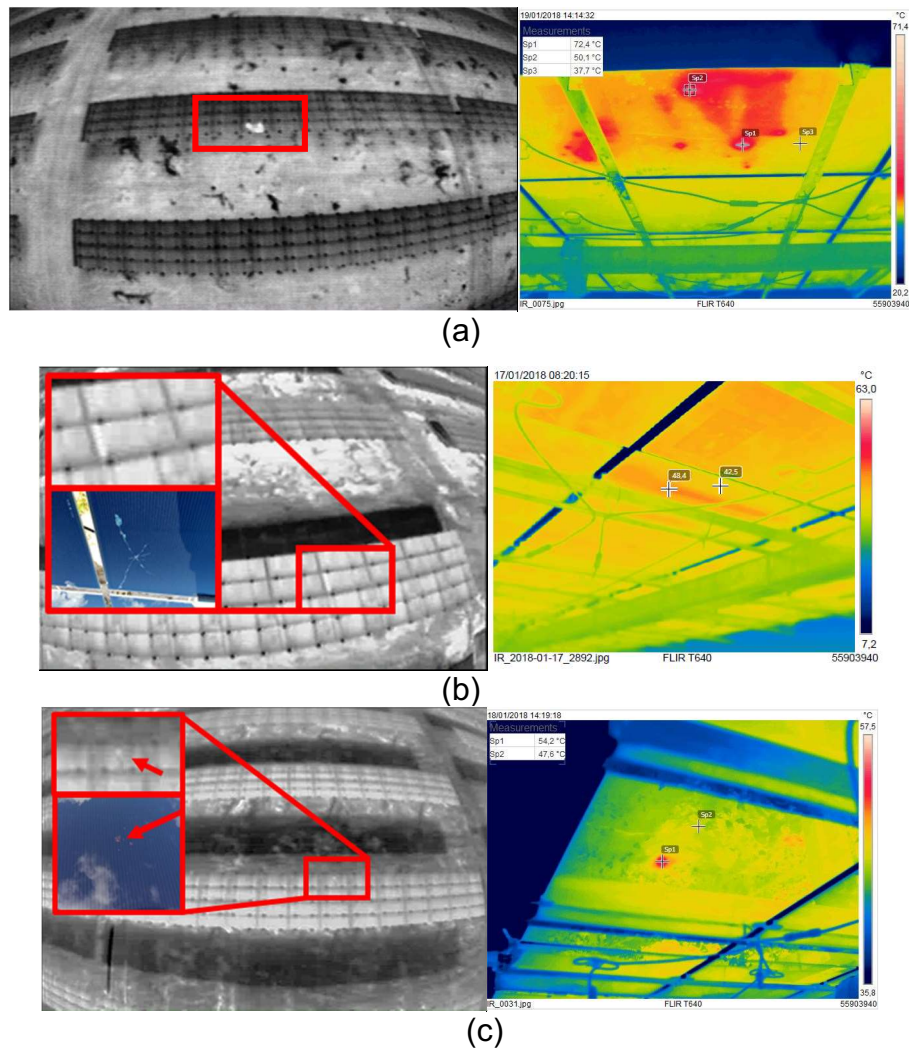
Figure 3-10 - Examples of hot spots detected in CdTe modules: (a) PV module with broken front glass. (b) PV module with broken front glass where a whole cell was

damaged (left corner of the module) (c) PV module with a delamination spot. Each image is accompanied by its correspondent hand-held IRT image.

This type of failure is easily spotted because it generates a "brighter" hot spot, due to the higher temperatures involved. This allows the defect to be detected from altitudes higher than 50 m. Figure 3-10 (b) also presents a module with broken glass, but in this case, only some cells in the PV module are hotter than the others and the temperature difference is much smaller (around 4 K), which makes detection more difficult. Figure 3-10 (c) shows a hot spot that revealed a delamination point in the PV module. This fault is much harder to be detected because of the small size and small temperature difference (less than 7 K).

3.5. CONCLUSIONS

In order to maximise uptime and increase capacity factors, this paper offers an analysis of the most common defects found during the commissioning phase of four different utility-scale PV power plants in Brazil, analysing PV module faults of two different technologies: c-Si and CdTe. Two different measurement equipment have been tested and compared, and as expected, the results show that System 2 provided a faster and easier experience. This is due to the integrated solution provided by the equipment, the better quality of its camera and GPS and the existence of a RGB camera on the UAV, what allows a quicker differentiation between faults and soiling and vegetation. Because of its advantages, System 2 is more expensive than System 1. However, results showed that this cost is compensated by reducing the inspection time, and therefore, reducing workmanship costs.

In terms of comparing real-time with post-flight fault analyses, the analyses carried out after or in between flights proved more efficient and required less time on-site. The duration of the inspection was also influenced by PV module technology and quality of the camera of the measurement system employed.

The most common problems found during the aerial inspections were hot spots due to soiling and vegetation, which caused shading of PV cells. They are not considered faults but can affect the outcomes of the aIRT and the total PV plant

downtime. They can be distinguished from actual damage of the PV cells through RGB images.

Among the actual faults of the PV systems detected during the flight campaign, the most common, in number of occurrences, were disconnected cell substrings, followed by disconnected strings, hot spots defects and modules with broken glass. However, when comparing the amount of lost power caused by each fault, the highest downtimes are caused by disconnected strings, followed by disconnected substrings and hot spots, with broken front glass in last.

The results of these flight campaigns are extremely important because they show the most common faults that can happen in the early operation of PV power plants and from that, operators can decide how to address and prevent them, maximising the uptime of utility-scale PV power plants.

4. DEVELOPMENT OF AUTOMATIC FAULT DETECTION ALGORITHM

This chapter is the transcription of the following paper:

Automatic Fault Detection of Utility-Scale Photovoltaic Solar Generators Applying Aerial Infrared Thermography and Orthomosaicking

Authored by: Aline Kirsten Vidal de Oliveira, Matheus Körbes Bracht, Mohammadreza Aghaei and Ricardo Rüther.

Abstract

As large-scale Photovoltaic (PV) power plants are being expanded in installation number and capacity, aerial infrared thermography (aIRT) has proven to be effective in detecting at different phases of their development, construction and commissioning to operation and maintenance. However, evaluating the aerial imagery over hundreds of hectares fields of PV arrays is very time-consuming and subject to human error. This paper proposes a complete framework for automatically detecting faults in large-scale PV power plants and their physical location inside the plant site. To this end, a Mask-RCNN algorithm is developed and fine-tuned for instance segmentation using a dataset of 93 samples collected in an aIRT flight campaign in Brazil. The results are combined with orthomosaic techniques to create an orthomap of the PV system with the highlighted faults. The proposed method has been tested to detect automatically the faults in two power plants. Several tests were performed to improve the algorithm's accuracy, including different pre-processing techniques and filters for the data. The final algorithm generated high-accuracy results for detecting and localizing hot spots in PV plants and disconnected substrings. The resulted maps could successfully show the location of this faults with a high accuracy (10% of false positives).

4.1. INTRODUCTION

At the beginning of 2022, the photovoltaics (PV) installation exceeded 1 TW which was an impressive milestone in the solar energy sector (ESKANDARI *et al.*, 2023). As solar PV energy conversion becomes one of the most promising energy sources for a sustainable and renewable energy future, reducing downtimes and assuring the technology's reliability and performance are of utmost importance. Especially in regions with a lack of specialized workforce and difficult access, developing reliable and cost-effective techniques for rapidly detecting faults in PV plants is urgent (OLIVEIRA *et al.*, 2020; TRIKI-LAHIANI *et al.*, 2018).

Among the recent advances in this area, the assessment of power plants by aerial inspections using Unmanned Aerial Vehicles (UAVs) is becoming widespread (AGHAEI *et al.*, 2014). The combination of drones with cameras that capture either RGB or infrared thermographic (IRT) images has proven to be effective in detecting faults in PV power plants in different stages of their operation (OLIVEIRA *et al.*, 2018, 2020). The technique has been called Aerial Infrared Thermography (aIRT).

However, evaluating the images captured through aerial inspections is very time-consuming and subject to human error. Therefore, automation techniques have been studied to assist the procedure (HENRY *et al.*, 2020; NIE *et al.*, 2020; OLIVEIRA, A. K. V. *et al.*, 2019). A solution to the problem is to use Digital Image Processing (DIP) to detect faults, as proposed by many authors (AGHAEI *et al.*, 2015; KIM *et al.*, 2017; ROGOTIS *et al.*, 2014; TSANAKAS *et al.*, 2015). A better way to approach the problem is to apply Artificial Neural Networks (ANNs) to categorize the different types of faults on PV modules, as they tend to be more assertive in more diverse image conditions. ANNs intend to mimic how the human brain performs a task of interest (MAYO; LEUNG, 2018). Among the many different architectures of ANNs, Convolutional Neural Networks (CNNs) have demonstrated clear superiority in visual recognition tasks such as image classification and object detection (GENG *et al.*, 2018).

One of the major concerns in the automatic evaluation of PV plants is the correct localization of faults and the cross-referencing with the terminology of areas and strings used in the field (OLIVEIRA *et al.*, 2022). This is extremely important to

allow the operation & maintenance personnel to perform corrective measures and precisely detect faulty PV strings in a timely manner, as many faults detected with aIRT do not produce any visible effect. This becomes even more relevant as the PV plant installations become larger and larger; a 1 GWp PV power plant can have a footprint larger than two thousand hectares.

A way to approach the problem is to generate orthomosaics of the PV plants, applying mosaicking techniques using RGB and thermographic images. This can help to improve sight perspective, providing a more expansive vision of the modules, enhancing resolution and facilitating the localization of faults (AGHAEI *et al.*, 2017).

Some recent studies (LÓPEZ-FERNÁNDEZ *et al.*, 2017; PARK; LEE, 2019; TSANAKAS *et al.*, 2017; Inspection of Photovoltaic Installations by Thermo-visual UAV Imagery Application Case: MoroccoZEFRI *et al.*, 2018) have shown that the combination of orthomapping with automatic detection of faults algorithms allows effective monitoring of PV power plants from the commissioning phase until the end of its operation. . This enables a follow-up of the evolution of the power plant faults and a better understanding of their roots and possible mitigation strategies which lead to an increase in the reliability and service lifetime of PV power plants. Given that, this paper aims to develop a methodology that combines aIRT inspections, automatic fault detection and classification using artificial intelligence algorithms and the reconstruction of orthomosaics reflecting the detection of faults. The main contributions of this study are summarized as follows:

a) Development of a fault detection algorithm on aIRT images highlighting its main challenges, shortcomings, and workarounds;

b) Utilization of an orthomosaic reconstruction software package describing the challenges that the workflow imposes for the automatic fault detection algorithms;

c) Evaluation of the impact of different flight configurations and datasets on the processing time and results;

d) Application of the proposed framework in real cases, evaluating the challenges imposed by real datasets.

The paper is arranged as follows: Section 2 presents the proposed methods and dataset. In section 3, we provided the results, followed by the discussion in section 4. Finally, section 5 wraps up the paper with a summary of the main outcomes.

4.2. METHOD

In this study, we propose a deep learning-based method to process aerial imagery automatically and produce a map of the faults of the PV power plant. A summary of the method described in this work is presented in Figure 4-1. In the flowchart, the steps shown in grey translate the processes followed to obtain the algorithm used in the framework's fault detection step.
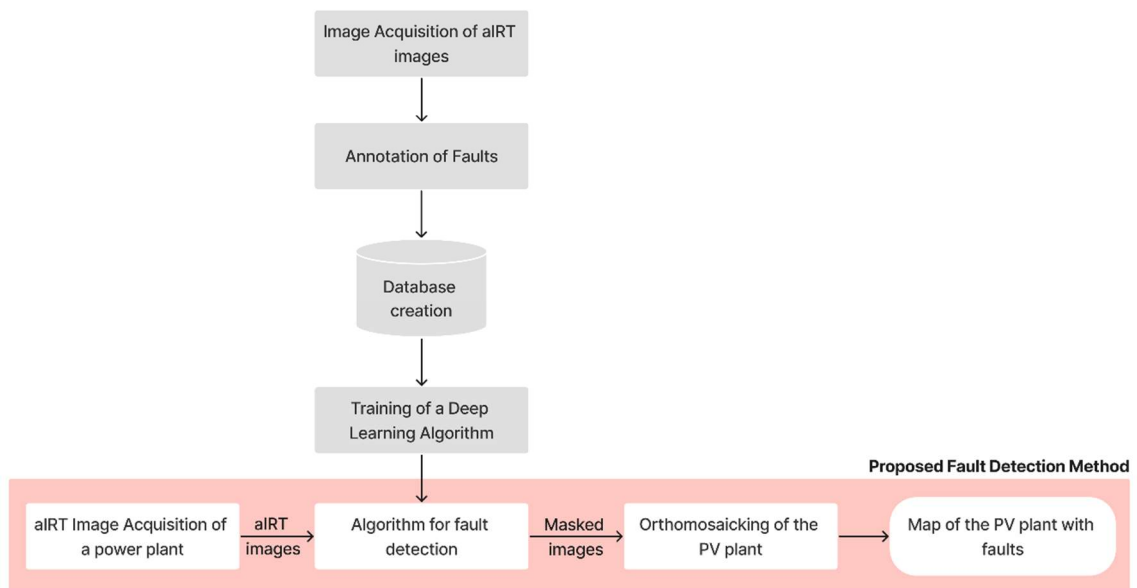
Figure 4-1 - Flowchart of the aIRT thermography imaging method developed to automatically detect faults in PV power plants.

The framework to create a map of faults in a specific power plant is highlighted in the figure in pink. It starts with the acquisition of aIRT images of the PV power plant. Then, the fault detection algorithm processes the images (still images taken from a

video stream), adding masks highlighting the faults over the original images. The masked images are combined through an orthomosaicking technique, resulting in the power plant map with the detected defects and failures highlighted. The following subsections describe these steps in more detail. The framework and the resulting algorithm are afterward tested in two test cases.

4.2.1. Development of the automatic fault detection algorithm

4.2.1.1. Creation of the dataset

A light commercial drone (UAV Matrice 200) with a lightweight infrared camera (Zenmuse XT2) was used for the dataset's creation. The Zenmuse XT2 takes both RGB and thermal images, with the specifications presented in Table 4-1.

Table 4-1 – Zenmuse XT2 properties.

Property	Camera	
Type	*RGB*	*Thermal*
Sensor size (mm)	7.44	10.88
Image resolution (px)	4000x3000	640x512
Focal length (mm)	8	13

The dataset consists of images stored in grayscale, and the intensity differences represent the temperature differences. The images were taken during a flight campaign in several commercial PV plants in Brazil. Some of the results obtained during the campaign are presented in (OLIVEIRA *et al.*, 2020). The faults encountered include disconnected substrings, disconnected strings, short-circuited strings and substrings, and hot spots caused by soiling, delamination and broken modules.

During the flights campaign, procedures and environmental conditions were followed according to the international standard IEC TS 62446-3 (INTERNATIONAL ELECTROTECHNICAL COMMISSION (IEC), 2017). The conditions include minimum environmental requirements such as clear sky conditions and a camera angle perpendicular to the modules to avoid reflections (KRENZINGER; DE ANDRADE, 2007). The flight altitude was set between 20 m and 40 m, depending on the site, which

allowed the detection of defects on the individual PV module level, and for an increased Field of View (FoV). Most flight routes were pre-set through GPS coordinates, so the flight was steady and the velocity constant.

The dataset consists of 93 IRT images with their corresponding ground-truth segmentation, which highlights the faulty modules in each image. The samples are either frames of aIRT videos or still images, and both are converted from the proprietary radiometric format of the camera to JPEG format. Images are annotated using the Annotation Tools developed by Bommes et al. (BOMMES, 2021; Computer vision tool for detection, mapping, and fault classification of photovoltaics modules in aerial IR videosBOMMES *et al.*, 2021). Based on the standards of (INTERNATIONAL ELECTROTECHNICAL COMMISSION (IEC), 2017; VATH, 2016), the detected faults include hot spots, disconnected substrings and strings, and short-circuited strings. Figure 4-2 shows some samples of the dataset with their annotations. Figure 4-2(a) is a frame of an aIRT video with two open strings highlighted. The other two samples are aIRT radiometric photos, where Figure 4-2(b) shows a disconnected substring and Figure 4-2(c) depicts a module with hot spots caused by a broken front glass. Tests were carried out holding a pre-processing step of the images, with a histogram equalization to improve the contrast in all of them.

(a) (b)

(c)
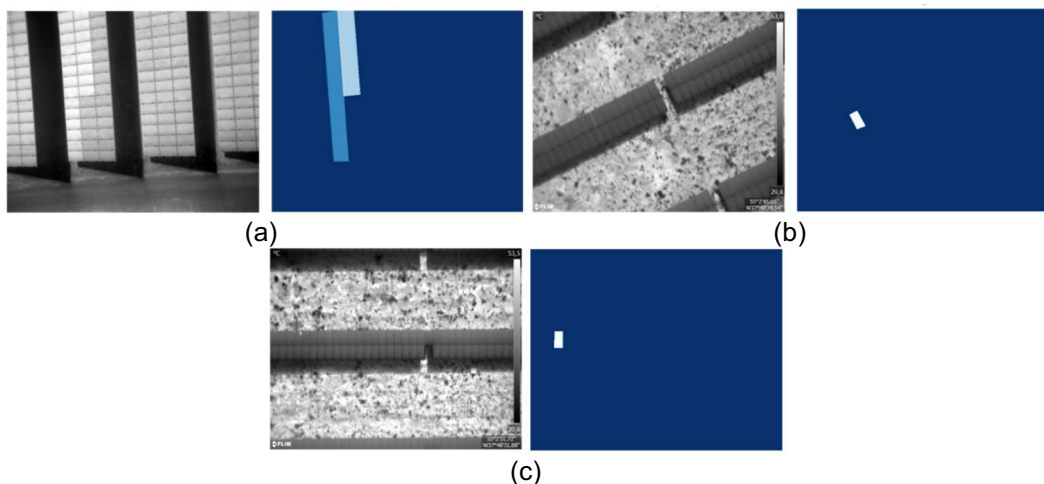
Figure 4-2 - Examples of the aIRT-image dataset samples, obtained from utility-scale PV power plants with faulty PV modules in Brazil.

Augmentation techniques are implemented to increase the dataset's number of samples. This process artificially enlarges the number of segments, helping to

improve the overall learning procedure and performance, feeding the model with varied data (KAMILARIS; PRENAFETA-BOLDÚ, 2018). Transformations included rotations, dataset segments cropping, scaling, and mirroring. Typically, 90% of the samples are used for training and 10% for validation.

4.2.1.2. Automatic Fault Detection

For the automatic classification, the fine-tuning of a Mask RCNN (Regional Convolutional Neural Network) is applied for instance segmentation using Keras and Tensor Flow (ABDULLA, 2017). The technique has been described in the literature to detect PV modules and systems (Computer vision tool for detection, mapping, and fault classification of photovoltaics modules in aerial IR videosBOMMES *et al.*, 2021; DÍAZ *et al.*, 2020; SIZKOUHI *et al.*, 2020, 2022) and faults in aIRT images (HUERTA HERRAIZ *et al.*, 2020; PIERDICCA *et al.*, 2018). The weights are initialized with pre-trained COCO weights (LIN *et al.*, 2014) and trained for 375 epochs (100 epochs for heads with a learning rate of 0.001 and 175 others for fine-tuning with a learning rate of 0.0001). The training output is the weights of the detection algorithm, whose inputs are the aIRT images and the outcome, binary images with the segmentation of the faults, which are afterwards highlighted over the original images. The flowchart presented in Figure 4-3 shows the schematic of the steps for this development.

Some figures of merit as the mean Average Precision (mAP) and F1-score are used to evaluate the algorithm's results.
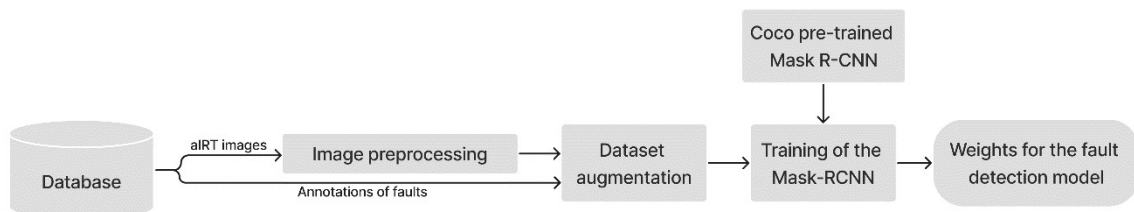
Figure 4-3 - Flowchart of the aIRT image evaluation method developed to automatically detect faults in large-scale PV power plants.

4.2.2. Orthomosaics reconstruction

Even with the automatic classification of the faults, the localization of modules or strings with problems within a power plant is challenging, as we have previously shown (OLIVEIRA *et al.,* 2021, 2022). We propose a method using an orthomosaic reconstruction of the PV power plant to facilitate the location of the faults which were previously automatically detected.

For this proposed workflow, the Bentley ContextCapture v10.20.0.4169 was employed (BENTLEY SYSTEMS, 2019). This software solution is a commercial package widely used in the field of photogrammetry. The software tool allows different reconstruction outputs for analysis and evaluation from the images taken over the area. The Bentley ContextCapture workflow is very clear and requires the user to perform several steps and setups actively. Initially, the acquired data must be verified regarding the position and rotation metadata, besides being subdivided into photo groups. Different photo groups are created to embrace different photo properties (like sensor size, focal length, principal point, and lens distortion/pose). These data are used to support the aerotriangulation process that follows. This step detects tie points in the photos and determines the correct image positioning and orientation. The process can either use the current camera position (e.g., GPS metadata) or control points for georeferencing. The next step is the reconstruction phase. The reconstruction framework is defined by these properties: spatial reference system, region-of-interest, tiling, retouching, and processing settings. Based on this process, several runs can be launched to generate a final deliverable. There are three ways to represent the reconstructed model using the ContextCapture software: 3D mesh model (e.g., 3MX Autodesk F8X, Google Earth KML), point cloud (LAS, POD) and orthomosaic and digital terrain model (TIFF, JPEG) (BENTLEY SYSTEMS, 2019).

- The computer used in the reconstructions has the following configurations:
- CPU: Intel Core i7-7700 CPU @ 3.60GHz
- GPU: Intel HD Graphics 630
- RAM: 8,00 GB
- Storage: SSD 256GB (LITEON CV3-8D256-11 SATA 256GB - 500MB/s reading and 360MB/s writing)

4.2.3. Case study

Two commercial-scale PV power plants are inspected to validate the proposed method. Figure 4-4 shows a flowchart with the framework overview used to evaluate the faults in the case study and to create an orthophoto with the plant defects. The acquired aIRT images of the power plants are pre-processed to pass through the Mask-RCNN model with the pre-trained weights. This process will generate masks of the faults of each sample in the data. The masks are then transferred back to the original aIRT images. Here, we imprint them as green segments with 10% of transparency.

If necessary, these images must be once more correlated to their GPS data since the masking of faults process removes this information from the images. After that, they can be processed with an orthomosaicking algorithm, which in this paper is carried out through the ContextCapture software. In this case, it does not require GPS data for processing the samples. Other software such as DroneDeploy require the GPS data on the images and therefore this previous step is important. The resulting orthophoto contains the overview of the power plant and the highlighted faults.
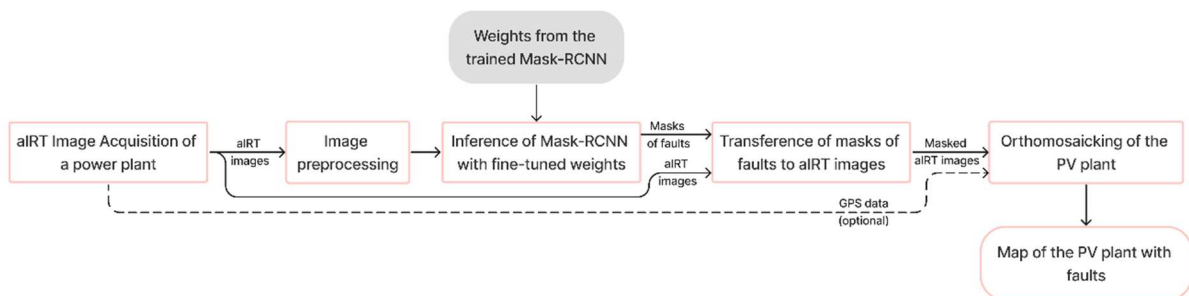
Figure 4-4 - Flowchart of the proposed method to automatically detect faults in PV power plants.

4.2.3.1. Sites description

Images acquired at a 3 MW PV power plant for research and development (R&D) in the South of Brazil (Test Case #1, at coordinates 28° South, 49° West) which were used to test the developed method. Fig. 5 shows a photograph of the fully monitored PV power plant, which consists of three different PV technologies divided

into blocks of 1 MW each. At the back of the photograph, next to the wind turbine, the plant's multi-crystalline silicon (mc-Si) portion is the focus of this work, with 4,199 Yingli Solar 245Wp mc-Si PV modules. The PV modules are fixed on ground-mounted racks tilted at 30 degrees, facing true North. The plant, test case #1 has a ground-mounted fixed structure facing northeast, tilted at 30°. It was installed in 2014 and damaged in 2016 because of the effects of an extreme meteorological condition (OLIVEIRA *et al.*, 2018). The damaged modules were replaced right after the incident.

Figure 4-5 - The 3 MW R&D utility-scale PV power plant in the South of Brazil which was used as Test Case #1 to validate the method proposed here.

Test Case #2 is a 400 kW PV power plant located in Northeast Brazil. The PV plant has been operating since 2014 and has 1,644 mc-Si modules installed in a ground-mounted fixed structure facing northeast, tilted at 15°.

4.2.3.2. Images Acquisition

The images acquired for the test case are frames of videos and photos captured using the same UAV (Matrice 200) equipped with the IRT camera (Zenmuse XT2). Flight procedures and environmental conditions were determined according to the standard IEC TS 62446-3 (INTERNATIONAL ELECTROTECHNICAL

COMMISSION (IEC), 2017), and the altitudes of the flights varied from 30 to 40 m. The flight settings were established using the DJI Pilot software. The route was set for an overlapping of 80%, according to the thermal camera's optical characteristics.

4.3. RESULTS

4.3.1. Automatic fault detection algorithm,

Several tests were carried out adjusting the hyperparameters of the Mask-RCNN network and adjusting the format of the annotation of the dataset. The best results obtained using the algorithm with the validation dataset (10% of the total number of samples) reached an AP of 90.5% and F1-score of 69.0%. Considering the small dataset used for training, these values are reasonable and can be improved by adding more samples.

Some false positives resulting from the algorithm included objects around the power plant, like cars and electrical components. Figure 4-6 presents an example of false detection in a vehicle and electrical box cover. This problem can be solved by adding images containing this type of object in the training set to show the algorithm that these are not PV modules.
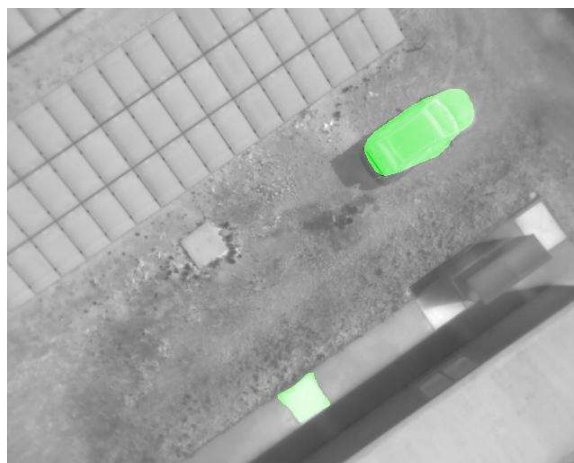
Figure 4-6 -Examples of false positives detected in aerial imagery of a car and an electrical box cover.

For testing purposes, one flight was carried out with the camera at a 0-degree angle, not facing the modules perpendicularly. As expected (KRENZINGER; DE ANDRADE, 2007), the consequence was the reflection of the sunlight interfering with the images. Those images were also processed in the algorithm to evaluate the robustness of the fault detection method. Unfortunately, it detected the sunlight as a fault (Figure 4-7(a)) or even overshadowed other defects because of its high-temperature intensity (Figure 4-7(b)). These problems could be avoided using techniques for reflection removal, such as the one described in (Computer vision tool for detection, mapping, and fault classification of photovoltaics modules in aerial IR videosBOMMES *et al.*, 2021). As already demonstrated in (OLIVEIRA *et al.*, 2021), the Sun's reflection is also a challenge for orthomosaic reconstruction, as it changes position between photos or frames, making it difficult for the software to find key points between images. Figure 4-8 shows an example of thermal orthophoto reconstruction that presents many errors because the Sun's reflection keeps repeating itself along the pictures. In the software ContextCapture, these reflections can be eliminated by adding "Masks" that highlight the parts of the image that should not be considered for the orthomosaic. Other software, e.g., DroneDeploy, has pre-processing algorithms that eliminate these problems (OLIVEIRA *et al.*, 2021).
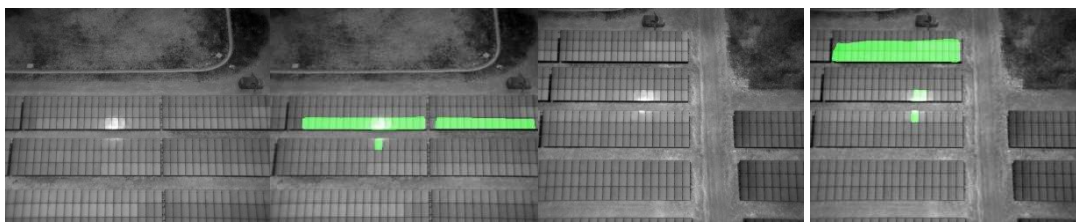
(a)   (b)

Figure 4-7 -Examples of erroneous results caused by Sun reflection over PV modules.
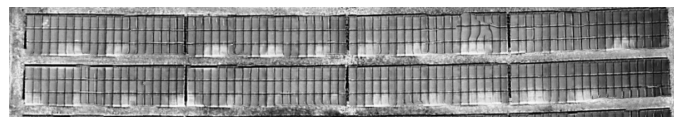
Figure 4-8 -Example of thermal orthophoto showing problems caused by Sun reflections.

In general, the major challenge of converting images into an orthomosaic is the software's ability to find key points among the photos. Because of that, it is fundamental that the faults are detected consistently in all images used for the reconstruction. However, with the small changes in the camera's focus and the image's brightness during the flight, variations in the algorithms' results are expected.

To tackle this problem, a tentative pre-processing of the dataset was carried out using the histogram equalization technique. The method aims to normalize the intensities of pixels among all the images to obtain a standard contrast along the samples. Some examples of results showing the effect of this pre-process are demonstrated in Figure 4-9. The equalization helped the algorithm to detect some of the open strings in the images, as indicated in Figure 4-9(a), where the histogram equalization enables the code to see the open string in the upper left corner. However, the process increases the number of false positives of the algorithm, especially in the case of modules with hot spots (as shown in Figure 4-9(b)). This is explained by the increase in the contrast inside the module, which turns any small tone change into a hot spot. The resulting F1-score using the pre-processing technique reached half the value of the results without it. Given these results, the histogram equalization step is not recommended.

(a)
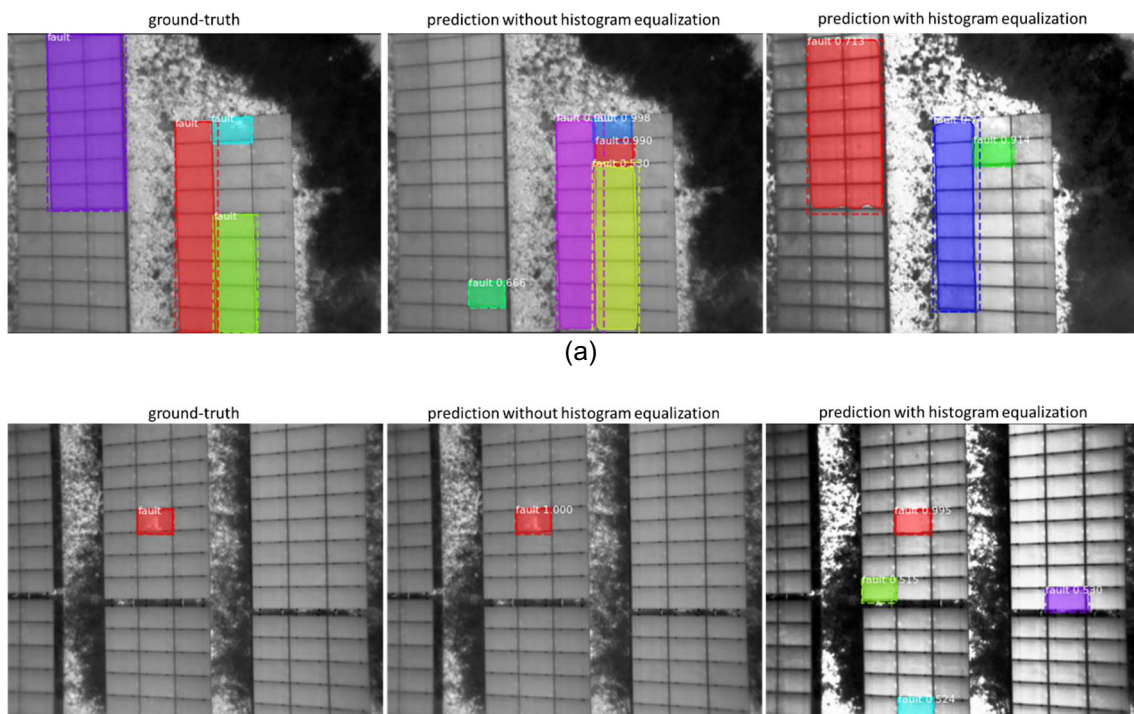
(b)
Figure 4-9 -Examples of the effect of histogram equalization of the samples in the results.

The proposed method could detect the faults in several data collection situations, including different directions of rows of modules. It had increased accuracy for hot spots, detecting them in different situations. Figure 4-10 presents one of these examples, where the algorithm could see the same hot spots in images of different days (5 months apart) under distinct environmental conditions. The angle of both images is also different and the photo on the right is taken at an altitude 5 m higher than the one on the left. Even then, the hot spot could be detected in both situations. The same does not happen for the disconnected string.
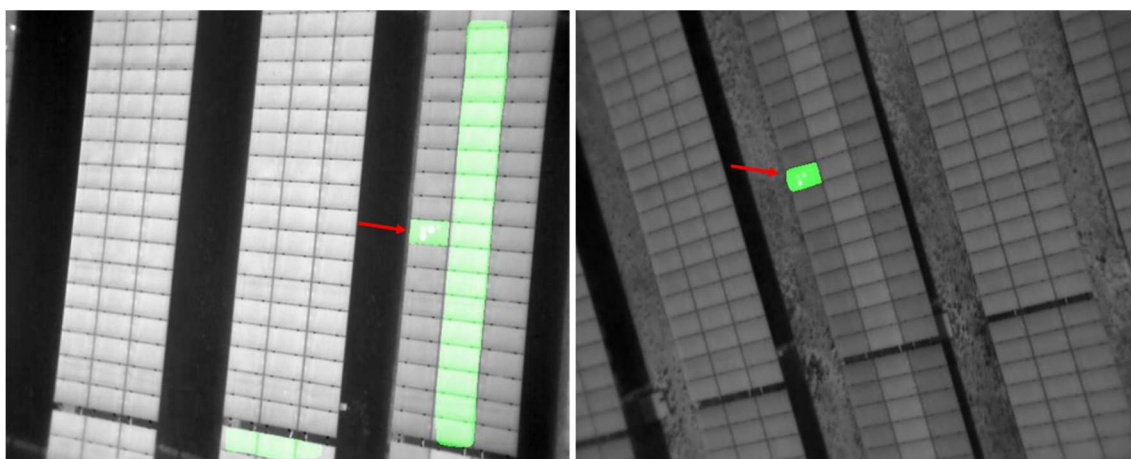
Figure 4-10 -The same hot spot detected in different aIRT flights acquired in different weather conditions and at different heights.

However, accuracy improved for faults that would appear fully on the image. Figure 4-11 presents 3 frames of an aIRT video containing detected and undetected hot spots. In the pictures, the defects are indicated with arrows, and the same color of arrow is used to indicate the same fault in a subsequent frame. As the defects move in the screen, the algorithm continues to detect them, as long as the whole module appears on the viewport of the image.

This type of failure is easily spotted because it generates a "brighter" hot spot, due to the higher temperatures involved. This allows the defect to be detected from altitudes higher than 50 m. Figure 3-10 (b) also presents a module with broken glass, but in this case, only some cells in the PV module are hotter than the others and the

temperature difference is much smaller (around 4 K), which makes detection more difficult. Figure 3-10 (c) shows a hot spot that revealed a delamination point in the PV module. This fault is much harder to be detected because of the small size and small temperature difference (less than 7 K).
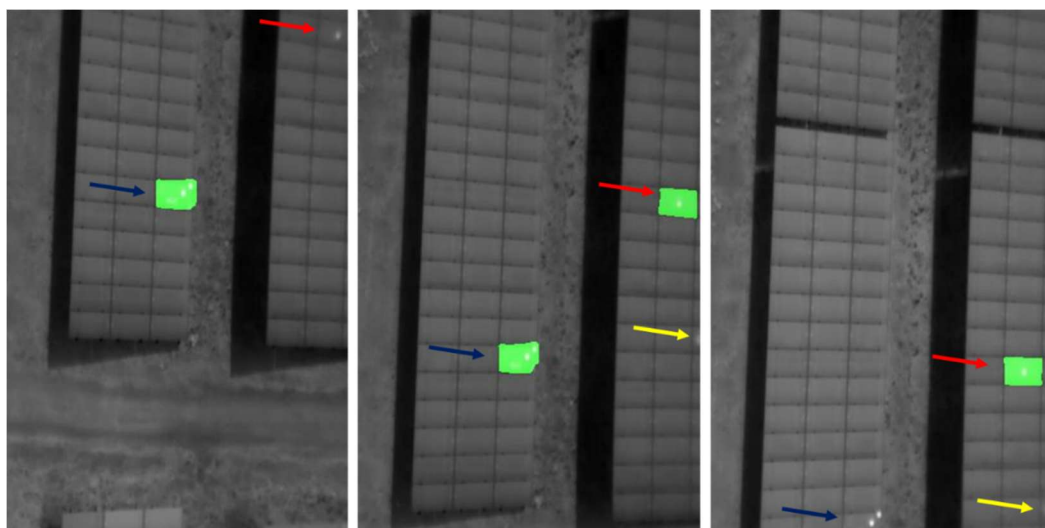
Figure 4-11 -Three frames of an aIRT video presenting detected and undetected hot spots in crystalline Si PV modules.

For the case of disconnected strings, as the faults are larger, images that comprise the whole defect are rare. Also, this defect highly depends on the contrast with other modules and panels to be detected, even by a human annotator. For these reasons, the detection accuracy of disconnected strings was much lower than that for seeing hot spots. Figure 4-12 shows examples of false detections, misdetections, and detections with erroneous shapes of disconnected strings. Because of the problems with this type of fault, the training dataset was re-annotated to remove disconnected strings. In this way, hot spots can be detected with higher accuracy. For clarity purposes, the initial dataset was labeled Dataset A and the one without disconnected strings was labeled Dataset B. The results of this test are presented in the following subsection. The accuracy of detecting short-circuited strings was also low due to the small number of samples of this type of fault in the training dataset. Because the patchwork pattern that identifies this image is similar to several hotspots in the modules, short circuits were kept in Dataset B.

(a)   (b)   (c)
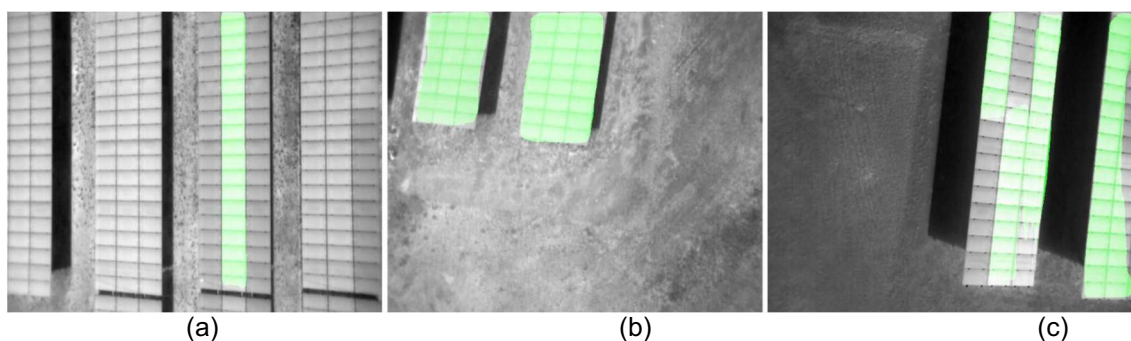
Figure 4-12 -Disconnected strings in aIRT images with erroneous detection results (painted light green): (a) shows a large number of disconnected strings (light gray in the image), but only one was detected by the algorithm (light green), (b) presents two connect panels that are detected as disconnected because of the lack of contrast with other panels and (c) presents some detected open strings, but the detection masks have irregular shapes.

4.3.2. Producing a PV plant orthomap with module faults

In order to transform the masked aIRT images into orthomaps with the software ContextCapture, different datasets were tested for both Test Cases #1 and #2. The best results were obtained using frames of aIRT videos recorded during the flights. The Zenmuse XT2 camera mounted on the UAV records videos at a frame rate of 8 Hz. Because the velocity of the flights was low (under 3 m/s), not all frames were necessary for the reconstruction. One of the tests performed consisted of comparing the effect of using two different dataset sizes for the method. Figure 4-13 and Table 4-2 show the results of this comparison. The figure shows two of the orthomosaics obtained for Test Case #1, using different sizes of datasets. The original video had around 4 minutes and, therefore, 1953 frames. The images show two tests carried out: one with 1/3 of the initial amount of frames (651 frames) and one with a sixth of the number of frames of the original video (325 frames). Tests with less than 300 frames could not produce a full orthomap.

The results show that both images are similar, differing in tone and some of the detected faults. Table 4-2 shows the difference in processing time between both tests and the detected faults, presenting true positives (TP) and false negatives (FN) of each type of fault.
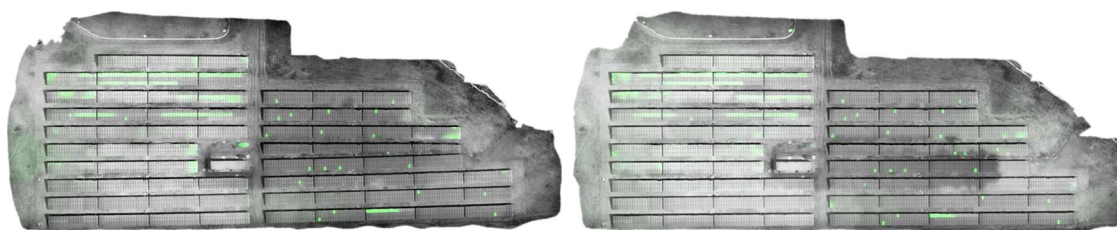
Figure 4-13 -Example of PV plant orthophoto of Test Case #1 with two sizes of datasets: 651 images (left) and 325 images (right).

Table 4-2 - Comparison of results with different sizes of datasets in Test Case #1.

No. of Images	Size of Orthomap (MP)	Processing time					Disconnected Strings			Hot Spots		Short-circuits		
		Inference	*Triangulation*	*Reconstruction*	*Total time*	*Time/image*	TP	PTP	FN	TP	FN	TP	FN	FP
651	213.3	1 h 34 min 43 s	11 min 34 s	29 min 40 s	2 h 15 min 57 s	12.5 s	8	8	8	21	7	0	1	7
325	106.5	48 min 51 s	4 min 51 s	17 min 16 s	1h 10 min 58 s	13.10 s	9	6	9	24	4	0	1	12

For the detection of disconnected strings, results of partial true positives (PTP), to describe open strings that are only partially highlighted. False positives are also presented in the table, including some erroneously highlighted modules and objects around the power plant that were marked as faults. The table shows that, in general, the results of the processing of a smaller dataset generated better results. One possible explanation is that with fewer pictures of the same fault, the distortions due to the lack of consistency of the algorithm are smaller. This result shows that more data will not necessarily improve the orthomap, but uniformity among the images. The results also corroborate the previously explained challenges of detecting open strings and short circuits.

Regarding the processing time, for the inference step, the tests were carried out using the platform Google Colab, whose processing capabilities vary along with the availability of the resources. In general, each image takes up to 9 seconds to be processed. This processing time does not change significally when using local computer resources. For the aerotriangulation and orthomap reconstruction steps, the computer caracteristics used for the processing are described in the method section, which is not a high-end equipment. Results shows that the required time is not proportional to the number of images processed. With that, reducing the dataset size in half does not necessarily mean reducing the processing time in half as well. However, the reduction of computer resources and the improvement in the results are significant.

The challenge of detecting disconnected strings also appeared in Test Case #2. Because of the effect shown in Figure 4-12(b), many false positives of open strings appear at the end of the panels, as shown in the left side of Figure 4-14. To avoid this effect, a mask filter was implemented, removing segments of faults larger than 25% of the picture. The results for this test case are shown on the right side of Figure 4-14. The highlighted part shows a zoomed image of one of the most affected parts of the left image. Table 4-3 also shows the quantitative results. The FP was reduced; however, the number of non-detected disconnected strings and hot spots increased minimally. Another way to mitigate this effect would be to increase the margin of the flight around the power plant. In this way, fewer images would be taken at the panels' borders, and fewer distortions would occur.
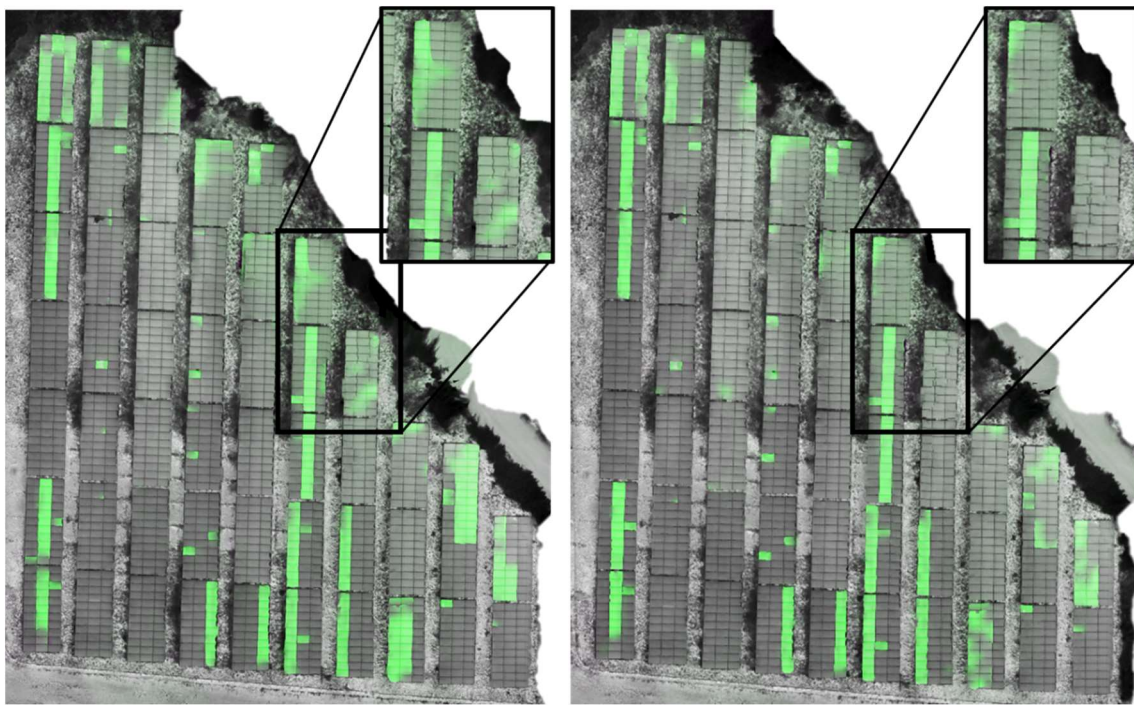
Figure 4-14 -Example of PV plant orthophoto of Test Case #2 without any filter for large faults (left) and with a filter to retain large masks (right).

Table 4-3 - Comparison of results of Test Case #2 with and without mask filter.

Mask Filter	Disconnected Strings			Disconnected Substrings		Hot Spots		Short-circuits		
	TP	PTP	FN	TP	FN	TP	FN	TP	FN	FP
No	14	6	1	2	1	27	2	0	0	11
Yes	12	8	1	2	1	26	8	0	0	8

As explained previously, an alternative way of improving the results was to train the DL algorithm with Dataset B (without disconnected strings). The results are shown in Figure 4-15 for test cases #1 (left) and #2 (right). Table 4-4 presents the quantitative results of these tests. It is visible that the FP highly decreased, and the precision of the detected hot spots increased. For Test Case #2, when detecting hot spots, the algorithm did not see less than 8.8% of the faults, proving to be adequately accurate for detecting this kind of fault. In Test Case #1, false negatives amounted to 14.3%. In this power plant, the algorithm could also partially detect the short-circuited string, which was detected as many PV modules with hot spots. Still, the number of false positives is significant, including a vehicle in Test Case #1, leading to the unnecessary task of extra checking work in the field.
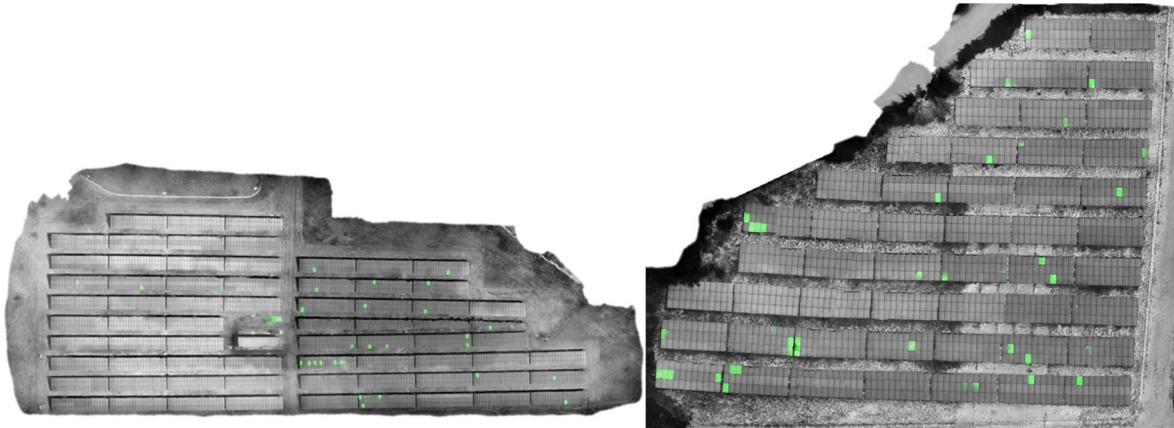
Figure 4-15 -Example of PV plant orthophoto of Test Case #1 (left) and #2 (right) trained with Dataset B.

Table 4-4 - Comparison of results of Test Cases #1 and #2 trained with Dataset B.

Test Case #	Disconnected Substrings		Hot Spots		Short-circuits			
	TP	FN	TP	FN	TP	PTP	FN	FP
1	2	1	24	4	0	1	0	1
2	2	1	31	3	0	0	0	6

4.4. DISCUSSION AND LIMITATIONS

The results were very promising in obtaining a satisfactory overview of the faults in the PV power plants with relatively low computational cost and time. Carrying out inspections in the field, under the sunlight in clear sky days in warm climates is exhausting. Therefore, quick methods to facilitate the work in the field are essential.

Another challenge in remote areas, where PV power plants are usually installed, is the access to high-performance computers and internet connection. The method proposed in this paper offers a feasible way to overcome these challenges.

The test sites where the method was tested are small-scale commercial power plants, and the amount of data and flight duration to cover the whole PV system were considerably small. However, the proposed method is scalable and replicable, so it can be expanded and applied in larger PV plants. It is recommended to discretize the acquired data into smaller blocks to reduce computational requirements.

This work is indicative of the feasibility of the proposed method, but there are several ways to improve the accuracy of the results. Using other software for the orthomosaic reconstruction part is one of these ways. There are many alternatives for the orthomosaicking process, including some open-source algorithms, such as OpenDroneMap (HIGUCHI; BABASAKI, 2018). This step can be improved by using the images' GPS data and a UAV with a high-precision RTK (Real Time Kinematic) positioning module.

The fault detection algorithm could also be improved by expanding the training dataset, including different layouts of power plants. Algorithms can also be implemented to remove the Sun's reflection and to remove false positives of objects around the power plant. The greatest challenge to be overcome is the detection of disconnected strings. This type of fault is extremely common and represents a significant loss of energy production (OLIVEIRA *et al.*, 2020). However, as it is usually easily detected by the monitoring system of the power plant, the algorithm could focus only on seeing hot spots and other types of faults.

4.5. CONCLUSIONS

This paper presented a framework to combine DL algorithms with orthomosaic techniques to create an orthomap of a PV power plant that automatically highlights the faults detected with aIRT. The results demonstrated that the proposed method effectively facilitates the localization of failures and defects in aerial inspections of PV power plants. Especially in the case of detecting hot spots and disconnected substrings, the processing tool proved to have high accuracy, in a quicker way, with

low computational resources required. Even with small datasets, it was possible to visually detect the different faults in the thermal orthomosaics produced.

Detecting disconnected strings and short circuits remains a challenge, given the size of the faults, which are typically more extensive than the viewport of the aIRT images and depend on the contrast with other photos to be detected.

5. CONCLUSIONS

The results of this work contribute to the development of the aIRT inspection technique, mainly in the context of Brazilian PV plants. First, the literature review presented in the first published paper provided an overview of the different algorithms used to automate the many parts of the inspection process and provided a clear understanding of the most common and effective methods to be employed and further developed.

The results of the inspections carried out in Brazil, and presented in the second published paper, are also significant because they show the most common failures that can happen at the beginning of the operation of PV plants. From these results, operators can decide how to solve and avoid these problems, maximizing the time of PV operation of utility-scale plants. Furthermore, these problems' technical and economic impacts on the PV system operator were presented. The produced images created an dataset that can be used to train ML algorithms focusing on Brazilian PV power plants.

Finally, in the third paper, currently under review, this thesis provided an innovative approach combining a DL algorithm with mosaicking techniques to offer a simple and effective way to detect and locate faults in PV plants using aIRT automatically. This method is innovative for the novel combination of DL and photogrammetry techniques and for training an instance segmentation network using data collected in Brazil. This is relevant because the country is subject to specific environmental conditions such as high irradiance and temperature and particular layout conditions that are not widespread in countries that have previously developed aIRT datasets, namely Europe and Asia. Therefore, developing automation algorithms with local datasets is extremely valuable and can be enhanced with a larger dataset to improve aIRT inspection across the country.

5.1. LIMITATIONS

This work has a few limitations specifically reported below to enable better replications and validations of the outcomes:

- The literature review focused on papers published until the time of submission of the review article (December of 2021) and on works that use algorithms to automatize aerial aIRT inspections, not including advancements in other inspection techniques such as electroluminescence and ultraviolet fluorescence.

- The results of the flight campaign published in the second paper are based on inspections held in Brazil during the commissioning phase of the PV plants under study. Therefore, the conclusions may not be replicable in older power plants and inspections held in other countries and conditions.

- The method proposed provides excellent accuracy for detecting hot spots in PV modules. However, detecting disconnected strings and short circuits is still a challenge and needs further improvement. This type of fault is widespread and represents a significant loss of energy production, although it is easily detected through supervisory systems.

- The dataset used for the algorithm's training was produced using data acquired in power plants in Brazil, including the layouts, type of soiling and environmental conditions of the local PV plants. Because of domain shift, it is important to expand the training dataset to implement this algorithm in other places.

- The validation of the proposed method was carried out for two small-scale PV plants. To expand the practice and apply it in larger PV plants, it is recommended to discretize the acquired data into smaller blocks to reduce computational requirements.

5.2. RECOMMENDATIONS FOR FUTURE DEVELOPMENTS

Given the limitations and opportunities highlighted by this work, some recommendations for future work are provided:

- This work indicates the feasibility of the proposed method, but there are several ways to improve the accuracy of the results.

Using other software or developing specific algorithms for the orthomosaic reconstruction part are some of these ways. There are many alternatives for the orthomosaicking process, including some open-source algorithms, such as OpenDroneMap (HIGUCHI; BABASAKI, 2018). This step can be improved by using the images' GPS data and a UAV with a high-precision RTK (Real Time Kinematic) positioning module.

- The fault detection algorithm could also be improved by expanding the training dataset, including different layouts of power plants. Algorithms can also be implemented to remove the Sun's reflection and false positives of objects around the power plant.

- The greatest challenge to be overcome by the method is the detection of disconnected strings. This type of fault is widespread and represents a significant energy production loss; therefore, its detection should be further investigated.

- In future work, to facilitate the visualization of the faults, it is suggested that the same orthomap is produced using visual images by correlating the location of the defects in the aIRT images with the visual images already taken at the same time.

- Future work should also explore the potential of combining Building Information Modelling tools (e.g. Revit) with aerial inspections data in order to obtain a virtual map of the site that allows the following up of the power plant along its operation time.

- The dataset used for training the algorithm should be further explored to contemplate datasets from diferent geographical regions and conditions. The exchange of data and academic collaborations are necessary to allow a fully automatic procedure to detect modules and faults on PV modules in different weather and layout conditions.

In conclusion, the technique of aIRT inspections is a promissing subject for increasing the uptime of PV power plants and is under the attention of academia and

the industry. The automatization of the technique is a fundamental issue and offers plenty of research and improvement opportunities.

REFERENCES

ABDULLA, W. **Mask R-CNN for object detection and instance segmentation on Keras and TensorFlow**. [*S. l.*]: Github, 2017.

ABSOLAR. **Panorama da solar fotovoltaica no Brasil e no mundo - Infográfico no. 48**. [*S. l.: s. n.*], 2022. Disponível em: https://www.absolar.org.br/mercado/infografico/. Acesso em: 2 nov. 2022.

ABUBAKAR, A.; MESCHINI ALMEIDA, C. F.; GEMIGNANI, M. A review of solar photovoltaic system maintenance strategies. *In*: 2021 14TH IEEE INTERNATIONAL CONFERENCE ON INDUSTRY APPLICATIONS, INDUSCON 2021 - PROCEEDINGS, 2021, [*s. l.*], . **Anais** [...]. [*S. l.*]: Institute of Electrical and Electronics Engineers Inc., 2021. p. 1400–1407.

ADDABBO, P.; ANGRISANO, A.; BERNARDI, M. L.; GAGLIARDE, G.; MENNELLA, A.; NISI, M.; ULLO, S. L. UAV system for photovoltaic plant inspection. **IEEE Aerospace and Electronic Systems Magazine**, [*s. l.*], v. 33, n. 8, p. 58–67, 2018. Disponível em: https://ieeexplore.ieee.org/document/8425583/.

AGÊNCIA NACIONAL DE ENERGIA ELÉTRICA (ANEEL). **Results of Generation Auction in the Regulated Environment**. [*S. l.: s. n.*], 2020. Disponível em: https://app.powerbi.com/view?r=eyJrIjoiZTZiNDhjNjctZTQ2NC00YzFmLTgxYTUtZm Y5YjEzNmI3MjdkIiwidCI6IjQwZDZmOWI4LWVjYTctNDZhMi05MmQ0LWVhNGU5Yz AxNzBlMSIsImMiOjR9. Acesso em: 2 jun. 2020.

AGÊNCIA NACIONAL DE ENERGIA ELÉTRICA (ANEEL). **Sistema de Informações de Geração (SIGA)**. [*S. l.: s. n.*], 2021. Disponível em: https://www.aneel.gov.br/siga. Acesso em: 11 jul. 2021.

AGHAEI, M. **Novel methods in control and monitoring of photovoltaic systems**. 2016. - Politecnico di Milano, [*s. l.*], 2016.

AGHAEI, M.; GRIMACCIA, F.; GONANO, C. A.; LEVA, S. Innovative Automated Control System for PV Fields Inspection and Remote Control. **IEEE Transactions on Industrial Electronics**, [*s. l.*], v. 62, n. 11, p. 7287–7296, 2015. Disponível em: http://ieeexplore.ieee.org/document/7230283/.

AGHAEI, M.; LEVA, S.; GRIMACCIA, F. PV power plant inspection by image mosaicing techniques for IR real-time images. **2017 IEEE 44th Photovoltaic Specialist Conference, PVSC 2017**, Portland, OR, USAp. 3462–3467, 2017. Disponível em: http://ieeexplore.ieee.org/document/7750236/.

AGHAEI, M.; OLIVEIRA, A. K. V.; RÜTHER, R. Fault Inspection by Aerial Infrared Thermography in a PV Plant after a Meteorological Tsunami. **Revista Brasileira de Energia Solar**, [*s. l.*], v. 10, n. 1, p. 17–25, 2019.

AGHAEI, M.; QUATER, P. B.; GRIMACCIA, F.; LEVA, S.; MUSSETTA, M. Unmanned

Aerial Vehicles in Photovoltaic Systems Monitoring Applications. **29th European Photovoltaic Solar Energy Conference and Exhibition (EU PVSEC 2014)**, [*s. l.*], n. 22-26 September, p. 2734–2739, 2014.

AHMED, W.; HANIF, A.; KALLU, K. D.; KOUZANI, A. Z.; ALI, M. U.; ZAFAR, A. Photovoltaic panels classification using isolated and transfer learned deep neural models using infrared thermographic images. **Sensors**, [*s. l.*], v. 21, n. 16, p. 1–14, 2021.

AKRAM, M. W. W.; LI, G.; JIN, Y. Y.; CHEN, X.; ZHU, C.; AHMAD, A. Automatic detection of photovoltaic module defects in infrared images with isolated and develop-model transfer deep learning. **Solar Energy**, [*s. l.*], v. 198, n. January, p. 175–186, 2020. Disponível em: https://doi.org/10.1016/j.solener.2020.01.055.

ALAJMI, M.; AWEDAT, K.; ALDEEN, M. S.; ALWAGDANI, S. IR thermal image analysis: An efficient algorithm for accurate hot-spot fault detection and localization in solar photovoltaic systems. *In*: IEEE INTERNATIONAL CONFERENCE ON ELECTRO INFORMATION TECHNOLOGY, 2019, [*s. l.*], . **Anais** [...]. [*S. l.*]: IEEE, 2019. p. 162–168. Disponível em: https://ieeexplore.ieee.org/document/8833855/.

ALFARO-MEJÍA, E.; LOAIZA-CORREA, H.; FRANCO-MEJÍA, E.; HERNÁNDEZ-CALLEJO, L. Segmentation of Thermography Image of Solar Cells and Panels. **Communications in Computer and Information Science**, [*s. l.*], v. 1152 CCIS, p. 1–8, 2020.

ALSAFASFEH, M.; ABDEL-QADER, I.; BAZUIN, B.; ALSAFASFEH, Q.; SU, W. Unsupervised fault detection and analysis for large photovoltaic systems using drones and machine vision. **Energies**, [*s. l.*], v. 11, n. 9, p. 1–18, 2018.

AMSTAD, D.; OLIVEIRA, A. K. V. de; HÄBERLE, A.; RÜTHER, R. Fault Inspection of CIGS PV Plant using Aerial Infrared Thermography. *In*: 36TH EUROPEAN PHOTOVOLTAIC SOLAR ENERGY CONFERENCE AND EXHIBITION (EU PVSEC), 2019, Marseille, France. **Anais** [...]. Marseille, France: [*s. n.*], 2019. p. 1569–1574. Disponível em: www.fotovoltaica.ufsc.br.

ARAICA, A.; RUÍZ, B. Performance of a Module and Defect Detection Algorithm for Aerial Infrared Images as a Function of the Flying Altitude. *In*: 32ND EUROPEAN PHOTOVOLTAIC SOLAR ENERGY CONFERENCE AND EXHIBITION, 2015, [*s. l.*], . **Anais** [...]. [*S. l.: s. n.*], 2015. p. 54–67. Disponível em: http://repositorio.unan.edu.ni/2986/1/5624.pdf.

ARENELLA, A.; GRECO, A.; SAGGESE, A.; VENTO, M. **Real time fault detection in photovoltaic cells by cameras on drones**. [*S. l.: s. n.*], 2017. 2017.v. 10317 LNCS. Disponível em: http://link.springer.com/10.1007/978-3-319-59876-5_68.

AROSH, S.; GHOSH, K.; PRAKASH, S.; DUTTAGUPTA, S. P. Development of Robust Algorithm for Autonomous System Health Monitoring of Ultra Large Scale Based Solar Farm. *In*: 33RD EUROPEAN PHOTOVOLTAIC SOLAR ENERGY CONFERENCE AND EXHIBITION, 2017, [*s. l.*], . **Anais** [...]. [*S. l.: s. n.*], 2017. p. 2413–2417.

BADRA, M. **Confira as 5 maiores usinas fotovoltaicas do Brasil**. [*S. l.: s. n.*], 2021. Disponível em: https://canalsolar.com.br/confira-as-5-maiores-usinas-fotovoltaicas-do-brasil/. Acesso em: 2 nov. 2022.

BAIG, H. R.; MURTAZA, A. F.; SALMAN, M. Recognition of Faulty Modules in a Photovoltaic Array Using Image Processing Techniques. **IEEEP NEW HORIZONS JOURNAL**, [*s. l.*], v. Vol No 97-, p. 22–27, 2018.

BALASUBRAMANI, G.; THANGAVELU, V.; CHINNUSAMY, M.; SUBRAMANIAM, U.; PADMANABAN, S.; MIHET□POPA, L. Infrared thermography based defects testing of solar photovoltaic panel with fuzzy rule□based evaluation. **Energies**, [*s. l.*], v. 16, n. 3, 2020.

BENTLEY SYSTEMS. **ContextCapture User Manual**. [*S. l.: s. n.*], 2019. Disponível em: https://docs.bentley.com/LiveContent/web/ContextCapture Help-v10/en/GUID-1D6739CD-B03D-4AFE-B6FA-6AF73D5476E1.html. .

BIZZARRI, F.; NITTI, S.; MALGAROLI, G. The use of drones in the maintenance of photovoltaic fields. **E3S Web of Conferences**, [*s. l.*], v. 119, p. 1–5, 2019.

BOMMES, L. **Grid-Annotation-Tool**. [*S. l.*]: GitHub, 2021. Disponível em: https://github.com/LukasBommes/Grid-Annotation-Tool. Acesso em: 8 nov. 2022.

BOMMES, L.; HOFFMANN, M.; BUERHOP-LUTZ, C.; PICKEL, T.; HAUCH, J.; BRABEC, C.; MAIER, A.; PETERS, I. M. Anomaly Detection in IR Images of PV Modules using Supervised Contrastive Learning. [*s. l.*], 2021. Disponível em: http://arxiv.org/abs/2112.02922.

BOMMES, L.; PICKEL, T.; BUERHOP-LUTZ, C.; HAUCH, J.; BRABEC, C.; PETERS, I. M. I. M. Computer vision tool for detection, mapping, and fault classification of photovoltaics modules in aerial IR videos. **Progress in Photovoltaics: Research and Applications**, [*s. l.*], v. 29, n. 12, p. 1236–1251, 2021.

BRAGA, M.; DO NASCIMENTO, L. R.; RÜTHER, R. Spectral modeling and spectral impacts on the performance of mc-Si and new generation CdTe photovoltaics in warm and sunny climates. **Solar Energy**, [*s. l.*], v. 188, p. 976–988, 2019. Disponível em: https://linkinghub.elsevier.com/retrieve/pii/S0038092X19306474.

BRAZILIAN MINISTRY OF MINES AND ENERGY. **Photovoltaic projects on energy auctions - Characteristics of PV projects on auctions from 2013 to 2018**. [*S. l.: s. n.*], 2018. Disponível em: http://www.epe.gov.br/sites-en/publicacoes-dados-abertos/publicacoes/PublicacoesArquivos/publicacao-184/EPE_DEE_NT_091_2018_r0 (English).pdf. Acesso em: 30 maio 2019.

BUERHOP-LUTZ, C.; PICKEL, T.; SCHEUERPFLUG, H.; DÜRSCHNER, C.; CAMUS, C.; HAUCH, J.; BRABEC, C. J. aIR-PV-Check of Thin-Film PV-Plants – Detection of PID and Other Defects in CIGS Modules. **32nd European Photovoltaic Solar Energy Conference and Exhibition**, [*s. l.*], p. 2021–2026, 2016.

BUERHOP, C.; BOMMES, L.; SCHLIPF, J.; PICKEL, T.; FLADUNG, A.; PETERS, I. M. Infrared imaging of photovoltaic modules: a review of the state of the art and future challenges facing gigawatt photovoltaic power stations. **Progress in Energy**, [*s. l.*], v. 4, n. 4, p. 042010, 2022.

BUERHOP, C.; JAHN, U.; HOYER, U.; LERCHER, B.; WITTMANN, S. **Abschlussbericht Machbarkeitsstudie Überprüfung der Qualität von Photovoltaik- Modulen mittels Infrarot-Aufnahmen**. [*S. l.: s. n.*], 2007.

BUERHOP, C.; PICKEL, T.; DALSASS, M.; SCHEUERPFLUG, H.; CAMUS, C.; BRABEC, C. J. AIR-PV-check: A quality inspection of PV-power plants without operation interruption. *In*: 2016 IEEE 43RD PHOTOVOLTAIC SPECIALISTS CONFERENCE (PVSC), 2016, Portland, OR, USA. **Anais** [...]. Portland, OR, USA: [*s. n.*], 2016. p. 1677–1681.

BUERHOP, Cl; SCHLEGEL, D.; NIESS, M.; VODERMAYER, C.; WEISSMANN, R.; BRABEC, C. J. Reliability of IR-imaging of PV-plants under operating conditions. **Solar Energy Materials and Solar Cells**, [*s. l.*], v. 107, p. 154–164, 2012. Disponível em: http://dx.doi.org/10.1016/j.solmat.2012.07.011.

BUERHOP, Claudia; WEISSMANN, R.; SCHEUERPFLUG, H.; AUER, R.; BRABEC, C. Quality Control of PV-Modules in the Field Using a Remote-Controlled Drone with an Infrared Camera. *In*: 27TH EUROPEAN PHOTOVOLTAIC SOLAR ENERGY CONFERENCE AND EXHIBITION, 2012, [*s. l.*], . **Anais** [...]. [*S. l.: s. n.*], 2012. p. 3370–3373.

CAMILO, J.; WANG, R.; COLLINS, L. M.; BRADBURY, K.; MALOF, J. M. Application of a semantic segmentation convolutional neural network for accurate automatic detection and mapping of solar photovoltaic arrays in aerial imagery. *In*: 2017 IEEE APPLIED IMAGERY PATTERN RECOGNITION (AIPR) WORKSHOP, 2018, [*s. l.*], . **Anais** [...]. [*S. l.: s. n.*], 2018. Disponível em: http://arxiv.org/abs/1801.04018.

CARLETTI, V.; GRECO, A.; SAGGESE, A.; VENTO, M. An intelligent flying system for automatic detection of faults in photovoltaic plants. **Journal of Ambient Intelligence and Humanized Computing**, [*s. l.*], v. 11, n. 5, p. 2027–2040, 2020. Disponível em: http://dx.doi.org/10.1007/s12652-019-01212-6.

CARNEIRO, A. C.; SILVA, R. R. V. Redes Neurais Convolucionais com Tensorflow: Teoria e Prática. *In*: III ESCOLA REGIONAL DE INFORMÁTICA DO PIAUÍ, 2017, [*s. l.*], . **Anais** [...]. [*S. l.: s. n.*], 2017. p. 382–406.

CIOACA, C.; POP, S.; BOSCOIANU, E. C.; BOSCOIANU, M. Aerial Infrared Thermography: A Scalable Procedure for Photovoltaics Inspections Based on Efficiency and Flexibility. **Applied Mechanics and Materials**, [*s. l.*], v. 772, n. July, p. 546–551, 2015.

CIPRIANI, G.; D'AMICO, A.; GUARINO, S.; MANNO, D.; TRAVERSO, M.; DI DIO, V. Convolutional neural network for dust and hotspot classification in PV modules. **Energies**, [*s. l.*], v. 13, n. 23, 2020.

COSTA, M. V. C. V. M. V. C. V. da; CARVALHO, O. L. F. de O. L. F.; ORLANDI, A. G. A. G.; HIRATA, I.; ALBUQUERQUE, A. O. A. O. de; SILVA, F. V. e. F. V.; GUIMARÃES, R. F. R. F.; GOMES, R. A. T. R. A. T.; JÚNIOR, O. A. C. O. A. de C. Remote sensing for monitoring photovoltaic solar plants in brazil using deep semantic segmentation. **Energies**, [*s. l.*], v. 14, n. 10, p. 1–15, 2021.

DA COSTA, C. H.; MORITZ, G. L.; LAZZARETTI, A. E.; MULINARI, B. M.; ANCELMO, H. C.; RODRIGUES, M. P.; OROSKI, E.; DE GOES, R. E. A Comparison of Machine Learning-Based Methods for Fault Classification in Photovoltaic Systems. *In*: 2019 IEEE PES INNOVATIVE SMART GRID TECHNOLOGIES CONFERENCE - LATIN AMERICA (ISGT LATIN AMERICA), 2019, [*s. l.*], . **Anais** [...]. [*S. l.*]: IEEE, 2019. p. 1–6. Disponível em: https://ieeexplore.ieee.org/document/8895279/.

DENIO, H. Aerial solar Thermography and condition monitoring of photovoltaic systems. *In*: 2012 38TH IEEE PHOTOVOLTAIC SPECIALISTS CONFERENCE, 2012, [*s. l.*], . **Anais** [...]. [*S. l.*]: IEEE, 2012. p. 000613–000618. Disponível em: http://ieeexplore.ieee.org/document/6317686/.

DHIMISH, M.; BADRAN, G. Photovoltaic Hot-Spots Fault Detection Algorithm Using Fuzzy Systems. **IEEE Transactions on Device and Materials Reliability**, [*s. l.*], v. 19, n. 4, p. 671–679, 2019.

DÍAZ, J. J. V.; VLAMINCK, M.; LEFKADITIS, D.; VARGAS, S. A. O.; LUONG, H. Solar panel detection within complex backgrounds using thermal images acquired by uavs. **Sensors (Switzerland)**, [*s. l.*], v. 20, n. 21, p. 1–16, 2020.

DING, Y.; CAO, R.; LIANG, S.; QI, F.; YANG, Q.; YAN, W. Density-Based Optimal UAV Path Planning for Photovoltaic Farm Inspection in Complex Topography. *In*: 2020 CHINESE CONTROL AND DECISION CONFERENCE (CCDC), 2020, [*s. l.*], . **Anais** [...]. [*S. l.*]: IEEE, 2020. p. 3931–3936. Disponível em: https://ieeexplore.ieee.org/document/9164257/.

DOLL, B.; PICKEL, T.; SCHREER, O.; ZETZMANN, C.; TEUBNER, J.; BUERHOP, C.; HAUCH, J.; CAMUS, C.; BRABEC, C. J. High through-put, outdoor characterization of silicon photovoltaic modules by moving electroluminescence measurements. *In*: INFRARED SENSORS, DEVICES, AND APPLICATIONS VIII, 2018, [*s. l.*], . **Anais** [...]. [*S. l.: s. n.*], 2018.

DOTENCO, S.; DALSASS, M.; WINKLER, L.; WURZNER, T.; BRABEC, C.; MAIER, A.; GALLWITZ, F.; WÜRZNER, T.; BRABEC, C.; MAIER, A.; GALLWITZ, F.; BAYERN, Z. A. E. Automatic detection and analysis of photovoltaic modules in aerial infrared imagery. *In*: 2016 IEEE WINTER CONFERENCE ON APPLICATIONS OF COMPUTER VISION, WACV 2016, 2016, [*s. l.*], . **Anais** [...]. [*S. l.*]: IEEE, 2016. p. 1–9. Disponível em: http://ieeexplore.ieee.org/document/7477658/.

DU, B.; HE, Y. Y.; HE, Y. Y.; DUAN, J.; ZHANG, Y. Intelligent Classification of Silicon Photovoltaic Cell Defects Based on Eddy Current Thermography and Convolution Neural Network. **IEEE Transactions on Industrial Informatics**, [*s. l.*], v. 16, n. 10, p. 6242–6251, 2020.

DUNDERDALE, C.; BRETTENNY, W.; CLOHESSY, C.; VAN DYK, E. E.; DYK, E. E. Photovoltaic defect classification through thermal infrared imaging using a machine learning approach. **Progress in Photovoltaics: Research and Applications**, [*s. l.*], v. 28, n. 3, p. 177–188, 2020. Disponível em: https://onlinelibrary.wiley.com/doi/abs/10.1002/pip.3191.

ELMOKADEM, T.; SAVKIN, A. V. Towards fully autonomous UAVs: A survey. **Sensors**, [*s. l.*], v. 21, n. 18, 2021.

ERGÜZEN, A.; SAIT, M. Using Image Processing Techniques for Automated Detection and Annotation of Faulty Regions in Thermal Infrared Images of PV Modules. **International Journal of Trend in Scientific Research and Development**, [*s. l.*], v. 4, n. 1, p. 892–895, 2019. Disponível em: https://www.ijtsrd.com/papers/ijtsrd29749.pdf%0Ahttps://www.ijtsrd.com/papers/ijtsrd 29749.pdf.

ESKANDARI, A.; AGHAEI, M.; MILIMONFARED, J.; NEDAEI, A. A weighted ensemble learning-based autonomous fault diagnosis method for photovoltaic systems using genetic algorithm. **International Journal of Electrical Power & Energy Systems**, [*s. l.*], v. 144, p. 108591, 2023. Disponível em: https://linkinghub.elsevier.com/retrieve/pii/S0142061522005877.

ET-TALEBY, A.; BOUSSETTA, M.; BENSLIMANE, M. Faults detection for photovoltaic field based on k-means, elbow, and average silhouette techniques through the segmentation of a thermal image. **International Journal of Photoenergy**, [*s. l.*], v. 2020, 2020.

FERNÁNDEZ, A.; USAMENTIAGA, R.; DE ARQUER, P.; FERNÁNDEZ, M. Á.; FERNÁNDEZ, D.; CARÚS, J. L. J. L.; FERNÁNDEZ, M. Robust detection, classification and localization of defects in large photovoltaic plants based on unmanned aerial vehicles and infrared thermography. **Applied Sciences (Switzerland)**, [*s. l.*], v. 10, n. 17, 2020.

FERRARA, C.; PHILIPP, D. Why do PV modules fail?. **Energy Procedia**, [*s. l.*], v. 15, n. 2011, p. 379–387, 2012. Disponível em: http://dx.doi.org/10.1016/j.egypro.2012.02.046.

FONSECA ALVES, R. H. R. H.; DEUS JÚNIOR, G. A. D. G. A. de; MARRA, E. G. E. G.; LEMOS, R. P. R. P. Automatic fault classification in photovoltaic modules using Convolutional Neural Networks. **Renewable Energy**, [*s. l.*], v. 179, p. 502–516, 2021. Disponível em: https://doi.org/10.1016/j.renene.2021.07.070.

GALLARDO-SAAVEDRA, S.; HERNÁNDEZ-CALLEJO, L.; DUQUE-PEREZ, O. Technological review of the instrumentation used in aerial thermographic inspection of photovoltaic plants. **Renewable and Sustainable Energy Reviews**, [*s. l.*], v. 93, n. May, p. 566–579, 2018. Disponível em: https://doi.org/10.1016/j.rser.2018.05.027.

GAO, X.; MUNSON, E.; ABOUSLEMAN, G. P.; SI, J. Automatic solar panel recognition and defect detection using infrared imaging. **Automatic Target Recognition XXV**, [*s.*

l.], v. 9476, n. May 2015, p. 94760O, 2015.

GENG, Q.; ZHOU, Z.; CAO, X. Survey of recent progress in semantic image segmentation with CNNs. **Science China Information Sciences**, [*s. l.*], v. 61, n. 5, p. 1–18, 2018.

GERD IMENES, A.; SAAD NOORI, N.; ANDREAS NESVAG UTHAUG, O.; KRONI, R.; BIANCHI, F.; BELBACHIR, N.; IMENES, A. G.; NOORI, N. S.; ANDREAS, O.; UTHAUG, N.; KRÖNI, R.; BIANCHI, F. A Deep Learning Approach for Automated Fault Detection on Solar Modules Using Image Composites. *In*: IEEE 48TH PHOTOVOLTAIC SPECIALISTS CONFERENCE (PVSC), 2021, [*s. l.*], . **Anais** [...]. [*S. l.: s. n.*], 2021. p. 1925–1930.

GIRARD, N.; TARABALKA, Y. End-to-end learning of polygons for remote sensing image classification. **International Geoscience and Remote Sensing Symposium (IGARSS)**, [*s. l.*], v. 2018-July, n. July, p. 2083–2086, 2018.

GOLOVKO, V.; KROSHCHANKA, A.; BEZOBRAZOV, S.; SACHENKO, A.; KOMAR, M.; NOVOSAD, O. Development of Solar Panels Detector. *In*: 2018 INTERNATIONAL SCIENTIFIC-PRACTICAL CONFERENCE ON PROBLEMS OF INFOCOMMUNICATIONS SCIENCE AND TECHNOLOGY, PIC S AND T 2018 - PROCEEDINGS, 2019, [*s. l.*], . **Anais** [...]. [*S. l.: s. n.*], 2019. p. 761–764.

GONZALEZ, R.; WOODS, R. **Digital image processing**. [*S. l.: s. n.*] 2002. Disponível em: http://mirror.klaus-uwe.me/ctan/biblio/bibtex/contrib/persian-bib/Persian-bib-userguide.pdf%5Cnhttp://ftp.neu6.edu.cn/mirrors/CTAN/biblio/bibtex/contrib/persian-bib/Persian-bib-userguide.pdf.

GRECO, A.; PIRONTI, C.; SAGGESE, A.; VENTO, M.; VIGILANTE, V. A deep learning based approach for detecting panels in photovoltaic plants. *In*: PROCEEDINGS OF THE 3RD INTERNATIONAL CONFERENCE ON APPLICATIONS OF INTELLIGENT SYSTEMS, 2020, New York, NY, USA. **Anais** [...]. New York, NY, USA: ACM, 2020. p. 1–7. Disponível em: https://dl.acm.org/doi/10.1145/3378184.3378185.

GRIMACCIA, F.; AGHAEI, M.; MUSSETTA, M.; LEVA, S.; QUATER, P. B. Planning for PV plant performance monitoring by means of unmanned aerial systems (UAS). **International Journal of Energy and Environmental Engineering**, [*s. l.*], v. 6, n. 1, p. 47–54, 2015. Disponível em: http://link.springer.com/10.1007/s40095-014-0149-6.

GRIMACCIA, F.; LEVA, S.; DOLARA, A.; AGHAEI, M. Survey on PV Modules' Common Faults After an O&M Flight Extensive Campaign Over Different Plants in Italy. **IEEE Journal of Photovoltaics**, [*s. l.*], v. 7, n. 3, p. 810–816, 2017. Disponível em: http://ieeexplore.ieee.org/document/7879865/.

GRIMACCIA, F.; LEVA, S.; NICCOLAI, A. PV plant digital mapping for modules' defects detection by unmanned aerial vehicles. **IET Renewable Power Generation**, [*s. l.*], v. 11, n. 10, p. 1221–1228, 2017. Disponível em: http://digital-library.theiet.org/content/journals/10.1049/iet-rpg.2016.1041.

GUERRIERO, P.; CUOZZO, G.; DALIENTO, S. Health diagnostics of PV panels by means of single cell analysis of thermographic images. *In*: 2016 IEEE 16TH INTERNATIONAL CONFERENCE ON ENVIRONMENT AND ELECTRICAL ENGINEERING (EEEIC), 2016, [*s. l.*], . **Anais** [...]. [*S. l.*]: IEEE, 2016. p. 1–6. Disponível em: http://ieeexplore.ieee.org/document/7555516/.

HANAFY, W. A.; PINA, A.; SALEM, S. A. Machine learning approach for photovoltaic panels cleanliness detection. *In*: ICENCO 2019 - 2019 15TH INTERNATIONAL COMPUTER ENGINEERING CONFERENCE: UTILIZING MACHINE INTELLIGENCE FOR A BETTER WORLD, 2019, [*s. l.*], . **Anais** [...]. [*S. l.: s. n.*], 2019. p. 72–77.

HAQUE, A.; BHARATH, K. V. S. K. V. S.; KHAN, M. A. M. A.; KHAN, I.; JAFFERY, Z. A. Z. A. Z. A. Fault diagnosis of Photovoltaic Modules. **Energy Science and Engineering**, [*s. l.*], v. 7, n. 3, p. 622–644, 2019.

HENRY, C.; POUDEL, S.; LEE, S.-W. S.-W. S.-W. S.-W.; JEONG, H. Automatic Detection System of Deteriorated PV Modules Using Drone with Thermal Camera. **Applied Sciences**, [*s. l.*], v. 10, n. 11, p. 3802, 2020. Disponível em: https://www.mdpi.com/2076-3417/10/11/3802.

HIGUCHI, Y.; BABASAKI, T. Failure detection of solar panels using thermographic images captured by drone. **7th International IEEE Conference on Renewable Energy Research and Applications, ICRERA 2018**, [*s. l.*], v. 5, p. 391–396, 2018.

HØIAAS, I.; GRUJIC, K.; IMENES, A. G.; BURUD, I.; OLSEN, E.; BELBACHIR, N. Inspection and condition monitoring of large-scale photovoltaic power plants: A review of imaging technologies. **Renewable and Sustainable Energy Reviews**, [*s. l.*], v. 161, n. February, p. 112353, 2022. Disponível em: https://doi.org/10.1016/j.rser.2022.112353.

HUERTA HERRAIZ, Á.; PLIEGO MARUGÁN, A.; GARCÍA MÁRQUEZ, F. P. F. P. Photovoltaic plant condition monitoring using thermal images analysis by convolutional neural network-based structure. **Renewable Energy**, [*s. l.*], v. 153, p. 334–348, 2020.

HWANG, H. P.-C.; KU, C. C.-Y.; CHAN, J. C.-C. Detection of malfunctioning photovoltaic modules based on machine learning algorithms. **IEEE Access**, [*s. l.*], v. 9, p. 37210–37219, 2021.

INTERNATIONAL ELECTROTECHNICAL COMMISSION (IEC). **IEC TS 62446-3 - Photovoltaic (PV) systems - Requirements for testing, documentation and maintenance - Part 3: Photovoltaic modules and plants - Outdoor infrared thermography**. Geneva: [*s. n.*], 2017.

IRENA. **Boosting Solar PV Markets: The Role of Quality Infrastructure**. Abu Dhabi: [*s. n.*], 2017.

IRENA. **Renewable Capacity Statistics 2022**. Abu Dhabi: The International Renewable Energy Agency, 2022. 2022. Disponível em: www.irena.org.

IRENA. **World Energy Transitions Outlook 2022: 1.5°C Pathway**. Abu Dhabi: International Renewable Energy Agency, 2022. 2022.

ISMAIL, H.; RAHMANI, A.; ALJASMI, N.; QUADIR, J. Stitching approach for PV panel detection. *In*: 2020 ADVANCES IN SCIENCE AND ENGINEERING TECHNOLOGY INTERNATIONAL CONFERENCES, ASET 2020, 2020, [*s. l.*], . **Anais** [...]. [*S. l.: s. n.*], 2020. p. 29–32.

J. VANEK; REPKO, I.; KLIMA, J.; PEROUTKA, T. Automatic Detection of Defective Solar Modules by Thermovision. **32nd European Photovoltaic Solar Energy Conference and Exhibition**, [*s. l.*], p. 1689–1699, 2016.

JAFFERY, Z. A. Z. A. Z. A.; DUBEY, A. K. A. K.; IRSHAD; HAQUE, A. Scheme for predictive fault diagnosis in photo-voltaic modules using thermal imaging. **Infrared Physics and Technology**, [*s. l.*], v. 83, n. April, p. 182–187, 2017. Disponível em: http://dx.doi.org/10.1016/j.infrared.2017.04.015.

JÄGER-WALDAU, A. Snapshot of photovoltaics-February 2020. **Energies**, [*s. l.*], v. 13, n. 4, 2020.

JEONG, H.; KWON, G.-R.; LEE, S.-W. Deterioration Diagnosis of Solar Module Using Thermal and Visible Image Processing. [*s. l.*], p. 1–14, 2020.

JUNIOR, C. F. C. **Uso de descritores morfológicos e cinemáticos na identificação automática de comportamentos de animais de laboratório**. 2011. 137 f. - Universidade Federal de Santa Catarina, [*s. l.*], 2011.

KAMILARIS, A.; PRENAFETA-BOLDÚ, F. X. Deep Learning in Agriculture: A Survey. **Computers and Electronics in Agriculture**, [*s. l.*], v. 147, n. 1, p. 70–90, 2018.

KARAKÖSE, M.; FIRILDAK, K. A shadow detection approach based on fuzzy logic using images obtained from PV array. *In*: 6TH INTERNATIONAL CONFERENCE ON MODELING, SIMULATION, AND APPLIED OPTIMIZATION, ICMSAO 2015 - DEDICATED TO THE MEMORY OF LATE IBRAHIM EL-SADEK, 2015, [*s. l.*], . **Anais** [...]. [*S. l.: s. n.*], 2015.

KARIMI, A. M.; FADA, J. S.; LIU, J.; BRAID, J. L. J. L.; KOYUTURK, M.; FRENCH, R. H. R. H. R. H.; KOYUTÜRK, M.; FRENCH, R. H. R. H. R. H.; KOYUTURK, M.; FRENCH, R. H. R. H. R. H. Feature Extraction, Supervised and Unsupervised Machine Learning Classification of PV Cell Electroluminescence Images. **2018 IEEE 7th World Conference on Photovoltaic Energy Conversion, WCPEC 2018 - A Joint Conference of 45th IEEE PVSC, 28th PVSEC and 34th EU PVSEC**, p. 418–424, 2018.

KIM, B.; SERFA JUAN, R. O.; LEE, D.-E.; CHEN, Z. Importance of image enhancement and CDF for fault assessment of photovoltaic module using IR thermal image. **Applied Sciences (Switzerland)**, [*s. l.*], v. 11, n. 18, 2021.

KIM, D.; YOUN, J.; KIM, C. Automatic Fault Recognition of Photovoltaic Modules

Based on Statistical Analysis of UAV Thermography. **The International Archives of the Photogrammetry, Remote Sensing and Spatial Information Sciences**, [*s. l.*], v. XLII-2/W6, n. 2W6, p. 179–182, 2017. Disponível em: https://www.int-arch-photogramm-remote-sens-spatial-inf-sci.net/XLII-2-W6/179/2017/.

KIM, D.; YOUN, J.; KIM, C. Automatic Photovoltaic Panel Area Extraction from UAV Thermal Infrared Images. **Journal of the Korean Society of Surveying, Geodesy, Photogrammetry and Cartography**, [*s. l.*], v. 34, n. 6, p. 559–568, 2016. Disponível em: http://koreascience.or.kr/journal/view.jsp?kj=GCRHBD&py=2016&vnc=v34n6&sp=559.

KÖNTGES, M.; KURTZ, S.; PACKARD, C. E. C.; JAHN, U.; BERGER, K. A.; KATO, K.; FRIESEN, T.; LUI, H.; ISEGHEM, Mike Van; LIU, H.; VAN ISEGHEM, M. **IEA PVPS Subtask 3.2: Review of Failures of Photovoltaic ModulesInternation Energy Agency (IEA) Photovoltaic Power Systems Programme**. [*S. l.: s. n.*], 2014.

KRENZINGER, A.; DE ANDRADE, A. C. Accurate outdoor glass thermographic thermometry applied to solar energy devices. **Solar Energy**, [*s. l.*], v. 81, n. 8, p. 1025–1034, 2007.

KUMAR, N. M.; CHOPRA, S. S.; DE OLIVEIRA, A. K. V.; AHMED, H.; VAEZI, S.; MADUKANYA, U. E.; CASTAÑÓN, J. M. Solar PV module technologies. *In*: PHOTOVOLTAIC SOLAR ENERGY CONVERSION. [*S. l.*]: Elsevier, 2020. p. 51–78. Disponível em: https://linkinghub.elsevier.com/retrieve/pii/B978012819610600003X.

KURUKURU, V. S. B.; HAQUE, A.; TRIPATHY, A. K.; KHAN, M. A. Machine learning framework for photovoltaic module defect detection with infrared images. **International Journal of System Assurance Engineering and Management**, [*s. l.*], 2021. Disponível em: https://doi.org/10.1007/s13198-021-01544-7.

LAFKIH, S.; ZAZ, Y. Solar panel monitoring using a video frames mosaicing. **Proceedings of 2016 International Renewable and Sustainable Energy Conference, IRSEC 2016**, [*s. l.*], p. 247–250, 2017.

LE, M.; LUONG, V. S.; NGUYEN, D. K.; DAO, V.-D.; VU, N. H.; VU, H. H. T. Remote anomaly detection and classification of solar photovoltaic modules based on deep neural network. **Sustainable Energy Technologies and Assessments**, [*s. l.*], v. 48, p. 101545, 2021. Disponível em: https://linkinghub.elsevier.com/retrieve/pii/S2213138821005579.

LEE, D. H.; PARK, J. H. Developing inspection methodology of solar energy plants by thermal infrared sensor on board unmanned aerial vehicles. **Energies**, [*s. l.*], v. 12, n. 15, 2019.

LEVA, S.; AGHAEI, M.; GRIMACCIA, F. PV power plant inspection by UAS : Correlation between altitude and detection of defects on PV modules. *In*: ENVIRONMENT AND ELECTRICAL ENGINEERING (EEEIC), 2015 IEEE 15TH INTERNATIONAL CONFERENCE ON, 2015, Rome, Italy. **Anais** [...]. Rome, Italy:

IEEE, 2015.

LI, Q.; FENG, Y.; LENG, Y.; CHEN, D. SolarFinder: automatic detection of solar photovoltaic arrays. *In*: PROCEEDINGS - 2020 19TH ACM/IEEE INTERNATIONAL CONFERENCE ON INFORMATION PROCESSING IN SENSOR NETWORKS, IPSN 2020, 2020, [*s. l.*], . **Anais** [...]. [*S. l.: s. n.*], 2020. p. 193–204.

LI, X.; LI, W.; YANG, Q.; YAN, W.; ZOMAYA, A. Y. A. Y. Edge Computing Enabled Unmanned Module Defect Detection and Diagnosis System for Large-scale Photovoltaic Plants. **IEEE Internet of Things Journal**, [*s. l.*], v. 4662, n. c, p. 1–1, 2020.

LI, X.; LI, W.; YANG, Q.; YAN, W.; ZOMAYA, A. Y.; MEMBER, S.; YANG, Q.; MEMBER, S.; YAN, W.; ZOMAYA, A. Y. An Unmanned Inspection System for Multiple Defects Detection in Photovoltaic Plants. **IEEE Journal of Photovoltaics**, [*s. l.*], v. 10, n. 2, p. 568–576, 2020. Disponível em: https://ieeexplore.ieee.org/document/8945396/.

LI, X.; YANG, Q.; LOU, Z.; YAN, W. Deep Learning Based Module Defect Analysis for Large-Scale Photovoltaic Farms. **IEEE Transactions on Energy Conversion**, [*s. l.*], v. 34, n. 1, p. 520–529, 2019. Disponível em: https://ieeexplore.ieee.org/document/8478340/.

LI, Q.; YU, K.; CHEN, D. SolarDiagnostics: Automatic damage detection on rooftop solar photovoltaic arrays. **Sustainable Computing: Informatics and Systems**, [*s. l.*], v. 32, p. 100595, 2021. Disponível em: https://linkinghub.elsevier.com/retrieve/pii/S2210537921000834.

LIAO, K. C.; LU, J. H. Using Matlab real-time image analysis for solar panel fault detection with UAV. **Journal of Physics: Conference Series**, [*s. l.*], v. 1509, n. 1, p. 012010, 2020. Disponível em: https://iopscience.iop.org/article/10.1088/1742-6596/1509/1/012010.

LIAO, K. C.; LU, J. H. Using UAV to detect solar module fault conditions of a solar power farm with ir and visual image analysis. **Applied Sciences (Switzerland)**, [*s. l.*], v. 11, n. 4, p. 1–21, 2021.

LIN, J.; JIANHUI, S.; XIN, L. Hot spots detection of operating PV arrays through IR thermal image using method based on curve fitting of gray histogram. *In*: MATEC WEB OF CONFERENCES, 2016, [*s. l.*], . **Anais** [...]. [*S. l.: s. n.*], 2016.

LIN, T. Y.; MAIRE, M.; BELONGIE, S.; HAYS, J.; PERONA, P.; RAMANAN, D.; DOLLÁR, P.; ZITNICK, C. L. Microsoft COCO: Common objects in context. **Lecture Notes in Computer Science (including subseries Lecture Notes in Artificial Intelligence and Lecture Notes in Bioinformatics)**, [*s. l.*], v. 8693 LNCS, n. PART 5, p. 740–755, 2014.

LÓPEZ-FERNÁNDEZ, L.; LAGÜELA, S.; FERNÁNDEZ, J.; GONZÁLEZ-AGUILERA, D. Automatic evaluation of photovoltaic power stations from high-density RGB-T 3D

point clouds. **Remote Sensing**, [*s. l.*], v. 9, n. 6, p. 1–19, 2017.

LUO, X.; LI, X.; YANG, Q.; WU, F.; ZHANG, D.; YAN, W.; XI, Z. Optimal path planning for UAV based inspection system of large-scale photovoltaic farm. **Proceedings - 2017 Chinese Automation Congress, CAC 2017**, [*s. l.*], v. 2017-Janua, p. 4495–4500, 2017.

MALOF, J. M.; BRADBURY, K.; COLLINS, L. M.; NEWELL, R. G. A Deep Convolutional Neural Network and a Random Forest Classifier for Solar Photovoltaic Array Detection in Aerial Imagery. **International Conference on Renewable Energy Research and Applications (ICRERA)**, [*s. l.*], v. 5, p. 650–654, 2016.

MANNO, D.; CIPRIANI, G.; CIULLA, G.; DI DIO, V.; GUARINO, S.; LO BRANO, V. Deep learning strategies for automatic fault diagnosis in photovoltaic systems by thermographic images. **Energy Conversion and Management**, [*s. l.*], v. 241, n. May, p. 114315, 2021. Disponível em: https://doi.org/10.1016/j.enconman.2021.114315.

MAYER, K.; WANG, Z.; ARLT, M. L.; NEUMANN, D.; RAJAGOPAL, R. DeepSolar for Germany: A deep learning framework for PV system mapping from aerial imagery. **SEST 2020 - 3rd International Conference on Smart Energy Systems and Technologies**, [*s. l.*], 2020.

MAYO, R. C.; LEUNG, J. Artificial intelligence and deep learning – Radiology's next frontier? **Clinical Imaging**, [*s. l.*], v. 49, n. July 2017, p. 87–88, 2018. Disponível em: https://doi.org/10.1016/j.clinimag.2017.11.007.

MEHTA, S.; AZAD, A. P.; CHEMMENGATH, S. A.; RAYKAR, V.; KALYANRAMAN, S. DeepSolarEye: Power Loss Prediction and Weakly Supervised Soiling Localization via Fully Convolutional Networks for Solar Panels. *In*: WACV 2018, 2017, [*s. l.*], . **Anais** [...]. [*S. l.: s. n.*], 2017. Disponível em: http://arxiv.org/abs/1710.03811.

MENÉNDEZ, O.; GUAMÁN, R.; PÉREZ, M.; CHEEIN, F. A. F. A. Photovoltaic modules diagnosis using artificial vision techniques for artifact minimization. **Energies**, [*s. l.*], v. 11, n. 7, 2018.

MONTANEZ, L. E.; VALENTIN-CORONADO, L. M.; MOCTEZUMA, D.; FLORES, G. Photovoltaic module segmentation and thermal analysis tool from thermal images. **arXiv**, [*s. l.*], n. Ropec, 2020.

MONTOYA, J. C. J. C.; MUÑOZ, C. Q. G. C. Q. G.; MÁRQUEZ, F. P. G. F. P. G. **Remote condition monitoring for photovoltaic systems**. [*S. l.*]: Elsevier Ltd., 2019. 2019. Disponível em: https://doi.org/10.1016/B978-0-08-101094-5.00009-5.

MORADI SIZKOUHI, A.; AGHAEI, M.; ESMAILIFAR, S. M. A deep convolutional encoder-decoder architecture for autonomous fault detection of PV plants using multi-copters. **Solar Energy**, [*s. l.*], v. 223, n. September 2020, p. 217–228, 2021. Disponível em: https://doi.org/10.1016/j.solener.2021.05.029.

MORADI SIZKOUHI, A. M.; MAJID ESMAILIFAR, S.; AGHAEI, M.; DE OLIVEIRA, A.

K. V.; RÜTHER, R. Autonomous Path Planning by Unmanned Aerial Vehicle (UAV) for Precise Monitoring of Large-Scale PV plants. *In*: 2019 IEEE 46TH PHOTOVOLTAIC SPECIALISTS CONFERENCE (PVSC), 2019, Chicago, IL, USA. **Anais** [...]. Chicago, IL, USA: IEEE, 2019. p. 1398–1402. Disponível em: https://ieeexplore.ieee.org/document/8980862/.

MORAGUEZ, M.; TRUJILLO, A.; DE WECK, O.; SIDDIQI, A. Convolutional Neural Network for Detection of Residential Photovoltalc Systems in Satellite Imagery. **International Geoscience and Remote Sensing Symposium (IGARSS)**, [*s. l.*], p. 1600–1603, 2020.

MUHAMMAD, B.; PRASAD, R.; NISI, M.; MENNELLA, A.; GAGLIARDE, G.; CIANCA, E.; MARENCHINO, D.; ANGRISANO, A.; BERNARDI, M.; ADDABBO, P.; ULLO, S. Automating the maintenance of photovoltaic power plants. *In*: 2017 GLOBAL WIRELESS SUMMIT (GWS), 2017, [*s. l.*], . **Anais** [...]. [*S. l.*]: IEEE, 2017. p. 6–11. Disponível em: http://ieeexplore.ieee.org/document/8300492/.

NAJIAH NURUL AFIFAH, A.; INDRABAYU; SUYUTI, A.; SYAFARUDDIN. A New Approach for Hot Spot Solar Cell Detection based on Multi-level Otsu Algorithm. **Proceedings - 2021 International Seminar on Intelligent Technology and Its Application: Intelligent Systems for the New Normal Era, ISITIA 2021**, [*s. l.*], p. 278–282, 2021.

NASCIMENTO, L. R. do; DE SOUZA VIANA, T.; CAMPOS, R. A.; RÜTHER, R. Extreme solar overirradiance events: Occurrence and impacts on utility-scale photovoltaic power plants in Brazil. **Solar Energy**, [*s. l.*], v. 186, n. January, p. 370–381, 2019. Disponível em: https://doi.org/10.1016/j.solener.2019.05.008.

NATARAJAN, K.; KUMAR, B. P.; KUMAR, V. S. Fault detection of solar PV system using SVM and thermal image processing. **International Journal of Renewable Energy Research**, [*s. l.*], v. 10, n. 2, p. 967–977, 2020.

NDIAYE, A.; CHARKI, A.; KOBI, A.; KÉBÉ, C. M. F.; NDIAYE, P. A.; SAMBOU, V. Degradations of silicon photovoltaic modules: A literature review. **Solar Energy**, [*s. l.*], v. 96, p. 140–151, 2013.

NGO, G. C. G. C.; MACABEBE, E. Q. B. E. Q. B. Image segmentation using K-means color quantization and density-based spatial clustering of applications with noise (DBSCAN) for hotspot detection in photovoltaic modules. *In*: 2016 IEEE REGION 10 CONFERENCE (TENCON), 2016, [*s. l.*], . **Anais** [...]. [*S. l.*]: IEEE, 2016. p. 1614–1618. Disponível em: http://ieeexplore.ieee.org/document/7848290/.

NIAZI, K.; AKHTAR, W.; KHAN, H. A. A.; SOHAIB, S.; NASIR, A. K. K. Binary Classification of Defective Solar PV Modules Using Thermography. *In*: 2018 IEEE 7TH WORLD CONFERENCE ON PHOTOVOLTAIC ENERGY CONVERSION (WCPEC) (A JOINT CONFERENCE OF 45TH IEEE PVSC, 28TH PVSEC & 34TH EU PVSEC), 2018, [*s. l.*], . **Anais** [...]. [*S. l.*]: IEEE, 2018. p. 0753–0757. Disponível em: https://ieeexplore.ieee.org/document/8548138/.

NIAZI, K. A. K.; AKHTAR, W.; KHAN, H. A.; YANG, Y.; ATHAR, S. Hotspot diagnosis for solar photovoltaic modules using a Naive Bayes classifier. **Solar Energy**, [*s. l.*], v. 190, n. February, p. 34–43, 2019. Disponível em: https://doi.org/10.1016/j.solener.2019.07.063.

NICCOLAI, A.; GANDELLI, A.; GRIMACCIA, F.; ZICH, R.; LEVA, S. Overview on Photovoltaic Inspections Procedure by means of Unmanned Aerial Vehicles. *In*: 2019 IEEE MILAN POWERTECH, 2019, [*s. l.*], . **Anais** [...]. [*S. l.*]: IEEE, 2019. p. 1–6. Disponível em: https://ieeexplore.ieee.org/document/8810987/.

NICCOLAI, A.; GRIMACCIA, F.; LEVA, S. Advanced asset management tools in photovoltaic plant monitoring: UAV-based digital mapping. **Energies**, [*s. l.*], v. 12, n. 24, 2019.

NIE, J.; LUO, T.; LI, H. Automatic hotspots detection based on UAV infrared images for large-scale PV plant. **Electronics Letters**, [*s. l.*], v. 56, n. 19, p. 993–995, 2020.

O'MAHONY, N.; CAMPBELL, S.; CARVALHO, A.; HARAPANAHALLI, S.; HERNANDEZ, G. V.; KRPALKOVA, L.; RIORDAN, D.; WALSH, J. Deep Learning vs. Traditional Computer Vision. **Advances in Intelligent Systems and Computing**, [*s. l.*], v. 943, n. Cv, p. 128–144, 2020.

OLIVEIRA, A. K. V.; AGHAEI, M.; MADUKANYA, U. E.; NASCIMENTO, L.; RÜTHER, R. Aerial Infrared Thermography of a Utility-Scale PV Plant After a Meteorological Tsunami in Brazil. *In*: 2018 IEEE 7TH WORLD CONFERENCE ON PHOTOVOLTAIC ENERGY CONVERSION (WCPEC) (A JOINT CONFERENCE OF 45TH IEEE PVSC, 28TH PVSEC & 34TH EU PVSEC), 2018, Waikoloa Village, HI, USA. **Anais** [...]. Waikoloa Village, HI, USA: IEEE, 2018. p. 0684–0689. Disponível em: https://ieeexplore.ieee.org/document/8548019/.

OLIVEIRA, A. K. V.; AGHAEI, M.; RÜTHER, R. Aerial infrared thermography for low-cost and fast fault detection in utility-scale PV power plants. **Solar Energy**, [*s. l.*], v. 211, n. September, p. 712–724, 2020. Disponível em: https://doi.org/10.1016/j.solener.2020.09.066.

OLIVEIRA, A. K. V.; AGHAEI, M.; RÜTHER, R. Automatic Fault Detection of Photovoltaic Array by Convolutional Neural Networks During Aerial Infrared Thermography. *In*: 36TH EUROPEAN PHOTOVOLTAIC SOLAR ENERGY CONFERENCE AND EXHIBITION (EU PVSEC), 2019, Marseille, France. **Anais** [...]. Marseille, France: [*s. n.*], 2019. p. 1302–1307. Disponível em: https://www.researchgate.net/publication/335950307.

OLIVEIRA, A. K. V. de; AGHAEI, M.; RÜTHER, R. Automatic Inspection of Photovoltaic Power Plants Using Aerial Infrared Thermography: A Review. **Energies**, [*s. l.*], v. 15, n. 6, p. 2055, 2022. Disponível em: https://www.mdpi.com/1996-1073/15/6/2055. Acesso em: 11 mar. 2022.

OLIVEIRA, A. K. V. de; BEDIN, C.; XAVIER DE ANDRADE PINTO, G.; MENDES FERREIRA GOMES, A.; HOSODA SOUZA REIS, G.; NASCIMENTO, L. R. do;

RÜTHER, R. Low-Cost Aerial Electroluminescence (aEL) of PV Power Plants. **2019 IEEE 46th Photovoltaic Specialists Conference (PVSC)**, Chicago, IL, USA, p. 0532–0537, 2019. Disponível em: www.fotovoltaica.ufsc.br.

OLIVEIRA, A. K. V.; BRACHT, M. K.; MELO, A. P.; LAMBERTS, R.; RÜTHER, R. Evaluation of Faults in a Photovoltaic Power Plant using Orthomosaics based on Aerial Infrared Thermography. **Conference Record of the IEEE Photovoltaic Specialists Conference**, [*s. l.*], p. 2604–2610, 2021.

PARK, J.; LEE, D. Precise Inspection Method of Solar Photovoltaic Panel Using Optical and Thermal Infrared Sensor Image Taken by Drones. **IOP Conference Series: Materials Science and Engineering**, [*s. l.*], v. 611, n. 1, p. 012089, 2019. Disponível em: https://iopscience.iop.org/article/10.1088/1757-899X/611/1/012089.

PATEL, A. V. A. V.; MCLAUCHLAN, L.; MEHRUBEOGLU, M. Defect Detection in PV Arrays Using Image Processing. *In*: 2020 INTERNATIONAL CONFERENCE ON COMPUTATIONAL SCIENCE AND COMPUTATIONAL INTELLIGENCE (CSCI), 2020, [*s. l.*], . **Anais** [...]. [*S. l.*]: IEEE, 2020. p. 1653–1657. Disponível em: https://ieeexplore.ieee.org/document/9457905/.

PEREIRA, E. B.; MARTINS, F. R.; GONÇALVES, A. R.; COSTA, R. S.; LIMA, F. J. L. de; RÜTHER, R.; ABREU, S. L. de; TIEPOLO, G. M.; PEREIRA, S. V.; SOUZA, J. G. de. **Atlas Brasileiro de Energia Solar**. 2a. Ediçãoed. São José dos Campos: INPE, 2017. 2017. Disponível em: http://urlib.net/rep/8JMKD3MGP3W34P/3PERDJE.

PÉREZ-GONZÁLEZ, A. É.; BENÍTEZ-MONTOYA, N.; JARAMILLO-DUQUE, Á.; CANO-QUINTERO, J. B. Coverage path planning with semantic segmentation for UAV in PV plants. **Applied Sciences (Switzerland)**, [*s. l.*], v. 11, n. 24, 2021.

PEREZ, R. M.; ARIAS, J. S.; MENDEZ-PORRAS, A. Solar panels recognition based on machine learning. **Proceedings - 4th Jornadas Costarricenses de Investigacion en Computacion e Informatica, JoCICI 2019**, [*s. l.*], p. 1–5, 2019.

PIERDICCA, R.; MALINVERNI, E. S. S.; PICCININI, F.; PAOLANTI, M.; FELICETTI, A.; ZINGARETTI, P. Deep Convolutional Neural Network for Automatic Detection of Damaged Photovoltaic Cells. **ISPRS - International Archives of the Photogrammetry, Remote Sensing and Spatial Information Sciences**, [*s. l.*], v. XLII–2, n. 2, p. 893–900, 2018. Disponível em: https://www.int-arch-photogramm-remote-sens-spatial-inf-sci.net/XLII-2/893/2018/.

PILLA, M.; GALMICHE, F.; MALDAGUE, X. Thermographic inspection of cracked solar cells. *In*: PROCEEDINGS OF SPIE - THE INTERNATIONAL SOCIETY FOR OPTICAL ENGINEERING, 2002, [*s. l.*], . **Anais** [...]. [*S. l.: s. n.*], 2002. p. 699–703.

PIVEM, T.; OLIVEIRA DE ARAUJO, F. de; OLIVEIRA DE ARAUJO, L. de; DE OLIVEIRA, G. S. Application of A Computer Vision Method for Soiling Recognition in Photovoltaic Modules for Autonomous Cleaning Robots. **Signal & Image Processing : An International Journal**, [*s. l.*], v. 10, n. 03, p. 43–59, 2019.

PLATINI REGES, J.; LIMA MOREIRA, F. D. F. D.; SANTOS BEZERRA, L. D. L. D.; RIPARDO DE ALEXANDRIA, A.; REBOUCAS FILHO, P. P. P. P. Thermographic Image Processing Application in Solar Followers. **IEEE Latin America Transactions**, [*s. l.*], v. 13, n. 10, p. 3350–3358, 2015.

QASEM, H.; MNATSAKANYAN, A.; BANDA, P. Assessing dust on PV modules using image processing techniques. *In*: CONFERENCE RECORD OF THE IEEE PHOTOVOLTAIC SPECIALISTS CONFERENCE, 2016, [*s. l.*], . **Anais** [...]. [*S. l.: s. n.*], 2016. p. 2066–2070.

QI, F.; LIANG, S.; CAO, R.; DING, Y.; YANG, Q.; YAN, W. Detection and Positioning of Keypoints in Small-scale Photovoltaic System Based on Object Detection Network and Aerial Sequence Images. *In*: 2020 CHINESE CONTROL AND DECISION CONFERENCE (CCDC), 2020, [*s. l.*], . **Anais** [...]. [*S. l.*]: IEEE, 2020. p. 4795–4800. Disponível em: https://ieeexplore.ieee.org/document/9164652/.

QUATER, P. B.; GRIMACCIA, F.; LEVA, S.; MUSSETTA, M.; AGHAEI, M. Light Unmanned Aerial Vehicles (UAVs) for cooperative inspection of PV plants. **IEEE Journal of Photovoltaics**, [*s. l.*], v. 4, n. 4, p. 1107–1113, 2014.

R. RASCH, G. BEHRENS, F.U. HAMELMANN, S. HANTELMANN, R. DREIMANN, J. A. W. Automated Thermal Imaging for Fault Detection on PV Systems. *In*: 31ST EUROPEAN PHOTOVOLTAIC SOLAR ENERGY CONFERENCE AND EXHIBITION, 2015, [*s. l.*], . **Anais** [...]. [*S. l.: s. n.*], 2015. p. 2147–2149.

REGALADO, M. J. P.; RUIZ, E. O.; PINZÓN, P. J. Study of defects in PV generators using image analysis techniques with Matlab. **Renewable Energy and Power Quality Journal**, [*s. l.*], v. 1, n. 12, p. 9–14, 2014. Disponível em: http://www.icrepq.com/icrepq'14/206.14-Regalado.pdf.

REN, Y.; YU, Y.; LI, J.; ZHANG, W. Design of photovoltaic hot spot detection system based on deep learning. **Journal of Physics: Conference Series**, [*s. l.*], v. 1693, n. 1, 2020.

RICO ESPINOSA, A.; BRESSAN, M.; GIRALDO, L. F. Failure signature classification in solar photovoltaic plants using RGB images and convolutional neural networks. **Renewable Energy**, [*s. l.*], v. 162, p. 249–256, 2020. Disponível em: https://doi.org/10.1016/j.renene.2020.07.154.

ROGGI, G.; NICCOLAI, A.; GRIMACCIA, F.; LOVERA, M. A Computer Vision Line-Tracking Algorithm for Automatic UAV Photovoltaic Plants Monitoring Applications. **Energies**, [*s. l.*], v. 13, n. 4, p. 838, 2020. Disponível em: https://www.mdpi.com/1996-1073/13/4/838.

ROGOTIS, S.; IOANNIDIS, D.; TSOLAKIS, a; TZOVARAS, D.; LIKOTHANASSIS, S. Early defect diagnosis in installed PV modules exploiting spatio-temporal information from thermal images. **QIRT2014 Conférence**, [*s. l.*], 2014.

RÜTHER, R.; NASCIMENTO, L. R. do; CAMPOS, R. A. Performance assessment

issues in utility-scale photovoltaics in warm and sunny climates. **Renewable Energy and Environmental Sustainability**, [*s. l.*], v. 2, p. 35, 2017.

SALAHAT, E.; ASSELINEAU, C.-A.; COVENTRY, J.; MAHONY, R. Waypoint Planning for Autonomous Aerial Inspection of Large-Scale Solar Farms. *In*: IECON 2019 - 45TH ANNUAL CONFERENCE OF THE IEEE INDUSTRIAL ELECTRONICS SOCIETY, 2019, [*s. l.*], . **Anais** [...]. [*S. l.*]: IEEE, 2019. p. 763–769. Disponível em: https://ieeexplore.ieee.org/document/8927123/.

SALAMANCA, S.; MERCHAN, P.; GARCIA, I. On the detection of solar panels by image processing techniques. *In*: 2017 25TH MEDITERRANEAN CONFERENCE ON CONTROL AND AUTOMATION, MED 2017, 2017, [*s. l.*], . **Anais** [...]. [*S. l.: s. n.*], 2017. p. 478–483.

SALAZAR, A. M.; MACABEBE, E. Q. B. Hotspots Detection in Photovoltaic Modules Using Infrared Thermography. *In*: MATEC WEB OF CONFERENCES, 2016, [*s. l.*], . **Anais** [...]. [*S. l.: s. n.*], 2016.

SCHMIDHUBER, J. Deep Learning in Neural Networks : An Overview. [*s. l.*], p. 1–88, 2014.

SEGOVIA RAMÍREZ, I.; DAS, B.; GARCÍA MÁRQUEZ, F. P. Fault detection and diagnosis in photovoltaic panels by radiometric sensors embedded in unmanned aerial vehicles. **Progress in Photovoltaics: Research and Applications**, [*s. l.*], n. May, p. 1–17, 2021. Disponível em: https://onlinelibrary.wiley.com/doi/10.1002/pip.3479.

SERFA JUAN, R. O. R. O.; KIM, J. Photovoltaic Cell Defect Detection Model based-on Extracted Electroluminescence Images using SVM Classifier. **2020 International Conference on Artificial Intelligence in Information and Communication, ICAIIC 2020**, [*s. l.*], p. 578–582, 2020.

SHA, W.; DAI, C.; JIANG, L. Design of patrol monitoring and control system for hot spot of solar photovoltaic module. *In*: PROCEEDINGS - 2019 INTERNATIONAL CONFERENCE ON INTELLIGENT COMPUTING, AUTOMATION AND SYSTEMS, ICICAS 2019, 2019, [*s. l.*], . **Anais** [...]. [*S. l.: s. n.*], 2019. p. 668–671.

SHEN, Y. Y.; CHEN, X.; ZHANG, J.; XIE, L.; ZHANG, K.; WEI, H. **A Robust Automatic Method for Removing Projective Distortion of Photovoltaic Modules from Close Shot Images**. [*S. l.: s. n.*], 2020. 2020.v. 12305 LNCS. Disponível em: http://link.springer.com/10.1007/978-3-030-60633-6_59.

SHEN, H.; ZHU, L.; HONG, X.; CHANG, W. **ROI extraction method of infrared thermal image based on GLCM characteristic imitate gradient**. [*S. l.: s. n.*], 2017. 2017.v. 771.

SHIHAO DING ; QIANG YANG ; XIAOXIA LI ; WENJUN YAN ; WEI RUAN. Transfer Learning based Photovoltaic Module Defect Diagnosis using Aerial Images. *In*: 2018 INTERNATIONAL CONFERENCE ON POWER SYSTEM TECHNOLOGY (POWERCON), 2018, [*s. l.*], . **Anais** [...]. [*S. l.*]: IEEE, 2018. p. 4245–4250.

SIZKOUHI, A. M. M.; AGHAEI, M.; ESMAILIFAR, S. M. S. M.; MOHAMMADI, M. R. R.; GRIMACCIA, F. Automatic Boundary Extraction of Large-Scale Photovoltaic Plants Using a Fully Convolutional Network on Aerial Imagery. **IEEE Journal of Photovoltaics**, [*s. l.*], v. 10, n. 4, p. 1061–1067, 2020. Disponível em: https://ieeexplore.ieee.org/document/9095250/.

SIZKOUHI, A. M. M.; ESMAILIFAR, S. M.; AGHAEI, M.; KARIMKHANI, M. RoboPV: An integrated software package for autonomous aerial monitoring of large scale PV plants. **Energy Conversion and Management**, [*s. l.*], v. 254, p. 115217, 2022.

SOUFFER, I.; SGHIOUAR, M.; SEBARI, I.; ZEFRI, Y.; HAJJI, H.; ANIBA, G.; I., S. S.; M., S.; I., S. S.; Y., Z.; H., H.; G., A. Automatic Extraction of Photovoltaic Panels from UAV Imagery with Object-Based Image Analysis and Machine Learning. *In*: S., Bennani; Y., Lakhrissi; G., Khaissidi; A., Mansouri; Y., Khamlichi (org.). **WITS 2020. Lecture Notes in Electrical Engineering**. vol 745ed. Singapore: Springer, 2021. v. 745, p. 699–709.

SRIDHARAN, N. V.; SUGUMARAN, V. Convolutional Neural Network based Automatic Detection of Visible Faults in a Photovoltaic Module. **Energy Sources, Part A: Recovery, Utilization and Environmental Effects**, [*s. l.*], v. 00, n. 00, p. 1–16, 2021. Disponível em: https://doi.org/10.1080/15567036.2021.1905753.

TRIBAK, H.; ZAZ, Y. Remote solar panels identification based on patterns localization. **Proceedings of 2018 6th International Renewable and Sustainable Energy Conference, IRSEC 2018**, [*s. l.*], p. 1–5, 2018.

TRIBAK, H.; ZAZ, Y. Solar Panels Frames Quality Assessment. **Proceedings of 2017 International Renewable and Sustainable Energy Conference, IRSEC 2017**, [*s. l.*], 2018.

TRIKI-LAHIANI, A.; BENNANI-BEN ABDELGHANI, A.; SLAMA-BELKHODJA, I. Fault detection and monitoring systems for photovoltaic installations: A review. **Renewable and Sustainable Energy Reviews**, [*s. l.*], v. 82, n. July 2017, p. 2680–2692, 2018. Disponível em: https://doi.org/10.1016/j.rser.2017.09.101.

TSANAKAS, J. A.; BOTSARIS, P. N. An infrared thermographic approach as a hot-spot detection tool for photovoltaic modules using image histogram and line profile analysis. **International Journal of Condition Monitoring**, [*s. l.*], v. 2, n. 1, p. 22–30, 2012. Disponível em: http://openurl.ingenta.com/content/xref?genre=article&issn=2047-6426&volume=2&issue=1&spage=22.

TSANAKAS, J. A.; BOTSARIS, P. N.; TSANAKAS, I.; BOTSARIS, P. N. On the Detection of Hot Spots in Operating Photovoltaic Arrays through Thermal Image Analysis and a Simulation Model. **Materials Evaluation**, [*s. l.*], v. 71, n. 4, p. 457–465, 2013.

TSANAKAS, J. A.; CHRYSOSTOMOU, D.; BOTSARIS, P. N.; GASTERATOS, A. Fault diagnosis of photovoltaic modules through image processing and Canny edge

detection on field thermographic measurements. **International Journal of Sustainable Energy**, [*s. l.*], v. 34, n. 6, p. 351–372, 2015. Disponível em: http://www.tandfonline.com/doi/abs/10.1080/14786451.2013.826223.

TSANAKAS, J. A.; HA, L. D.; AL SHAKARCHI, F. Advanced inspection of photovoltaic installations by aerial triangulation and terrestrial georeferencing of thermal/visual imagery. **Renewable Energy**, [*s. l.*], v. 102, p. 224–233, 2017. Disponível em: http://dx.doi.org/10.1016/j.renene.2016.10.046.

TSANAKAS, J. A. J. A.; HA, L.; BUERHOP, C. Faults and infrared thermographic diagnosis in operating c-Si photovoltaic modules: A review of research and future challenges. **Renewable and Sustainable Energy Reviews**, [*s. l.*], v. 62, p. 695–709, 2016. Disponível em: http://dx.doi.org/10.1016/j.rser.2016.04.079.

ULRIKE JAHN; HERZ, M.; KÖNTGES, M.; PARLEVLIET, D.; PAGGI, M.; TSANAKAS, I.; STEIN, J. S.; BERGER, K. A.; RANTA, S.; FRENCH, R. H.; RICHTER, M.; TANAHASHI, T. **Review on Infrared and Electroluminescence Imaging for PV Field Applications**. IEA PVPS: [*s. n.*], 2018.

UMA, J.; MUNIRAJ, C.; SATHYA, N. Diagnosis of Photovoltaic (PV) Panel Defects Based on Testing and Evaluation of Thermal Image. **Journal of Testing and Evaluation**, [*s. l.*], v. 47, n. 6, p. 20170653, 2019. Disponível em: http://www.astm.org/doiLink.cgi?JTE20170653.

UMAIR, M.; FARHAJ, H.; MASUD, M.; DAD, K.; ZAFAR, A. A machine learning framework to identify the hotspot in photovoltaic module using infrared thermography. **Solar Energy**, [*s. l.*], v. 208, n. July, p. 643–651, 2020. Disponível em: https://doi.org/10.1016/j.solener.2020.08.027.

VATH. Electrical Infrared Inspections ▪ Low Voltage. [*s. l.*], n. February, p. 17, 2016.

VENKATESH, S. N. S. N.; SUGUMARAN, V. A combined approach of convolutional neural networks and machine learning for visual fault classification in photovoltaic modules. **Proceedings of the Institution of Mechanical Engineers, Part O: Journal of Risk and Reliability**, [*s. l.*], v. 236, n. 1, p. 148–159, 2022.

VERGURA, S. Correct Settings of a Joint Unmanned Aerial Vehicle and Infrared Camera System for the Detection of Faulty Photovoltaic Modules. **IEEE Journal of Photovoltaics**, [*s. l.*], v. 11, n. 1, p. 124–130, 2021.

VERGURA, S.; FALCONE, O. Filtering and processing IR images of PV modules. **Renewable Energy and Power Quality Journal**, [*s. l.*], v. 1, n. 9, p. 1209–1214, 2011.

VERGURA, S.; MARINO, F. Quantitative and Computer-Aided Thermography-Based Diagnostics for PV Devices: Part I-Framework. **IEEE Journal of Photovoltaics**, [*s. l.*], v. 7, n. 3, p. 822–827, 2017.

VOULODIMOS, A.; DOULAMIS, N.; DOULAMIS, A.; PROTOPAPADAKIS, E. Deep Learning for Computer Vision: A Brief Review. **Computational Intelligence and**

Neuroscience, [*s. l.*], v. 2018, p. 1–13, 2018. Disponível em: https://www.hindawi.com/journals/cin/2018/7068349/.

WANG, M.; CUI, Q. Q.; SUN, Y.; WANG, Q. Photovoltaic panel extraction from very high-resolution aerial imagery using region–line primitive association analysis and template matching. **ISPRS Journal of Photogrammetry and Remote Sensing**, [*s. l.*], v. 141, p. 100–111, 2018. Disponível em: https://doi.org/10.1016/j.isprsjprs.2018.04.010.

WANG, Q.; PAYNABAR, K.; PACELLA, M. Online automatic anomaly detection for photovoltaic systems using thermography imaging and low rank matrix decomposition. **Journal of Quality Technology**, [*s. l.*], 2021.

WANG, N.; SUN, Z.-L.; ZENG, Z.; LAM, K.-M. Effective Segmentation Approach for Solar Photovoltaic Panels in Uneven Illuminated Color Infrared Images. **IEEE Journal of Photovoltaics**, [*s. l.*], v. 11, n. 2, p. 478–484, 2021. Disponível em: https://ieeexplore.ieee.org/document/9292949/.

WANG, P.; YANG, W.; SHEN, Y.; ZHOU, L. The Fault Diagnosis for Photovoltaic Array with the Technique of Infrared/Visible Image Fusion. *In*: PROCEEDINGS OF SPIE - THE INTERNATIONAL SOCIETY FOR OPTICAL ENGINEERING, 2003, [*s. l.*], . **Anais** [...]. [*S. l.: s. n.*], 2003. p. 658–661.

WAQAR AKRAM, M.; LI, G.; JIN, Y. Y.; CHEN, X.; ZHU, C.; ZHAO, X.; ALEEM, M.; AHMAD, A. Improved outdoor thermography and processing of infrared images for defect detection in PV modules. **Solar Energy**, [*s. l.*], v. 190, n. March, p. 549–560, 2019. Disponível em: https://doi.org/10.1016/j.solener.2019.08.061.

WEI, S.; LI, X.; DING, S.; YANG, Q.; YAN, W. Hotspots Infrared detection of photovoltaic modules based on Hough line transformation and Faster-RCNN approach. *In*: 2019 6TH INTERNATIONAL CONFERENCE ON CONTROL, DECISION AND INFORMATION TECHNOLOGIES (CODIT), 2019, [*s. l.*], . **Anais** [...]. [*S. l.*]: IEEE, 2019. p. 1266–1271. Disponível em: https://ieeexplore.ieee.org/document/8820333/.

WEINREICH, B.; HAAS, R.; ZEHNER, M.; BECKER, G. Optimierung thermografischer Fehleranalyseverfahren auf Multi-MW-PV-Kraftwerke. **26th PV-Symposium Bad Staffelstein**, [*s. l.*], n. 1, p. 10, 2011.

WEN, W.; LI, S.; ZHOU, F.; LI, M.; XIE, Q. Q.; CHEN, S. Stain detection method of solar panel based on spot elimination. **2021 IEEE 2nd International Conference on Big Data, Artificial Intelligence and Internet of Things Engineering, ICBAIE 2021**, [*s. l.*], n. Icbaie, p. 820–824, 2021.

WU, J.; CHAN, E.; YADAV, R.; GOPALAKRISHNA, H.; TAMIZHMANI, G.; YADAV, R.; CHAN, E.; WU, J.; TAMIZHMANI, G. Durability evaluation of PV modules using image processing tools. *In*: PROCEEDINGS OF SPIE - THE INTERNATIONAL SOCIETY FOR OPTICAL ENGINEERING, 2018, [*s. l.*], . **Anais** [...]. [*S. l.: s. n.*], 2018. p. 36.

WU, F.; ZHANG, D.; LI, X.; LUO, X.; WANG, J.; YAN, W.; CHEN, Z.; YANG, Q. Aerial image recognition and matching for inspection of large-scale photovoltaic farms. *In*: 2017 INTERNATIONAL SMART CITIES CONFERENCE (ISC2), 2017, [*s. l.*], . **Anais** [...]. [*S. l.*]: IEEE, 2017. p. 1–6. Disponível em: http://ieeexplore.ieee.org/document/8090792/.

XI, Z.; LOU, Z.; SUN, Y.; LI, X.; YANG, Q.; YAN, W. A Vision-Based Inspection Strategy for Large-Scale Photovoltaic Farms Using an Autonomous UAV. *In*: 2018 17TH INTERNATIONAL SYMPOSIUM ON DISTRIBUTED COMPUTING AND APPLICATIONS FOR BUSINESS ENGINEERING AND SCIENCE (DCABES), 2018, [*s. l.*], . **Anais** [...]. [*S. l.*]: IEEE, 2018. p. 200–203. Disponível em: https://ieeexplore.ieee.org/document/8572557/.

XIE, Y.; SHEN, Y. Y.; ZHANG, K.; ZHANG, J. Efficient Region Segmentation of PV Module in Infrared Imagery using Segnet. **IOP Conference Series: Earth and Environmental Science**, [*s. l.*], v. 793, n. 1, 2021.

XIE, X.; WEI, X.; WANG, X.; GUO, X.; LI, J.; CHENG, Z. Abnormal target tracking and localization algorithm for UAV PV inspection scenarios. **IOP Conference Series: Materials Science and Engineering**, [*s. l.*], v. 768, n. 7, 2020.

XIE, X.; WEI, X.; WANG, X.; GUO, X.; LI, J.; CHENG, Z. Photovoltaic panel anomaly detection system based on Unmanned Aerial Vehicle platform. **IOP Conference Series: Materials Science and Engineering**, [*s. l.*], v. 768, n. 7, 2020.

YANG, M.; JI, J.; GUO, B. Soiling Quantification Using an Image-Based Method: Effects of Imaging Conditions. **IEEE Journal of Photovoltaics**, [*s. l.*], v. 10, n. 6, p. 1780–1787, 2020. Disponível em: https://ieeexplore.ieee.org/document/9184067/.

ZECH, M.; RANALLI, J. Predicting PV Areas in Aerial Images with Deep Learning. **Conference Record of the IEEE Photovoltaic Specialists Conference**, [*s. l.*], v. 2020-June, p. 0767–0774, 2020.

ZEFRI, Y.; ELKCTTANI, A.; SEBARI, I.; LAMALLAM, S. A. Inspection of Photovoltaic Installations by Thermo-visual UAV Imagery Application Case: Morocco. **Proceedings of 2017 International Renewable and Sustainable Energy Conference, IRSEC 2017**, [*s. l.*], p. 1–6, 2018. Disponível em: https://ieeexplore.ieee.org/document/8477241/.

ZEFRI, Y.; ELKETTANI, A.; SEBARI, I.; LAMALLAM, S. A. S. A. Thermal Infrared and Visual Inspection of Photovoltaic Installations by UAV Photogrammetry—Application Case: Morocco. **Drones**, [*s. l.*], v. 2, n. 4, p. 41, 2018.

ZEFRI, Y.; SEBARI, I.; HAJJI, H.; ANIBA, G. Developing a deep learning-based layer-3 solution for thermal infrared large-scale photovoltaic module inspection from orthorectified big UAV imagery data. **International Journal of Applied Earth Observation and Geoinformation**, [*s. l.*], v. 106, p. 102652, 2022. Disponível em: https://doi.org/10.1016/j.jag.2021.102652.

ZEFRI, Y.; SEBARI, I.; HAJJI, H.; ANIBA, G. In-depth investigation of applied digital photogrammetry to imagery-based RGB and thermal infrared aerial inspection of large-scale photovoltaic installations. **Remote Sensing Applications: Society and Environment**, [*s. l.*], v. 23, n. February, p. 100576, 2021. Disponível em: https://doi.org/10.1016/j.rsase.2021.100576.

ZHANG, H.; HONG, X.; ZHOU, S.; WANG, Q. Infrared Image Segmentation for Photovoltaic Panels Based on Res-UNet. *In*: LECTURE NOTES IN COMPUTER SCIENCE (INCLUDING SUBSERIES LECTURE NOTES IN ARTIFICIAL INTELLIGENCE AND LECTURE NOTES IN BIOINFORMATICS). [*S. l.: s. n.*], 2019. v. 11857 LNCS, p. 611–622. Disponível em: http://link.springer.com/10.1007/978-3-030-31654-9_52.

ZHANG, D.; WU, F.; LI, X.; LUO, X.; WANG, J.; YAN, W.; CHEN, Z.; YANG, Q. Aerial image analysis based on improved adaptive clustering for photovoltaic module inspection. *In*: 2017 INTERNATIONAL SMART CITIES CONFERENCE (ISC2), 2017, [*s. l.*], . **Anais** [...]. [*S. l.*]: IEEE, 2017. p. 1–6. Disponível em: http://ieeexplore.ieee.org/document/8090798/.

ZHANG, P.; ZHANG, L.; WU, T.; ZHANG, H.; SUN, X. Detection and location of fouling on photovoltaic panels using a drone-mounted infrared thermography system. **Journal of Applied Remote Sensing**, [*s. l.*], v. 11, n. 1, p. 016026, 2017.

ZYOUT, I.; OATAWNEH, A. Detection of PV solar panel surface defects using transfer learning of the deep convolutional neural networks. **2020 Advances in Science and Engineering Technology International Conferences, ASET 2020**, [*s. l.*], 2020.

APPENDIX A – SHARED AUTHORSHIP AGREEMENT

The co-author of the third paper that is included in this thesis provided written consent to include it herein. The consent is presented in this Appendix.

Term of agreement for the use of journal paper

This document attests that I, Matheus Körbes Bracht, co-author of the paper "Automatic Fault Detection of Utility-Scale Photovoltaic Solar Generators Applying Aerial Infrared Thermography and Orthomosaicking", submitted to the journal Solar Energy in November 2022, agree with the use of the article specified here for the use of the doctoral thesis of the student Aline Kirsten Vidal de Oliveira (first author of the paper), supervised by Prof. Ricardo Rüther, of the Programa de Pós Graduação em Engenharia Civil (PPGEC) of the Universidade Federal de Santa Catarina (UFSC) and co-supervised by Mohammadreza Aghaei, PhD.

Florianópolis, November 10, 2022.

Matheus Körbes Bracht – co-autor